Author:
Watson, Erin O

Title:
The impact of genotoxic damage on mammary epithelial cell fate

The Impact of Genotoxic Damage on Mammary Epithelial Cell Fate

Erin Olivia Watson

A dissertation submitted to the University of Bristol in accordance with the requirements for award of the degree of Cellular and Molecular Medicine (MRes) in the School of Cellular and Molecular Medicine, Faculty of Life Sciences

July 2022

Word count: 25,615

Acknowledgements

I am extremely grateful to my supervisor, Dr. Bethan Lloyd-Lewis, for her inspirational enthusiasm, patience and support throughout this project, as well as her invaluable expertise. I am also indebted to my panel member, Dr. Parthive Patel, who's feedback was incredibly instructive. I would like to extend thanks to Laura Bevan who's practical (and moral) support was endlessly helpful. Also to Tracey Collard, for her practical assistance and advice in the lab and to Dr. Francisca Segers, for all her guidance regarding the bioinformatics analysis. Lastly, I'd like to acknowledge my coursemates, who's friendship has kept my spirits high during this process.

Abstract

The mammary gland is a highly dynamic organ that undergoes waves of proliferation, cell death and regeneration throughout female reproductive life. This activity requires the support of adult tissue stem/progenitor cells. The branched mammary epithelium is comprised of a basal cell layer surrounding an inner luminal cell layer. Lineage tracing studies have demonstrated that lineage-restricted progenitor cells maintain the luminal and basal compartments postnatally under physiological conditions. However, 'reprogramming' of these cells causing the reacquisition of multipotency and generation of cells of the opposing lineage is triggered by certain conditions, including genotoxic (DNA) damage. This process, termed plasticity, is thought to play an important role in breast cancer. Thus, understanding how genotoxic damage affects mammary epithelial cell plasticity has the potential to improve breast cancer chemo-prevention and treatment. Here, I established 3D organoid cultures from transgenic lineage tracing mouse models that enable basal and luminal epithelial cell fate mapping to investigate genotoxic damage-induced fate plasticity. I showed that organoids faithfully recapitulate the *in vivo* structure and behaviour of mammary epithelial cells and confirmed their suitability for *in vitro* lineage tracing. Using 3D organoid culture, I demonstrated that cisplatin-induced DNA damage does not generate plasticity in basal or luminal cells *in vitro*. Interestingly, administration of cisplatin *in vivo* led to basal cell plasticity. This suggests that genotoxic damage-induced plasticity may be mediated by signals from the mammary microenvironment. Investigation of two candidate mediating factors, namely Interleukin-1ß and the TNF inhibitor Adalimumab that have previously been implicated in epithelial cellular plasticity, revealed that while IL-1ß failed to induce plasticity in basal or luminal cells *in vitro*, subtle evidence of basal cell plasticity was seen with Adalimumab treatment. Alongside, I interrogated available RNA sequencing data to identify novel putative microenvironmental factors mediating mammary cell plasticity that could be investigated in future studies.

Author’s declaration

I declare that the work in this dissertation was carried out in accordance with the requirements of the University's Regulations and Code of Practice for Research Degree Programmes and that it has not been submitted for any other academic award. Except where indicated by specific reference in the text, the work is the candidate's own work. Work done in collaboration with, or with the assistance of, others, is indicated as such. Any views expressed in the dissertation are those of the author.

SIGNED: .....Erin Watson..... DATE: 21/07/2022

Contents

List of Figures and Tables

1. Introduction

The mammary gland is one of the most fascinating biological systems. A highly conserved mammalian organ, it's function is to produce and secrete milk to feed offspring. It is unique among its epithelial organ counterparts as it develops solely in females and predominantly postnatally. It also undergoes cycles of growth and regression during oestrus and pregnancy. This remarkable regeneration potential is attributed to the presence of adult mammary stem and progenitor cells. This provides an ideal system to study adult stem cell dynamics and fate specification in development outside of the embryo. As presumptive targets for transformation in breast cancer, the fate dynamics of adult mammary stem cells are subject to intense investigation.

1.1 Mammary Gland Development

In mice, the mammary gland begins to develop via the formation of two milk lines on top of the ectoderm at embryonic day 10.5 (E10.5) (Lloyd-Lewis et al. 2018) (Figure 1A). On E11.5, structures termed mammary placodes, consisting of clustered epithelial cells, form. By E13.5, these placodes have sunk into the dermis below, triggering condensation of mesenchymal cells to form the mammary mesenchyme. The mesenchyme further differentiates into two layers, one of which forms the mammary fat pad precursor at approximately E14.5. The period from E15.5 until the end of embryonic mammary development at E18.5 is dominated by epithelial cell proliferation, elongation and invasion into the fat pad to form a primitive mammary glandular tree (Inman et al. 2015).

This basic structure present at birth grows in proportion with body development until puberty. Puberty is triggered by an increase in gonadotropin levels, leading to the secretion of the ovarian hormones oestrogen and progesterone (Slepicka, Somasondara and Dos Santos, 2021), which the mammary gland responds to by forming an intricate ductal network through a process termed branching morphogenesis (Lloyd-Lewis et al. 2018). This is driven by the proliferation of cells within structures named Terminal End Buds (TEBs) (Figure 1B). These structures reside at the tips of the developing branches and are thought to harbour the putative stem cells which are responsible for this process. By the end of puberty, the TEBs deteriorate and leave the fat pad fully populated by a bi-layered mammary epithelium, consisting of lumens enclosed by luminal cells, surrounded by a layer of basal cells (Lloyd-Lewis et al. 2017). These mammary cells are distinguished by the

differential expression of specific marker proteins (Figure 1C). Once this stage of development is reached, the mammary gland becomes relatively quiescent, with modest cycles of expansion and regression coordinating with the oestrus cycle.

In adulthood, pregnancy prompts further remodelling of the mammary gland whereby alveolar (milk-producing) cells specialise from the luminal cell population, resulting in a dense, highly branched structure to facilitate milk production and let down (Lloyd-Lewis et al. 2017). The contractile activity of basal cells ensures that milk produced by alveolar cells is transported through the ductal tree towards the nipple (Stevenson et al. 2020). Once offspring are weaned and lactation arrests, the alveolar cells die in a programme of cell death referred to as involution and the mammary gland returns to its pre-pregnancy state. However, future pregnancies will trigger further rounds of cell proliferation and regeneration of alveolar cells to support subsequent young (Lloyd-Lewis et al. 2017) (Figure 1B).

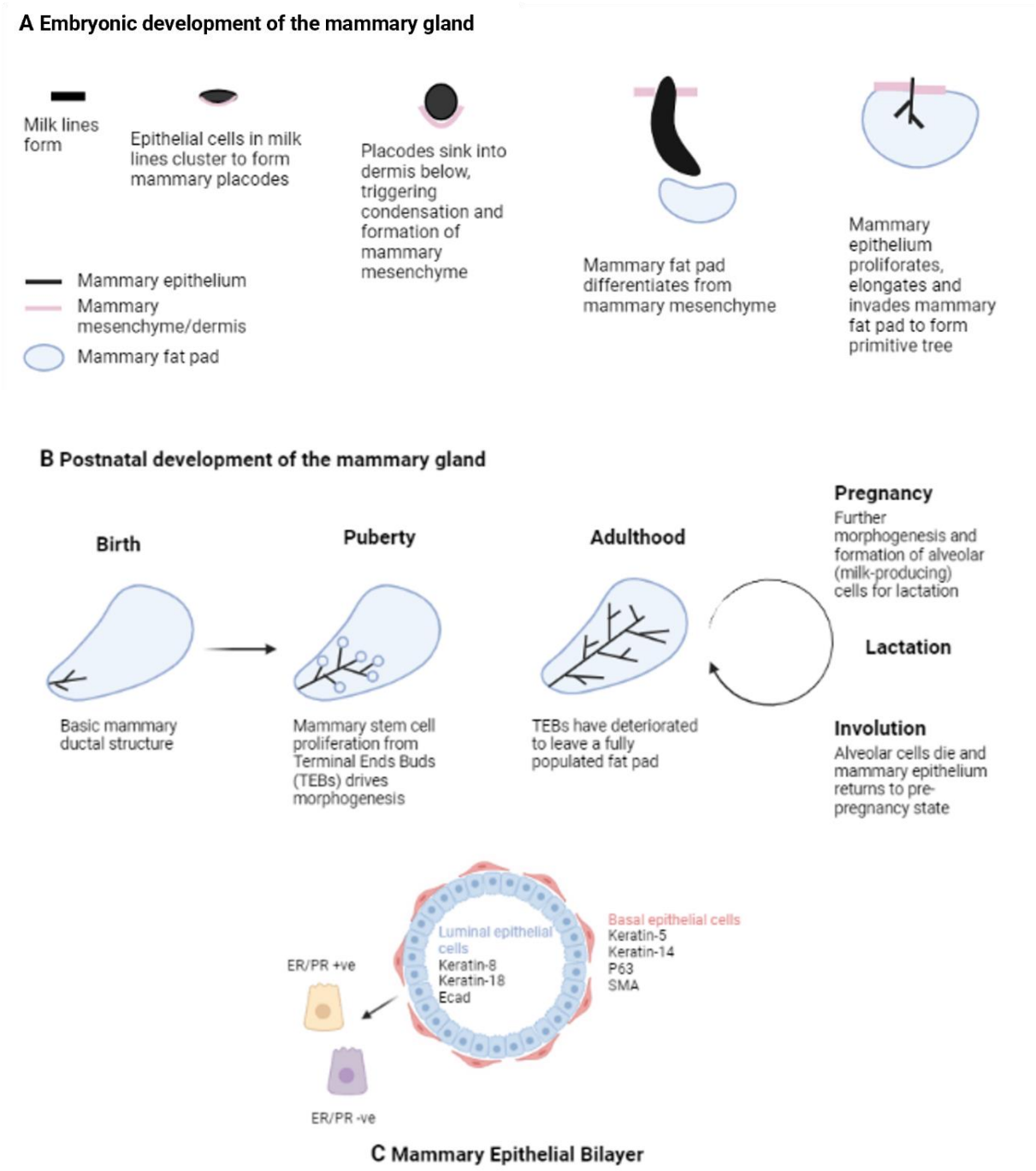

Figure 1: An overview of mammary gland development. A: Embryonic mammary gland development begins with the specification of milk lines, which form mammary placodes that invade the mammary fat pad and elongate/proliferate to form a basic mammary tree upon birth. B: Postnatal mammary gland development initiates with puberty, whereby hormonal signalling triggers morphogenesis which generates a branched ductal network, primarily driven by proliferation of mammary stem cells (MaSCs) in Terminal End Buds (TEBs). The TEBs regress at the end of puberty to leave a mature mammary ductal network filling the entire fat pad during adulthood. Pregnancy during adulthood stimulates further morphogenesis to form a dense network and differentiation of luminal cells into milk-producing alveolar cells for lactation. At the end of lactation, the alveolar cells die in a process termed involution, returning the mammary gland to its pre-pregnancy state. C: The mammary epithelial bilayer is the basic unit of the mammary gland. Examples of specific genes expressed in luminal and basal mammary epithelial cells are shown. Embryonic mammary development adapted from Honvo-Hueto and Turchet (2015). Created in BioRender.com.

The remodelling and regenerative events that occur during the development and maintenance of the mammary gland suggest the presence of a stem cell population capable of generating and regenerating the cells required and subsequently lost during pregnancy, lactation and involution. This concept was first demonstrated experimentally during pioneering studies in the 1950s that led to the development of the mammary transplantation assay (Lloyd-Lewis et al. 2017).

1.2 Mammary stem cell identification: Mammary transplantation assay

The mammary transplantation assay was developed by DeOme et al. in experiments in 1959, when fragments of mammary epithelia were taken from a host mouse and implanted into the mammary fat pad of a recipient mouse which had been cleared of its existing mammary epithelia (Figure 2). The epithelial fragments were able to regenerate an entire mammary ductal tree in the recipient fat pad, indicating the presence of cells able to generate both basal and luminal epithelial cells within the postnatal mammary gland (DeOme et al. 1959). Although adult stem cells are often recruited for tissue repair and regeneration, adult development and maintenance is rarely dictated by these cells as in most systems development occurs in embryonic stages. The possibility that these putative stem cells may play an active role in the adult mammary gland invites further investigation into their precise identity and differentiation potential.

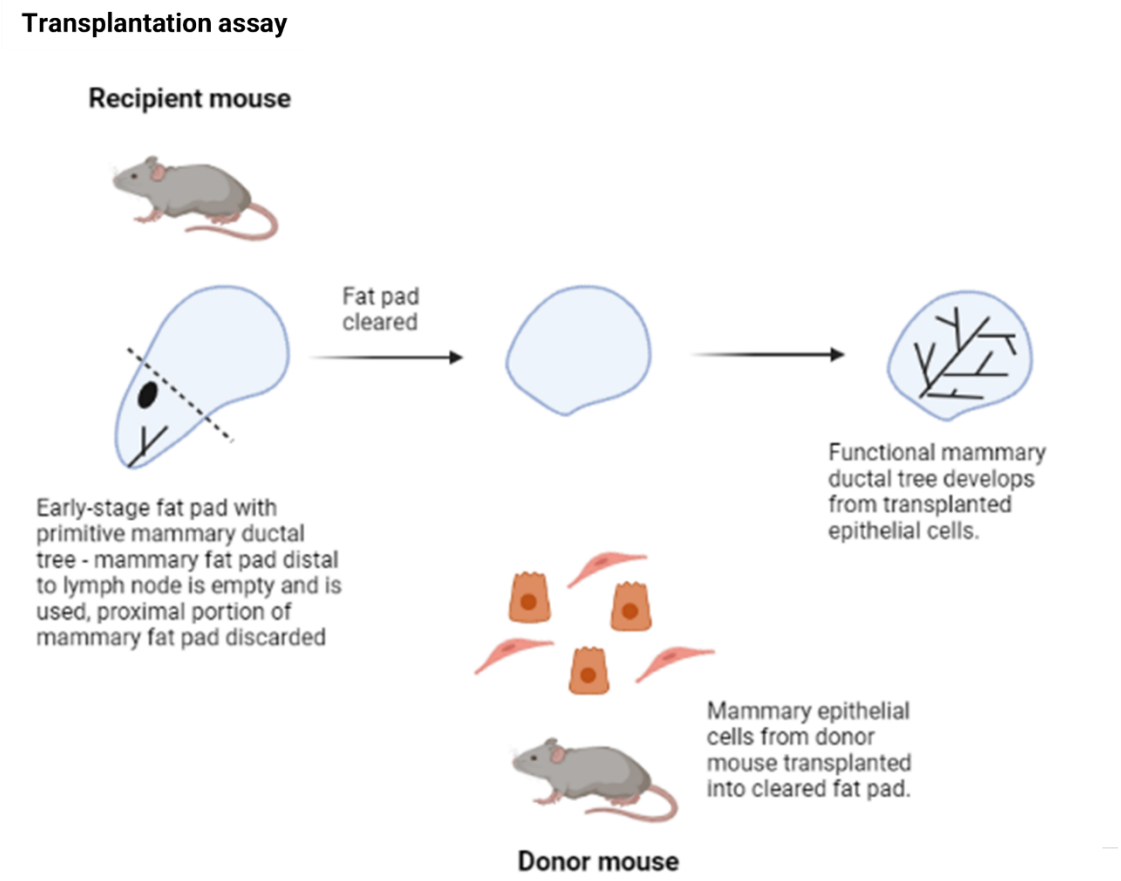

Figure 2: Schematic of a mammary transplantation assay. The section of fat pad distal to the lymph node of a recipient mouse in the early stages of development is used as it is empty of epithelium (the proximal section is discarded). Mammary epithelial fragments or cells from a donor mouse are isolated and transplanted into the 'cleared' fat pad. Any resulting mammary duct that develops will have arisen from the transplanted donor cells. Created in BioRender.com.

Due to the observation that both basal and luminal cells were generated upon transplantation of mammary epithelia dissociated into single cells, the search for the mammary stem cell population initially focused on a multipotent cell capable of generating both cell types. Confirmation of this suspected multipotency requires the use of a technique called lineage tracing, whereby a cell of interest is marked in a way that its fate and the fate of its progeny can be followed over time. The need for technologies that allow in situ fate mapping becomes more apparent when considering the non-physiological nature of mammary transplantation assays, which move cells from a complex microenvironment complete with neighbouring epithelial cells and stromal components to a comparatively barren mammary fat pad which has been cleared of host epithelia. The behaviour of transplanted cells in this recipient fat pad may therefore not mimic their behaviour in their natural microenvironment (Van Keymeulen et al. 2011).

1.3 Mammary stem cell identification: Lineage Tracing

The first lineage tracing experiments aimed at determining the potency of mammary stem cells in development were population-based or 'mosaic' lineage tracing experiments performed by Van Keymeulen et al. in 2011. These experiments used the Cre-recombinase system which allows temporal regulation of label induction (typically at levels between 5 and 50% (Van Keymeulen et al. 2011, Wuidart et al. 2016)) and subsequent tracking of cell fate specification over time (Figure 3).

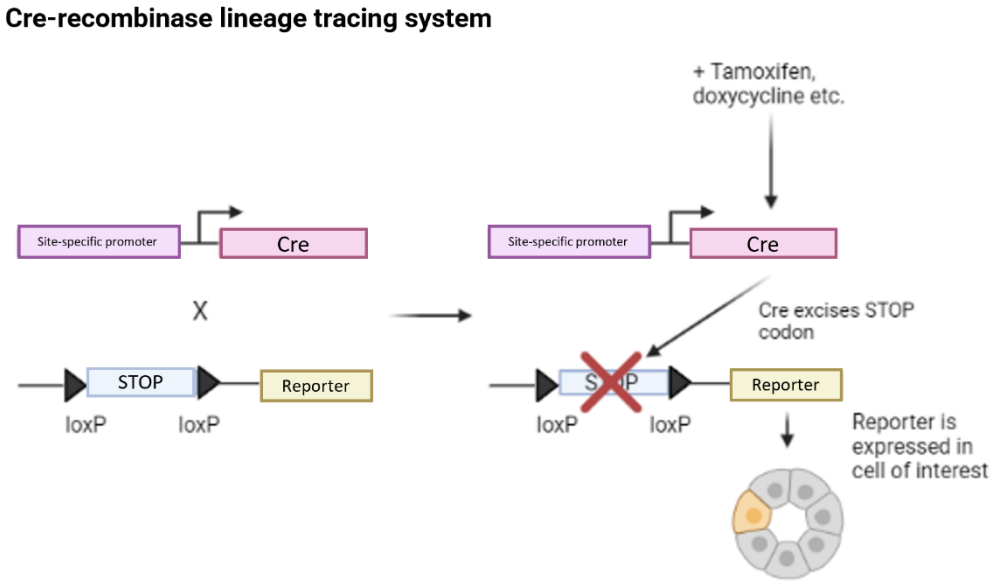

Figure 3: Diagram illustrating the Cre-recombinase system for lineage tracing. Cell type-specific expression of Cre is achieved through cell-specific promoters lying upstream of the Cre recombinase gene. Addition of e.g. tamoxifen or doxycycline (dependent on the receptor the Cre recombinase gene is coupled to) activates expression of Cre recombinase, which recombines loxP sites to excise a STOP codon lying upstream of a reporter gene e.g. Green Fluorescent Protein. This enables time-specific labelling of cells of interest by a reporter gene, which is passed to progeny. Created in BioRender.com.

Due to the observation that embryonic mammary cells express Keratin 14 (K14), Van Keymeulen et al. used the K14 promoter to target a doxycycline-inducible Cre-recombinase to K14-expressing cells, where excision of loxP sites activated yellow fluorescent protein (YFP) labelling. By administering a single dose of doxycycline to pregnant K14/Cre/YFP mice at embryonic day 17, it was confirmed that K14-expressing cells represent bipotent stem cells able to produce both luminal and basal mammary epithelial cells in the mouse embryo. To investigate whether this K14-expressing population contains bipotent cells postnatally, K14/Cre/YFP activity was induced in mice over puberty and adulthood. This resulted in the exclusive labelling of basal cells with no evidence of luminal cell labelling. Tracing of labelled cells over several weeks during puberty and adulthood resulted in clones composed of only

basal cells, indicating that K14-expressing basal progenitors become lineage-restricted (i.e.unipotent) postnatally (Van Keymeulen et al. 2011). Analogous studies using luminal gene promoters (K8 and 18) to drive Cre expression revealed that the luminal compartment is also maintained postnatally by unipotent luminal progenitors (Van Keymeulen et al. 2011).

To understand the contrast between this result and those observed during transplantation experiments, YFP-labelled K14+ cells were transplanted to the cleared mammary fat pad of immunodeficient mice with and without unlabelled luminal cells. Without luminal cells, a normal mammary gland complete with YFP-labelled basal and luminal cells developed. However, transplantation alongside unlabelled luminal cells restricted labelling to the basal compartment. This suggests that the transplantation process itself triggers multipotency in otherwise unipotent progenitors and that the luminal cells may be restricting the bipotency of basal cells in physiological conditions – a concept further investigated by Centonze et al. in later work (discussed below). These unipotent progenitors appear to maintain the basal and luminal compartments in the pubertal and adult mammary gland following its initial generation by a multipotent embryonic stem cell. Whilst it is not possible to disprove the presence of multipotent stem cells, postnatal mammary gland development and the homeostatic maintenance of the mammary gland does not appear to rely on them (Van Keymeulen et al. 2011).

1.4 Mammary stem cell identification: Overcoming Obstacles in Lineage Tracing

Despite excitement caused by the revelation of a new role for postnatal mammary progenitors through population-based/'mosaic' lineage tracing, several limitations to this technique exist which must be considered. Firstly, this method relies on the assumption that molecular markers chosen to drive labelling (e.g. K14 and K8) specifically and consistently label putative mammary stem/progenitor cells (Lloyd-Lewis et al. 2018). However, K14 and K8 have been shown not to label these cells exclusively and distinct molecular markers for mammary stem cells have yet to be identified (Seldin, Le Guelte and Macara, 2017). K8 has in fact been demonstrated to preferentially label a subset of luminal cells (Davis et al. 2016). Thus, the use of the K8 promoter to drive Cre-recombinase expression may 'select' for a particular population of luminal cells to label and trace. The lack of desired specificity of promoters can result in a phenomenon termed 'Clone Convergence', particularly in studies

where labelling is induced at levels above clonal density. This occurs when the promoter driving the labelling system 'leaks', causing labelling of an incorrect population of cells which become intermixed with the desired targeted cells. Although the level of labelling is quite low in these systems due to the low efficiency of recombination, it is not low enough to accurately trace a single cell and its progeny. Therefore (in the context of lineage tracing of mammary epithelial cells), it is impossible to distinguish between a 'leaky' labelling system causing the independent labelling of two adjacent cells of different lineages e.g. a basal cell next to a luminal cell, or whether the labelled luminal cell represents the progeny of a labelled, bipotent basal cell, or vice versa. As such, a single instance of promiscuous labelling of an untargeted cell and subsequent proliferation of this cell may give the false impression of the existence of bipotent progenitors (Davis et al. 2016). Furthermore, as previously mentioned, while the level of labelling induced by Cre-recombinase systems varies between models, it is generally quite low due to poor recombination efficiencies. As a result, rare multipotent mammary stem cells may be missed (Van Keymeulen et al. 2011). The confounding impact of these limitations when investigating the cell fate specification of particular populations can be seen when considering the findings of Rios et al. (2014). By using newly constructed lineage tracing mouse lines using the luminal-specific promoter Elf5 and the basal-specific promoter K5, their results suggested the existence of bipotent stem cells during puberty and adulthood, for example through the identification of tdTomato-positive luminal cells when using a K5-tdTomato lineage tracing mouse model (Rios et al. 2014).

Saturation lineage tracing is a method that can be used to address the limitations presented by the population-based lineage tracing techniques mentioned above. This technique involves labelling almost 100% of cells of a particular lineage to investigate the dilution of the label. In the context of lineage tracing of mammary epithelial cells, if saturation lineage tracing of basal cells was performed and unlabelled basal cells emerged over time (therefore diluting the label), this would suggest that they originated from an unlabelled, bipotent luminal progenitor (Figure 4). Wuidart et al. (2016) performed this experiment using a doxycycline-inducible system to avoid the toxicity and perturbed mammary development induced when using high levels of tamoxifen in Cre-ERT (oestrogen receptor-fused Cre-recombinase) based models. After continuous doxycycline

administration during the entirety of pubertal development in K14-Cre-YFP mice, 97% of basal cells were labelled with YFP and no labelled luminal cells emerged during postnatal development, pregnancy and lactation, demonstrating that K14+ basal progenitors are unipotent. Saturation levels of labelling of K8+ cells was also achieved and analysis 5 months later demonstrated no dilution of the label, demonstrating the presence of a unipotent progenitor that maintains luminal cells (Wuidart et al. 2016).

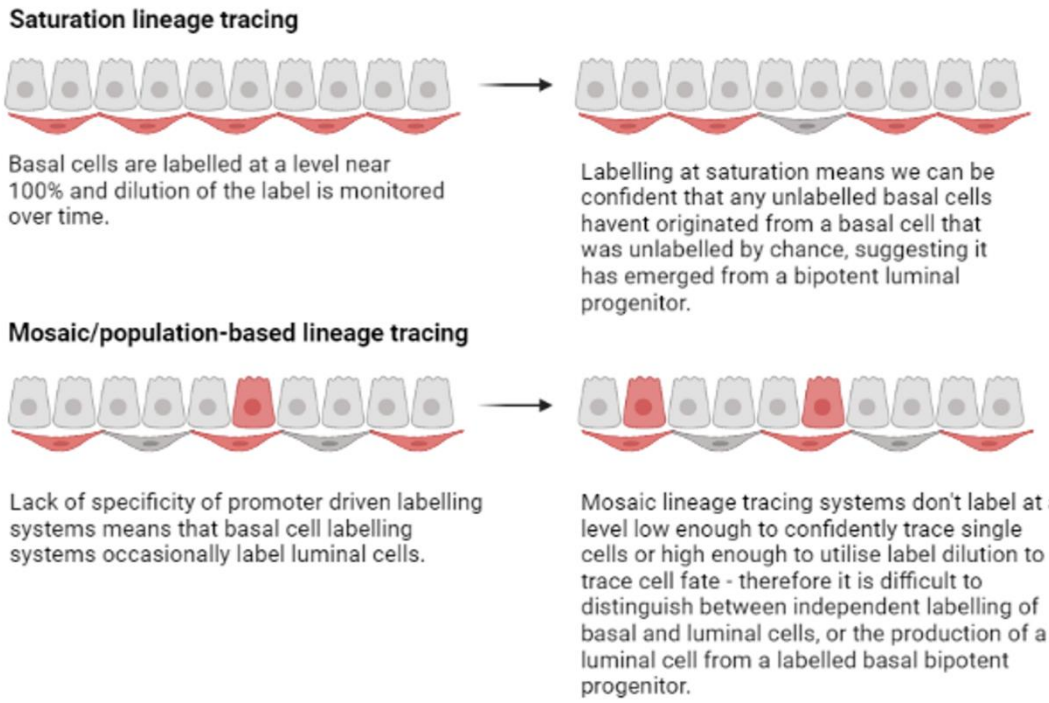

Figure 4: Saturation lineage tracing labels almost 100% of cells, meaning label dilution can be used to investigate the fate potential of progenitors. The lower level of labelling achieved using population-based/mosaic approaches, coupled with 'leaky' promoters causing labelling of the opposing cell lineage, means clone convergence can confound results. This phenomenon makes it difficult to distinguish between independent labelling events marking adjacent basal and luminal cells, or the existence of a bipotent basal progenitor producing a labelled luminal cell (or vice versa). Created in BioRender.com

Two further neutral lineage tracing techniques have also provided evidence for the presence of lineage-restricted progenitors in the pubertal and adult mammary gland. Both methods utilise systems that can label any cell, overcoming the issues presented by systems driven by 'lineage-specific' promoters that can be promiscuous, or potentially only label particular lineage subsets (Figure 5).

The $R26^{[CA]30}$ reporter mouse model enables single cell tracing with high confidence. It relies on rare frame-shift mutations occurring during DNA replication causing expression of a reporter gene, allowing the labelling and tracing of single cells (Figure 5A). In this model,

large ductal regions comprising of B-glucosidase+ basal cells only and separate regions consisting of B-glucosidase+ luminal cells only were observed, suggesting the presence of unipotent progenitors in developing ducts (Davis et al. 2016, Lloyd-Lewis et al. 2018). However, this system requires cells to be actively cycling, and therefore likely fails to label a potential quiescent population of multipotent stem cells. In addition, it is not possible to control the timing of labelling in this system. Without knowing at which stage of mammary development the cells were labelled, it is difficult to understand how the potential and contribution to development of a cell changes over time. The R26-CreERT2 Confetti reporter mouse model overcomes this issue, as it allows the temporal regulation of label expression in an unbiased manner (due to the universal Rosa26 promoter driving both Cre and Confetti expression). The stochastic induction of 4 different fluorescent reporters also allows for distinct clones to be identified with confidence, minimising the risk of clone convergence (Figure 5B). By administering a single, low dose of tamoxifen to 4 week old mice and incorporating a 3 week chase, the progeny of cells labelled at the onset of puberty could be tracked. This model also suggested that postnatally, distinct luminal and basal unipotent progenitors maintain the mammary gland (Davis et al. 2016, Scheele et al. 2017, Lloyd-Lewis et al. 2018) (Figure 6).

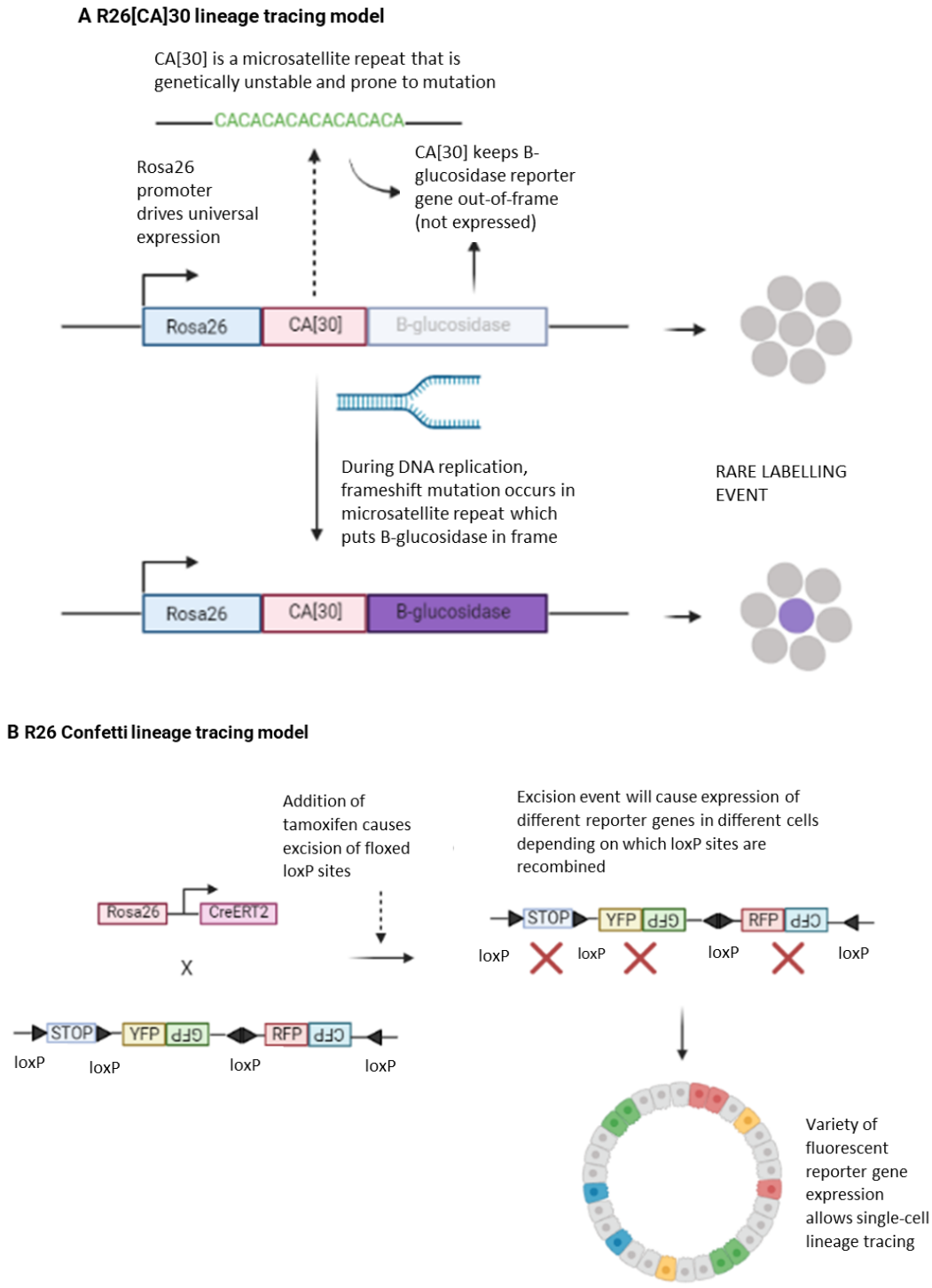

Figure 5: Schematic of R26$^{CA[30]}$ lineage tracing model (A) and R26-CreERT2 Confetti lineage tracing model (B). A: The R26$^{CA[30]}$ lineage tracing model relies on rare frame-shift mutations occurring during DNA replication putting a modified out-of-frame B-glucosidase gene in frame, leading to expression. This event is targeted by the inclusion of a CA[30] microsatellite repeat positioned upstream of the B-glucosidase reporter, which is inherently unstable and prone to mutation. The entire construct is driven by the universal Rosa26 promoter, leading to expression in any cell type. B: The R26-CreERT2 Confetti lineage tracing model allows temporal regulation of universal reporter gene expression, which can reliably label single cells due to the possibility of expression of 4 different reporter genes depending on which loxP sites are recombined. Adapted from Lloyd-Lewis et al. (2018). Created in BioRender.com.

Several additional lineage tracing studies targeting specific subsets of mammary cells support the conclusion that postnatal mammary gland development and tissue homeostasis is mediated by distinct unipotent luminal and basal progenitors under physiological contexts (Figure 6). For example, population-based lineage tracing using a Cre-recombinase directed to Axin2+ cells (a gene target of the Wnt pathway) suggested that Axin2 marked either luminal or basal cells at different developmental timepoints, but never both during the same window (van Amerongen, Bowman and Nusse, 2012). Furthermore, targeting Cre-recombinase downstream of the Smooth Muscle Actin (aSMA) promoter (which marks basal cells) also demonstrated that basal cells do not contribute to the luminal epithelial layer postnatally (Prater et al. 2014). Finally, the use of this system downstream of the Lgr6 promoter, which is known to mark stem cells in other organs such as the lung and skin, also provided evidence of unipotent progenitors postnatally (Blaas et al. 2016).

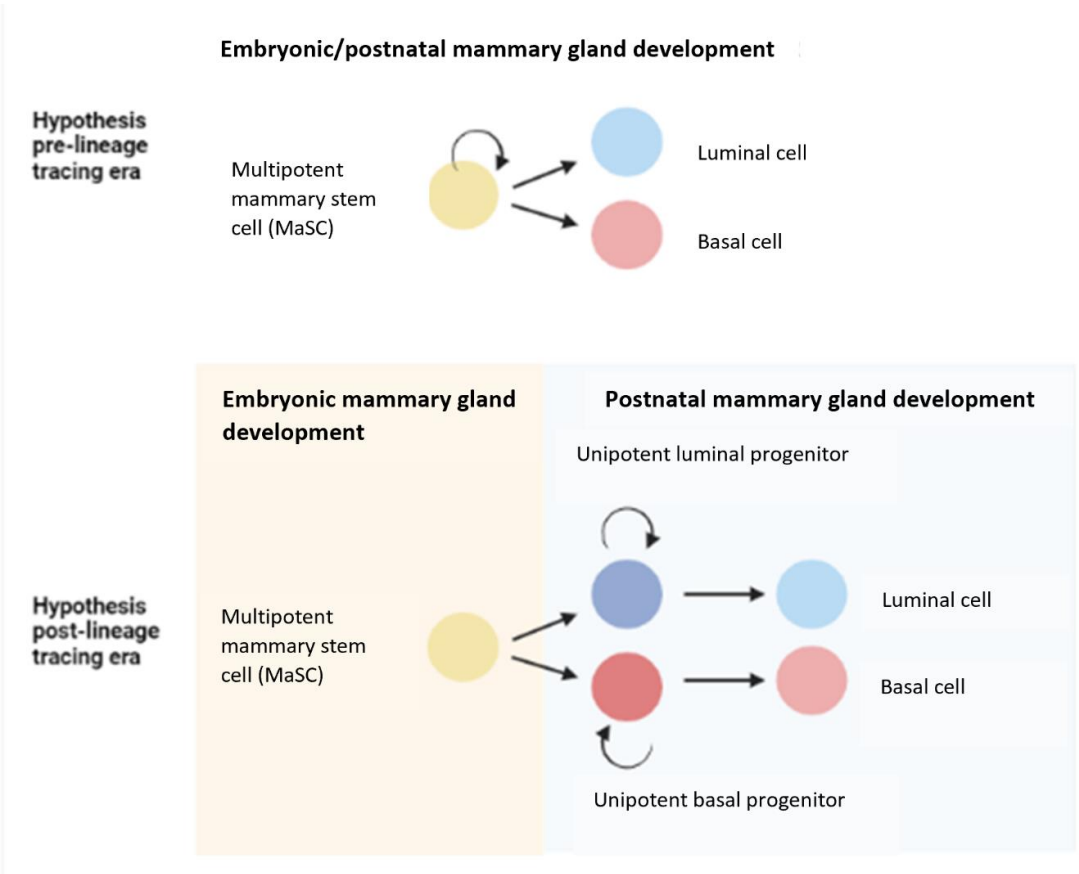

Figure 6: Hypothesised hierarchy of epithelial cells in the mammary gland. Transplantation experiments (whereby individual mammary epithelial cells could generate an entire mammary gland when transplanted to a cleared mammary fat pad) lead to the belief that multipotent mammary stem cells generated both luminal and basal epithelial cells during embryonic, pubertal and adult mammary gland development. However, lineage tracing experiments during puberty and adulthood demonstrating the retention of reporter genes in distinct cellular (i.e. luminal and basal) subsets over time suggested that although a multipotent mammary stem cell drives embryonic development, pubertal and adult development and maintenance of the mammary gland is driven by distinct unipotent basal and luminal progenitors. Adapted from Lloyd-Lewis et al. (2017). Created in BioRender.com.

1.5 Mammary stem cells: Reactivating multipotency in lineage-restricted progenitors

Although maintenance of the adult mammary gland is governed by distinct unipotent progenitors, various studies have demonstrated that certain conditions, such as transplantation as mentioned above, cause unipotent mammary epithelial progenitors to reacquire multipotent capabilities. This is termed cellular 'plasticity', which broadly refers to a change in cell identity or fate. This suggests that under normal, physiological conditions, bipotency in lineage-specific epithelial progenitors is actively restricted; which, in the context of mammary basal cells, is supported by the observation that transplanting basal progenitors alongside luminal cells maintains basal progenitor unipotency (Van Keymeulen et al. 2011).

Centonze et al. (2020) explored this hypothesis further by utilising a mouse model that allowed the fluorescent labelling of mammary basal cells alongside the ablation of luminal cells (via the specific induction of diphtheria toxin A in K8-expressing cells). In the absence of luminal ablation, clones arising from labelled basal cells remained lineage restricted as expected. However, triggering luminal cell ablation resulted in the appearance of bi-lineage clones, with around 6% of luminal cells becoming fluorescently labelled *in vivo*. This suggests that luminal cell ablation activates bipotency in basal progenitors. This effect persisted in the presence of anti-inflammatory treatment, suggesting the activation of bipotency in basal cells is not dependent on immune cell recruitment to the ablated site. The activation of bipotency in basal cells in response to luminal cell ablation was also mimicked in mammary epithelial organoid culture, suggesting that this was mediated by a cell intrinsic mechanism. RNA sequencing data pointed to Tumour Necrosis Factor (TNF) as a significant mediator in the restriction of basal progenitor bipotency. In support, TNF inhibition using the anti-TNF antibody Adalimumab indeed stimulated bipotency in basal progenitors in the absence of injury, suggesting a potential mechanism whereby luminal cell secretion of TNF maintains the unipotency of basal progenitors in physiological conditions (Centonze et al. 2020).

Oncogene expression has also been shown to induce cell fate plasticity in unipotent progenitors, potentially by re-activating embryonic-like transcriptional programs. For example, Van Keymeulen et al. (2015) and Koren et al. (2015) demonstrated that mutant Pik3ca (one of the most commonly mutated genes in breast cancer) expression in either luminal or basal cells specifically reactivated bipotency in normally lineage-restricted

progenitors. Furthermore, it was demonstrated that luminal cells expressing mutant Pik3ca were able to reconstitute the mammary gland in transplantation assays, marking a reactivation of bipotency in normally unipotent luminal progenitors. This is particularly remarkable considering wildtype luminal cells, unlike basal cells, are highly inefficient at reconstituting entire mammary glands in transplantation assays, requiring transplantation at high numbers and the presence of a solubilized basement matrix such as Matrigel. Oncogenic expression of PyMT and ErbB2 in luminal cells (using the Whey Acidic Protein (WAP) promoter) also induced cellular plasticity and re-acquisition of multipotent capacity in normally lineage-restricted luminal progenitors (Hein et al. 2016). The observation that oncogene expression can cause plasticity has important implications for the breast cancer field, which I will discuss below.

1.6 Breast cancer

Breast cancer is the most common cancer in females (Van Keymeulen et al. 2015) and the leading cause of cancer death in women worldwide (Bray et al. 2018) Originating in the mammary gland, breast tumours are classified as distinct subtypes depending on the expression of certain receptors or markers. The three main groups are hormone receptor-positive breast cancer, HER2-positive breast cancer and triple-negative breast cancer. The different tumour molecular signatures and histological appearances reflect differences in prognosis, treatment regimen and therapeutic responsiveness (Figure 7) (Vinuesa-Pitarch, Ortega-Álvarez and Rodilla, 2022).

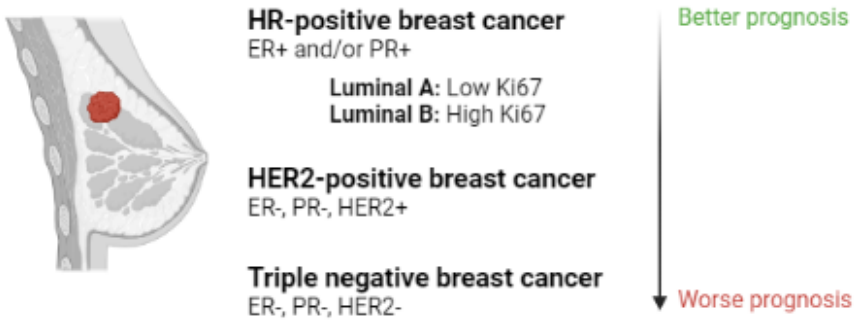

Figure 7: Classification of breast cancer subtypes. Breast cancer is a highly heterogeneous disease classified into distinct subtypes based on histological expression and molecular signatures. The three main subtypes are Hormone Receptor (HR)-positive (defined by high oestrogen and/or progesterone receptor expression). This subtype can be further classified into Luminal A or B subtypes depending on Ki67 expression. HER2-positive breast cancer is defined by high expression of the receptor tyrosine kinase ErbB2/HER2 in tumours, which typically lack hormone receptor expression. Triple negative breast cancer is defined by an absence of hormone receptor and ErbB2/HER2 expression. Adapted from Vinuesa-Pitarch, Ortega-Álvarez and Rodilla (2022). Created in BioRender.com.

This high level of heterogeneity between breast cancers is also reflected intra-tumourally due to evolution of tumour cells in response to variations in the tumour microenvironment (Sumbal et al. 2020). Intra-tumour heterogeneity poses challenges for accurate diagnosis and treatment of breast cancers and contributes to therapy resistance, disease relapse and metastasis, which all maintain the high burden this cancer has on society (Kahn et al. 2021).

The longevity and extensive self-renewal properties of stem/progenitor cells provide ample opportunity for the accumulation of transforming and/or tumour-initiating genetic mutations. As a result, several studies aimed at identifying the cell-of-origin of distinct breast cancer subtypes have focused on the unipotent progenitor populations present in the pubertal and adult mammary gland. Indeed, observational studies support the implication of mammary progenitor cells in cancer initiation. For example, the incidence of breast cancer following the enormous radiation exposure triggered by the nuclear bombing of Hiroshima and Nagasaki during World War Two was highest in females who were entering puberty at the time of the attack — a time when mammary stem/progenitor cell activity is increased (Tiede and Kang, 2011). Similarly, epidemiological studies have revealed a protective effect of early pregnancy on lifetime breast cancer risk, which may relate to the forced differentiation of mammary progenitors and resulting reduction in the size of the progenitor pool as a result of pregnancy (Meier-Abt and Bentires-Alj, 2014).

However, as discussed above, the ability of oncogenic transformation to induce plasticity in mammary epithelial cells means that a tumour's phenotype may not necessarily reflect its initiating cell-of-origin. Indeed, several studies suggest that breast cancers possessing basal characteristics likely arise from luminal progenitors (Molyneux et al. 2010, Hein et al. 2016). For example, Molyneux et al. (2010) demonstrated that only luminal progenitors harbouring BRCA1 deletions mimicked basal-like breast cancers molecularly and histologically. Targeting mutant BRCA1 to basal progenitors, on the other hand, drove the formation of rare adenomyoepitheliomas which had a similar molecular signature but a vastly different histological appearance (Molyneux et al. 2010). This reinforces the need to better understand the role of physiological and oncogene-induced mammary epithelial cell plasticity to inform breast cancer susceptibility, initiation, diagnosis and treatment.

1.7 The role of genotoxic damage in mammary epithelial plasticity?

Breast cancer is commonly treated using genotoxic agents, such as cisplatin and irradiation. These therapeutics take advantage of the rapid proliferation that is characteristic of cancer cells, which make them more susceptible to damage than quiescent, differentiated cells. Furthermore, cancer cells often harbour defective DNA damage response pathways which can be targeted by genotoxic agents.

The transmission of genetic information from a cell to its daughter during replication must be accurate to preserve genome integrity and proper cell function. As such, cells have developed complex DNA damage response (DDR) mechanisms to sense any errors in this process and repair them in a timely manner to avoid the transmission of DNA damage (such as single and double strand breaks, crosslinks and mutations) to daughter cells. If transmitted, this damage can have potentially devastating consequences in the form of cellular transformation or apoptosis. Faced with constant metabolic and environmental insults including reactive oxygen species and ionizing radiation, these mechanisms are incredibly efficient (Liang et al. 2009).

Small changes to DNA, such as single strand breaks, are commonly repaired by Base Excision Repair (BER) or Nucleotide Excision Repair (NER), whereby damaged DNA is excised and replaced with newly synthesised DNA. In contrast, double strand breaks (DSBs) are repaired by homologous recombination and non-homologous end joining (NHEJ) (Figure 8). Homologous recombination involves the excision of faulty DNA and resynthesis of the original sequence using a sister chromatid as a template, whereas NHEJ directly joins the two ends generated by a double strand break. In doing so, NHEJ may inadvertently introduce new mutations into DNA sequences. DNA damage repair mechanisms involve the complex interactions of protein effectors that work in concert to resolve DNA errors (Lord and Ashworth, 2012). However, if the damaged DNA cannot be repaired, cells undergo cell death by the activation of caspase-dependent apoptosis (Siddik, 2003).

DNA damage repair pathways can be exploited therapeutically in cancer treatment in various ways. Simply introducing DNA damage in cancerous cells to stimulate apoptosis is one example and forms the basis of many chemotherapeutics used in cancer treatment, such as cisplatin. Cisplatin interacts with DNA to form crosslinks between DNA strands (Lord and Ashworth, 2012), which often lead to strand breaks when repair via NER is attempted.

As cancer cells divide rapidly and therefore replicate their DNA more frequently, they are inherently more vulnerable to the introduction of DNA crosslinks and subsequent strand breaks. These strand breaks lead to apoptosis of cancer cells either as a direct result of their severity or as a result of defective DDR pathways that are often harboured by cancerous cells leading to an inability of the cell to repair the damage (Siddik, 2003).

Genomic instability is a common feature of cancers and in some cases of the disease it is evident that faulty DNA damage repair pathways generate genomic instability and thus the cancerous phenotype (Figure 8). Perhaps the most well-known example in breast and ovarian cancers is mutations in the DDR pathway proteins BRCA1 and BRCA2, which prevent effective DNA damage repair via homologous recombination. As a result of this, individuals affected by these mutations have a high chance of developing breast cancer in their lifetimes. Evidence also suggests that oncogene activation can be a preceding step in the process of cancer development by generating genomic instability and thus activating the DDR pathway, which becomes dysregulated following further mutations. For example, the activation of the oncogene RAS can cause double-strand breaks due to multiple stalled replication forks. These replication forks are induced through hyperproliferation stimulated by RAS expression but fail due to a lack of dinucleotides available to complete the replication process. These double-strand breaks activate the DDR pathway, which must become dysregulated to facilitate cancer progression. Perturbed DDR pathways impair a cell's ability to repair damage and as such can render cancer cells vulnerable to chemotherapeutics. The crosslinks introduced by cisplatin treatment are less likely to be resolved in affected cancer cells, leading to higher levels of apoptosis. The cytotoxic effects of cisplatin make it one of the most impactful chemotherapeutics in the cancer field (Lord and Ashworth, 2012).

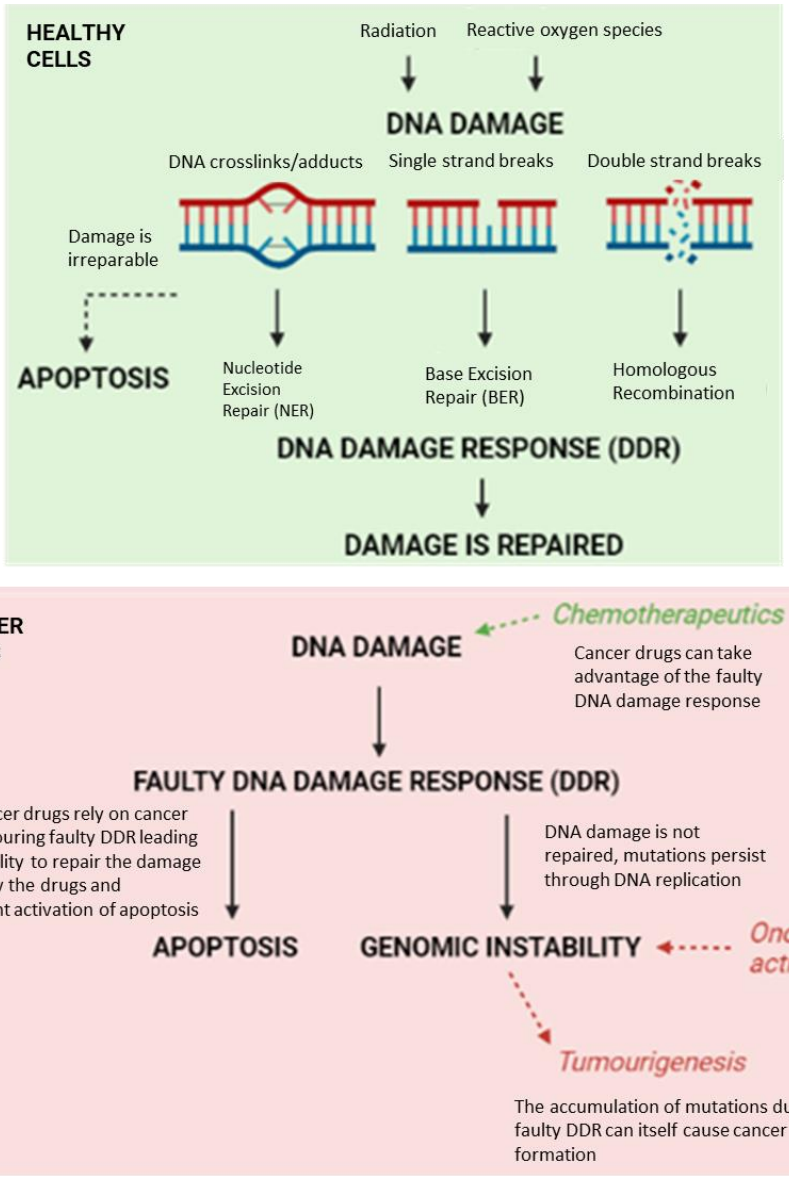

Figure 8: Summary of the DNA Damage Response (DDR) in healthy and cancerous cells. In healthy cells, the DNA damage response detects various forms of DNA damage (e.g. single and double strand breaks, crosslinks) and performs repairs through a number of mechanisms depending on the damage caused (e.g. NER, BER, HR). If the damage is too great for repair, the apoptotic programme is activated. Cancer cells often harbour a faulty DDR system which can be exploited therapeutically – many cancer drugs induce DNA damage that cannot be repaired and thus apoptosis is triggered. However, faulty DDR can contribute to tumourigenesis if DNA damage is not repaired and persists throughout replication, causing mutation accumulation and genomic instability. Oncogene activation is another generator of genomic instability that can lead to tumourigenesis.

Although cisplatin, amongst other chemotherapeutics, has arguably been revolutionary in the treatment of many cancers (including breast cancer), its poor selectivity for cancer cells means it also damages healthy, wildtype cells. This non-specificity causes a range of side effects experienced by patients taking these drugs (Oun, Moussa and Wheate, 2018). Recently, a study by Seldin and Macara (2020) demonstrated an additional unexpected effect of DNA damaging agents on normal (genetically wildtype) mammary epithelial cells. When investigating the effect of cisplatin treatment on mammary epithelial cell fate by

genetic lineage tracing, they observed increased proliferation, hyperplasia and lineage specification defects in basal cells. They showed that in response to cisplatin treatment, basal cells lost the expression of typical basal markers, and instead started expressing luminal marker proteins. Alongside, these basal cells became displaced into the mammary duct lumens. This response contrasts greatly with the apoptotic effect of cisplatin in cancerous cells.

Interestingly, physical wounding had no effect on mammary basal cell behaviour, suggesting the response is specific to genotoxic injury. Further investigation into an analogous phenotype observed in epidermal (skin) basal cells suggested that signals from nearby stromal fibroblasts played an important role in this process. They showed that the ablation of fibroblasts dramatically reduced the proliferative and defective specification responses of epidermal basal cells in response to cisplatin exposure. Transplantation of fibroblasts from mice with cisplatin-treated back skin to an untreated mouse was sufficient to generate a similar response in the unexposed mouse. Moreover, RNA sequencing of the fibroblasts concerned suggested that the cytokine Interleukin-1ß released by fibroblasts in response to cisplatin led to the fate specification defects and hyperplastic response seen in the skin. Whether a similar mechanism underpins the phenotype observed in the mammary epithelium in response to cisplatin remains to be elucidated.

The observation that genotoxic injury can promote plasticity in the form of fate specification defects in mammary epithelial cells (Seldin and Macara, 2020) coupled with previous evidence that mammary epithelial plasticity may play a role in breast cancer initiation (Van Keymeulen et al. 2015, Koren et al. 2015, Hein et al. 2016, Vinuesa-Pitarch, Ortega-Álvarez and Rodilla, 2022) demands further investigation into the mechanisms underpinning fate plasticity in the normal breast. Understanding the mechanisms underpinning the plasticity of normal mammary epithelial cells and the contribution of cellular plasticity to breast tumourigenesis has important implications for our understanding of breast cancer susceptibility, tumour initiation and how best to treat this intractable disease.

1.8 Project aims

Despite many advances in the field, much remains to be elucidated regarding the role of mammary stem cells in the postnatal mammary gland, in both physiological and

regenerative/injury contexts. The innate plasticity of mammary epithelial cells is an especially understudied area. A better understanding of the ability of mammary epithelial cells to reacquire bipotency in certain conditions would contribute to revealing the role plasticity plays in mammary gland maintenance/homeostasis and disease, in particular cancer, as well as in tissue repair. This knowledge would almost certainly benefit patients in the form of improved prevention, diagnosis and treatment options for breast cancer amongst other diseases, in addition to enhancing the understanding of this fascinating system and its development.

To better understand mammary epithelial cell plasticity, it is necessary to assess physiological levels of plasticity and whether this capacity for reprogramming varies with epithelial cell type. The molecular mechanisms underpinning cellular plasticity also remains unclear, for example whether epithelial cells transition through hybrid/transient states. In addition, it is important to address whether the cellular response to genotoxic injury differs depending on cell type.

During this project, I aim to begin addressing these questions by characterising the impact of genotoxic damage on basal and luminal mammary epithelial cell fate and behaviour using 3D culture of mammary epithelial organoids derived from transgenic lineage tracing mouse models. Specifically, I will perform the following aims:

Aim 1: Analysis of cell plasticity in response to genotoxic agents *in vitro*.

I will combine genetic lineage tracing approaches in mammary epithelial organoids with 2D and 3D immunofluorescence imaging and flow cytometry to:

Aim 1.1: Quantify baseline levels of plasticity in basal and luminal mammary cells under physiological conditions.

Aim 1:2 Investigate the impact of genotoxic damage on luminal and basal cell fate specification (using lineage-specific cell markers) and behaviour (including proliferation and apoptosis).

Aim 2: Identify the gene expression changes underpinning cellular plasticity in response to genotoxic agents and cell ablation.

I will interrogate and cross-compare published RNA sequencing datasets of epithelial cells exposed to genetic cell ablation and genotoxic agents to identify genes and pathways that underpin cellular plasticity during damage-induced tissue regeneration.

2. Materials and Methods

2.1.1 Hardware

Reagent/Resource	Source	Identifier
Forceps (straight)	SLS	INS4280
Forceps (curved)	SLS	INS4292
Straight dissecting scissors (112 mm)		INS4812
Scalpel blade no10	SLS	INS4670
Scalpel handle no3	SLS	INS4603
70 µm cell strainer	BD Biosciences	352350
1 ml syringe	Fisher Scientific	15889142
25G and 27G needles	BD Biosciences	300600/300635
Millex® 33 mm Millipore Express® (PES)/Fast Flow and low protein binding. 0.22 GP 200 ml < 100 µl	Sigma	SLGP033RS
Ibidi dishes	Thistle	80827
Ibidi µ-Slide 8 Well high Glass Bottom: #1.5H (170 µm +/- 5 µm) D 263 M Schott glass, sterilized	Thistle	80807
40 µm cell strainer	Fisherbrand	11587522 / 22363547
24 well plate	Thermofisher	TKT-190-010Y
Elkay liquipette fine time	SLS	127-P406-000
5 ml stripettes	Sarstedt	86.1253.001
T80 flasks (Tissue culture treated)	Nunc/Fisher	TKT-130-370U5/TKT-130-220Q
Class coverslips 16 mm thickness number 1	VWR	631-0152
2 mm PAP pen	Merck	Z672548-1EA
Aqua/polymount	Generon	18606-20
PurePlus 0.2 ml 8-Well PCR Tube Strips with attached bubble cap lid strip	Fisher Scientific	16644142
Falcon 12x75 mm tube (polystyrene) – Cell strainer cap	Corning/Fisher	352235
Falcon 12x75 mm tube (polystyrene) - No cap	SLS	352008

2.1.2 Mammary organoid culture

Reagent/Resource	Source	Identifier
Growth factor reduced, Phenol red free Matrigel	BD Biosciences	356231
Fetal Bovine Serum	Gibco/Invitrogen	105000064
Glutamax	Invitrogen	35050-038
Penicillin/Streptomycin	Invitrogen	15140122
Leibovitz's L-15	Invitrogen	11415049
Red blood cell lysis buffer	Sigma	R7757
Dulbecco's Modified Eagle Medium	Invitrogen/Sigma	Invitrogen: 41966052, Sigma D6545
Collagenase A from Clostridium histolyticum	Roche	11088793001
Trypsin from porcine pancreas	Sigma	T5266
TrypLE express enzyme	Life Tech	12605010
Dulbecco's Modified Eagle Medium/F-12 (phenol red free)	Invitrogen	21331046 or 21041033
HEPES	Invitrogen	15630-056
N2 supplement	Thermofisher	12587-010
B27 supplement	Thermofisher	17502048
Fungizone	Bio-Techne	B23192
Bovine Serum Albumin	Sigma	A7030
Mouse recombinant noggin	Peprotech	250-38
Recombinant human neuregulin-1	R&D	5898-NR-050
Human recombinant R-spondin1	R&D	3474-RS-050
Y27632 Rock Inhibitor	Sigma	Y0503
Cell recovery solution	Corning	354253
4-hydroxytamoxifen	Sigma	H7904
Tamoxifen free base	Sigma	T5648
Cisplatin	Merck	P4394
Recombinant mouse IL-1 beta	R&D	401-ML/CF
Adalimumab — a2010 Selleckchem	Stratech	A2010-SEL-5mg

2.1.3 Immunostaining of organoids (wholemount and paraffin-embedded sections)

Reagent/Resource	Source	Identifier
Triton-X100 molecular grade	VWR	A4975.0500
Goat Serum	Sigma	G9023-5ML

Ascorbic Acid	Sigma	A4544
Citric acid	Sigma	C8532-500G
4,6-diamidino-2-phenylindole (DAPI) dilactate	Sigma	D9564
Paraformaldehyde, 16% w/v aq. Soln., methanol free, Alfa Aesa	Fisher Scientific	11400580
Aqua/polymount	Generon	18606-20

2.1.4 Genotyping and Endpoint PCR for IL-6 and Cox-2

Reagent/Resource	**Source**	**Identifier**
EDTA	Promega	V4231
NaOH	Sigma	221465
Trisma Base	Sigma	T1503
dNTP mix	Promega	U1511
dNTPs (Separate)	Promega	U1420
GoTaq® G2 Hot Start Taq Polymerase	Promega	M7405
100bp ladder	Promega	G8291
Primers	Sigma	Custom

2.1.5 Flow cytometry

Reagent/Resource	**Source**	**Identifier**
Dispase	Sigma/Merck/Roche	D4693
Dnase	Sigma/Merck/Roche	D4527
Hanks' Balanced Salt Solution (HBSS)	Gibco	24020091
Trustain FcX	Biolegend	101319
GFP calibration beads	Takara	632594
BD Big beads	BD	560499
EDTA	Promega	V4231

2.1.6 Antibodies – primaries (for immunofluorescence)

Antibody	**Company**	**Species**	**Cat #**	**Concentration**
K8	DHSB	Rat	Troma-I - Supernatant 1.0 ml	Wholemount organoids and sections 1:200, wholemount

				mammary tissue 1:100
GFP	Abcam	Chicken	ab13970	Wholemount organoids, wholemount mammary tissue and sections 1:200
GFP	Invitrogen	Chicken	A10262	
GFP	Sicgen	Goat	AB0020-200	
Ki67	Abcam	Rabbit	ab15580	
P63	Abcam	Mouse	ab735	
SMA	Abcam	Rabbit	ab5694	
K5	Biolegend	Rabbit	905504/905502	
CC3	Cell Signalling	Rabbit	9661S	
yH2AX	Cell Signalling	Rabbit	9718	
NF-KB	Santa Cruz	Rabbit	sc-114 (discontinued)	Sections 1:300

2.1.7 Antibodies – secondaries (for immunofluorescence)

Antibody	**Fluorochrome**	**Species**	**Company**	**Cat #**	**Concentration**
goat anti-mouse IgG	Alexa 488	Goat	Life Tech	A11001	Wholemount 1:500, Sections 1:500 – 1:1000
goat anti-rabbit IgG	Alexa 488	Goat	Life Tech	A11008	
goat anti-chicken IgG	Alexa 488	Goat	Life Tech	A-11039	
goat anti-rat IgG	Alexa 488	Goat	Life Tech	A11006	
goat anti-rabbit IgG	Alexa 568	Goat	Life Tech	A-11011	
goat anti-rat IgG	Cy-3	Goat	Life Tech	A10522	
goat anti-mouse IgG	Alexa 647	Goat	Life Tech	A-21236	
goat anti-rat IgG	Alexa 647	Goat	Life Tech	A-21247	
goat anti-rabbit IgG	Alexa 647	Goat	Life Tech	A-21245	
goat anti-chicken IgG	Alexa 647	Goat	Life Tech	A-21449	

2.1.8 Antibodies – flow cytometry

Antibody (+Fluorochrome)	Source	Identifier
DRAQ7 (APC/Cy7)	Biostatus	DR71000
EpCAM (BV786)	Biolegend	118245
CD49f (APC)	Biolegend	313645
Lineage (AF700) CD31 CD45 TER119	Biolegend	103127 102443 116220

2.1.9 RNA extraction

Reagent/Resource	Source	Identifier
TRIzol	ThermoFisher	15596026
Chloroform	Sigma	C2432
Isopropanol	Sigma	109827
Ethanol	Sigma	PLHA01143
Rneasy mini kit	Qiagen	74101

2.1.10 cDNA synthesis

Reagent/Resource	Source	Identifier
SuperScript IV VILO Master Mix (without ezDNAse)	ThermoFisher	11756050

2.1.11 RT-qPCR

Reagent/Resource	Source	Identifier
PowerUp SYBR Green Master Mix	ThermoFisher	A25741

2.2 Mouse models and procedures

All animal procedures were performed by Dr. Bethan Lloyd-Lewis under licence according to the Animals (Scientific Procedures) Act 1986 and the European Union Directive 86/609 and were approved by the local animal ethics committee at the University of Bristol. All mouse strains used have been previously described. Mice were purchased from The Jackson Laboratory and maintained on a C57BL6 background: K5Cre^{ERT2} mice (B6N.129S6(Cg)-Krt5tm1.1(cre/ERT2)Blh/J, stock no. 029155), K8Cre^{ERT2} mice (Tg(Krt8-cre/ERT2)17Blpn, stock no. 017947) and ROSA26^{mTmG} (B6.129(Cg)-Gt(ROSA)26Sor<tm4(ACTBtdTomato-EGFP)Luo>/J, stock no. 007676). All animals were housed in a 12 h light/12 h dark cycle facility in cages with access to food and water at all times. K5Cre^{ERT2} and K8Cre^{ERT2} (Van Keymeulen et al. 2011) were crossed to the double fluorescent reporter ROSA26^{mTmG} (Muzumdar et al. 2007). We exclusively used female mice. All mice were all euthanised by dislocation of the neck or exposure to CO_2 at rising concentrations.

GFP reporter expression was induced in K8Cre^{ERT2}-mTmG and K5Cre^{ERT2}-mTmG mice by intraperitoneal injection of tamoxifen free base (Sigma cat#: T5648) prepared in sunflower oil containing 10% ethanol (0.1 mg per g of mouse body weight). Two tamoxifen doses were administered, scheduled 2 days apart. Two days following the final tamoxifen dose, 15 µl of 4 mM cisplatin (Sigma cat#: P4394) and PBS vehicle were injected into the exposed contralateral 4th mammary fat pads just below the 4th nipple via a 5-7 mm cutaneous incision. During this procedure, mice were anesthetised using Isofluorane (induction at 4 l/min, maintenance at 1.5 – 2 l/min), and provided with the analgesics carprofen (50 mg/ml, dose dependent on weight) and buprenorphine (0.3 mg/ml, dose dependent on weight) administered subcutaneously before pre-surgery preparation. Incisions were closed using wound clips, which were removed ~7 days post-surgery. Mouse body temperature was maintained throughout the procedure using a heated pad, with mice housed in a pre-warmed cage (28°C) during recovery.

2.3 Organoid culture

2.3.1 Organoid culture medium

2.3.1.1 Base media

Ingredient	Amount (ml)
DMEM/F12 containing 1x Penicillin/Streptomycin, 1x Glutamax + 10mM HEPES	47.5
N2 supplement	0.5
B27 supplement	1.0
Fungizone	1.0

2.3.1.2 Growth factors — reconstitution

- Noggin: 200 mg/ml in filter sterilised PBS/0.1% BSA
- Neuregulin-1: 100 mg/ml in sterile PBS
- R-spondin1 : 100 µg/ml in sterile PBS

2.3.1.3 Complete media

Ingredient	Amount	Dilution	Final concentration
Base media	50 ml	-	-
Noggin (200 µg/ml)	25 µl	1:2000	100 ng/ml
Neuregulin (100 µg/ml)	50 µl	1:1000	100 ng/ml
R-spondin (100 µg/ml)	25 µl	1:2000	50 ng/ml

2.3.2 Primary mammary epithelial cell isolation - organoid culture establishment

Uninduced female K5- and K8-mTmG mice were euthanised by dislocation of the neck or exposure to CO_2 at rising concentrations. The 4^{th} and 5^{th} mammary fat pads were subsequently dissected and lymph nodes removed. The fat pads were dipped in 70% Ethanol (EtOH) and placed in Leibovitz's L-15/10% Fetal Bovine Serum/Penicillin-Streptomycin-Glutamine (L-15/10% FBS/PSG) media on ice during the dissection. The tissue was then minced on a 10 cm plastic dish using scissors and razor blades to form a fine pulp.

The minced tissue was transferred to the collagenase/trypsin digestion mix (Trypsin 1.5 mg/ml, Collagenase A 3 mg/ml in serum free L-15/PSG media, filtered through a 0.22 µm filter) and incubated on a horizontal rocker at 37^{o}C for 1 hour to 1 hour 30 minutes. The tissue solution was agitated more vigorously every 15 minutes. Once fully digested, the tissue solution was centrifuged at 1500 rpm for 5 minutes. The supernatant was aspirated and the remaining pellet washed in L-15/10% FBS/PSG media (approx. 5 ml/mouse) and centrifuged at 1500 rpm for 5 minutes. The supernatant was once again aspirated and the pellet resuspended in 1 ml red blood cell (RBC) lysis buffer and incubated at room temperature for 5 minutes. 10 ml of L-15/10% FBS/PSG media was added and the solution centrifuged at 1500 rpm for 5 minutes. The supernatant was aspirated and the pellet resuspended in 1 ml of Dulbecco's Modified Eagle Medium (DMEM)/10% FBS/PSG media with a P1000 pipette. The suspension was transferred into a T80 tissue culture flask, 12 ml of DMEM/10%FBS+PSG added and gently shaken in a horizontal plane. The flask was incubated for 1 hour 15 minutes at 37^{o}C and 5% CO_2 to separate fibroblasts (which adhere to the flask) from epithelial cells (which do not). After incubation, the flask was shaken in horizontal plane and the media pipetted off into a 15 ml falcon. The cell suspension was centrifuged at 1500 rpm for 5 minutes, supernatant aspirated and pellet resuspended in 1 ml TrypLE. The suspension was incubated at 37°C for 5 minutes. Then, 9 ml of DMEM/10%FBS/PSG was added and the solution centrifuged at 1500 rpm for 5 minutes. The supernatant was aspirated, the pellet resuspended in 1 ml DMEM/F-12/PSG and filtered through a 70 µm cell strainer. 9 ml of DMEM/F-12/PSG was added and the solution centrifuged at 1500 rpm for 5 minutes. The supernatant was aspirated, pellet washed in 10 ml DMEM/F-12/PSG and the solution centrifuged at 1500 rpm for 5 minutes to ensure that serum-medium containing media has been washed out. The supernatant was aspirated and the epithelial organoid pellet resuspended well in the required volume of Matrigel. Typically 50 µl Matrigel per well of a 24-well plate was used, or 20 µl Matrigel per well of an 8-well ibidi or labtek plate. The plate was pre-warmed in the incubator and once the organoid-matrigel drops were added, the plate was returned to the incubator for 10 minutes. Then, complete media (described above) was added to each well (500 µl per well of a 24-well plate, 250 µl of media per well of an 8-well ibidi/labtek plate). Organoids were supplemented with fresh complete media every 2 days.

2.3.3 Organoid passage

Around 7-10 days after seeding, organoids were passed. Organoids were also passed if the culture contained a lot of dead cells/debris or was contaminated by other cell types e.g. fibroblasts. The media was aspirated from the organoids and 200 µl pre-chilled Corning Cell Recovery solution or 500 µl DMEM/F-12/PSG was added to the wells. The wells were scraped with a P1000 pipette tip to break up the Matrigel and the suspension pipetted up and down. All pipette tips used to handle the organoid suspension were pre-coated in 2.5% Bovine Serum Albumin/Phosphate Buffered Saline (BSA/PBS) to minimise material loss in pipette tips. The suspension was added to a 15 ml falcon tube and incubated on ice for 20 to 40 minutes until the Matrigel matrix was broken down. The wells were washed with DMEM/F-12/PSG (approx. 500 µl) to maximise material recovery and resulting suspension added to a separate 15 ml falcon tube. After incubation on ice, both suspensions were centrifuged at 1500 rpm for 5 minutes. The supernatant in each falcon tube was discarded and the pellet from the falcon containing the wash was resuspended in 1ml DMEM/F-12/PSG and added to the initial falcon tube. 12 ml DMEM/F-12/PSG was added to the falcon tube and the suspension centrifuged at 1500 rpm for 5 minutes. The supernatant was aspirated and the pellet resuspended in 12 ml DMEM/F-12/PSG and centrifuged at 1500 rpm for 5 minutes. The supernatant was aspirated and the pellet resuspended in the desired volume of Matrigel (see above). Drops were pipetted onto a pre-warmed plate and incubated at 37^{o}C for 10 minutes before adding complete media to each well.

2.3.4 Organoid trypsinising for expansion

When organoid structures had grown very large/branched, organoids were trypsinised for expansion. The media was aspirated and organoids removed from the Matrigel using the same procedure as for passaging (described above). Following the final wash after Matrigel removal, the supernatant was removed and the organoid pellet resuspended in 1 ml TrypLE. The suspension was agitated by pipetting approx. 10 times and incubated for 5 minutes at 37°C (after 3 minutes, the falcon was mixed gently by flicking the bottom of tube). After 5 minutes, 9 ml of DMEM/F-12/PSG was added to the suspension and it was centrifuged at 1500 rpm for 5 minutes. The supernatant was discarded and pellet resuspended in 1 ml DMEM/F-12/PSG and filtered through a 70 µm cell strainer into a 50 ml falcon tube. The original 15 ml falcon tube was washed with 9 ml cold DMEM/F-12/PSG and filtered through

the strainer. The filtered suspension was centrifuged at 1500 rpm for 5 minutes. The supernatant was discarded and pellet resuspended in the desired volume of Matrigel (see above). Drops were pipetted onto a pre-warmed plate and incubated at 37^{o}C for 10 minutes before adding complete media to each well (see above).

2.3.5 Freezing organoids for storage

Organoids were removed from the Matrigel following the same procedure as for passaging (described above). Following the final wash step, the supernatant was aspirated and pellet resuspended in cryomedia at a density equivalent to 6 wells per 1 ml cryomedia per cryovial. The cryovials were placed in a Mr Frosty freezing container at -80°C and transferred to -80°C storage boxes after few days.

2.3.6 Reconstitution of organoids from frozen

Cryovials were thawed in a 37°C water bath and the contents added to 12 ml DMEM/F-12/PSG media and centrifuged at 1500 rpm for 5 minutes. The supernatant was aspirated and the pellet washed with 12 ml DMEM/F-12/PSG and centrifuged at 1500 rpm for 5 minutes. The supernatant was again aspirated and the pellet resuspended in the desired volume of Matrigel before being added to a pre-warmed plate (see above). The growth media was supplemented with Y-27632 (10 µM) for the first 5 days for improved viabilities.

2.3.7 4-hydroxytamoxifen treatment of organoids

4-hydroxytamoxifen (4-OHT) was obtained from Sigma (cat#: H7904). A 10 mM concentration stock solution was made by adding 1.29 ml of ethanol directly to 5 mg powdered 4-OHT. A 10 µM working solution was made by diluting 10 mM stock 1:1000 in sterile PBS. This working solution was added to aliquots of complete media at concentrations of 25 nM, 50 nM and 100 nM for the initial titration experiment and 200 nM, 500 nM and 1 µM thereafter. 4-OHT-containing media was added to the organoid wells for 24 hours. After 24 hours, 4-OHT-containing media was removed and the organoids were washed 2-3 x 5 minutes in PBS to ensure 4-OHT was fully removed. Standard complete media was then added to the organoid wells.

2.3.8 Cisplatin treatment of organoids

Cisplatin was obtained from Sigma (cat#: P4394). A 4 mM concentration working solution was made by adding 20.8 ml of sterile PBS to 25 mg of Cisplatin. This working solution was added to aliquots of complete media at concentrations of 5 µM, 10 µM, 25 µM and 50 µM for the initial titration and 1 µM, 2.5 µM, 5 µM and 10 µM thereafter. Cisplatin-containing media was added to the organoid wells for 24 hours. After 24 hours, cisplatin-containing media was removed and the organoids were washed 2-3 x in PBS to ensure cisplatin was fully removed before culturing in standard complete media.

2.3.9 Interleukin-1β and Adalimumab treatment of organoids

Recombinant mouse Interleukin-1beta (IL-1β) was obtained from R&D systems (cat#: 401-ML-005/CF). The 0.2 mg/ml stock solution of IL-1β was diluted 1:100 in sterile PBS (filter sterilised with a 0.22 µM filter) to give a 2000 ng/ml working solution. This working solution was added to aliquots of complete media at concentrations of 5 ng/ml, 10 ng/ml and 20 ng/ml for the initial titration experiment and 20 ng/ml thereafter for the desired timecourses. For short timecourse experiments, IL-1β-containing media was added to the organoid wells every two days for one week. For long timecourse experiments, IL-1β-containing media was added to the organoid wells every two days for two weeks. At the end of the experiments organoids were washed 2-3 x in PBS to ensure all traces of IL-1β were removed before processing for further analysis.

Adalimumab was obtained from Stratech (cat#: A2010-SEL-5mg). The 5 mg/ml stock solution was diluted 1:100 in PBS to make 50 µg/ml working solution, which was added to aliquots of complete media at concentrations 2 µg/ml and 5 µg/ml for the initial treatment regime. Adalimumab-containing media (2 µg/ml or 5 µg/ml) was added to the organoid wells for 48 hours, after which the organoids were washed 2-3 x in PBS to remove Adalimumab-containing media before culturing in standard complete media for 3 days. The treatment regime was later amended and 5 µg/ml Adalimumab-containing media was added to the organoid wells for 5 days before washing organoids 2-3 x in PBS and processing for analysis.

2.4 Wholemount staining of organoids embedded in Matrigel

The complete media was aspirated and the organoids washed for 5 minutes in PBS. The organoids were fixed in 4% paraformaldehyde (4% PFA) for 1 hour at room temperature. The PFA was then removed and the organoids washed 3 x 10 minutes in PBS-Triton X-100 (0.25%). The organoids were permeabilised in PBS-Triton X-100 (1%) for 1 hour at room temperature, followed by 3 x 5 minute washes in PBS-Triton X-100 (0.25%). The organoids were blocked for 1 hour at room temperature in blocking buffer (10% Normal Goat Serum (NGS) in PBS-Triton X-100 (1%), approx. 200 µl per well of an 8-well ibidi dish). The organoids were then incubated with primary antibodies diluted in antibody dilution buffer (5% NGS in PBS-Triton X-100 (0.25%), approx. 150 µl per well of an 8 well ibidi) overnight at 4^{o}C. The following day the primary antibodies were removed from the organoids and the organoids washed 3 x 10 minutes in PBS-Triton X-100 (0.25%). The organoids were incubated with secondary antibodies diluted in antibody dilution buffer for 4 hours at room temperature in the dark and from this step forwards the organoids were protected from light. The secondary antibodies were aspirated and the organoids washed 2 x 10 minutes in PBS-Triton X-100 (0.25%). The organoids were then incubated with DAPI (5 µg/ml, approx. 10 µM) diluted in PBS for 30 min at room temperature. After DAPI was removed the organoids were washed 2 x 10 minutes in PBS-Triton X-100 (0.25%) and stored in standard PBS at 4^{o}C prior to imaging. Images were acquired using a Leica TCS SP8 inverted confocal microscope.

2.5 Organoid embedding for sectioning

Protocol adapted from Przepiorski, A. et al. (2018). Media was aspirated from the organoids and the organoids were fixed in 4% Paraformaldehyde for 1 hour at room temperature. The organoids were then washed with PBS for 10 minutes. The PBS was aspirated and the Matrigel drops scooped from the plates using a small spatula before being added to an embedding mould in 1.5% agarose gel. The agarose blocks were left to solidify and trimmed. The blocks were given 30 minute to 1 hour washes in 30%, 50% and 70% ethanol (in this order) and submitted in 70% ethanol to the histology facility for paraffin embedding and sectioning.

2.6 Immunohistochemistry of paraffin-embedded tissue sections

Mounted tissue sections on glass slides were deparaffinised by washing 3 x 10 minutes in coplin jars containing histoclear. Subsequently, the slides were washed 1 x 5 minutes in coplin jars containing 100% ethanol, 90% ethanol, 70% ethanol, 50% ethanol and double distilled water (ddH_2O) (in this order). The slides were then incubated in 0.01 M sodium citrate (pH=6.0) brought to the boil on a hot plate for 20 minutes. The slides were cooled for approx. 30 minutes before washing 1 x 2 minutes in a coplin jar of ddH_2O. The slides were then washed 1 x 15 minutes in PBS-Triton X-100 (0.5%) (this was dotted onto slides using a Pasteur pipette to maximise wax pen efficiency). Liquid adjacent to the samples on the slides was wiped away using a lint-free tissue and the samples were circled with a PAP (wax) pen before blocking buffer (10% Normal Goat Serum (NGS) in PBS-Triton X-100 (0.25%)) was added to the samples (approx. 70 µl buffer p. sample). The slides were blocked for 1 hour in a humid chamber at room temperature. The blocking buffer was tipped off the slides and replaced with primary antibodies diluted in antibody dilution buffer (5% NGS in PBS-Triton X-100 0.25%, approx. 70 µl p. sample). The slides were left overnight in a humid chamber at 4^{o}C. The following day the primary antibody solution was tipped off the slides and the slides were washed 1 x 1 minute in PBS in a coplin jar followed by 2 x 5 minute washes in PBS-Triton X-100 (0.25%) dotted on with a Pasteur pipette. The secondary antibodies were added (diluted in antibody dilution buffer) and slides incubated for 1 hour in a humid chamber at room temperature. From this point onwards slides were protected from light. Subsequently, the secondary antibodies were tipped off the slides and the slides were washed 1 x 1 minute in PBS in a coplin jar followed by 2 x 5 minute washes in PBS-Triton X-100 (0.25%) dotted on with a Pasteur pipette. DAPI was applied to the slides (approx. 70 µl per sample, dilution (1 µg/ml) prepared in PBS) and the slides were incubated for 10 minutes in the dark at room temperature. The slides were then washed 2 x 5 minutes in PBS-Triton X-100 (0.25%). The slide adjacent to the samples was dried using lint-free tissue and a small volume of mounting medium (e.g. AquaPoly Mount) was applied to the samples (one dot per sample). Coverslips were applied and bubbles removed. The slides were stored at 4^{o}C and protected from light. Images were acquired using a Leica DMI6000 inverted epifluorescence microscope.

2.7 CUBIC clearing of mammary tissue

For tissue clearing, samples were immersed in CUBIC Reagent 1A (urea (10% w/w), N,N,N',N'-tetrakis (2-hydroxypropyl) ethylenediamine (5% w/w), triton X-100 (10% w/w) in distilled water) at 37°C for 2-3 days. Tissues were then washed 3 x 1 hour in PBS and blocked overnight in 10% Normal Goat Serum (NGS) in PBS-Triton-X-100 (0.5%) with a volume that covered the tissues (typically 500 µl). Tissues were washed 3 x 1 hour in PBS before adding primary antibodies diluted in blocking buffer (1:100 – 1:200) for 4 days at 4°C (again using a volume that covered tissues). Tissues were washed 3 x 1 hour in PBS. Secondary antibodies diluted in PBS (1:500) were added for 2 days at 4°C. Tissues were washed 1 x 1 hour in PBS before being incubated in DAPI (10 µM in PBS) for 2-3hrs. Tissues were washed 1 x 1 hour in PBS before being immersed in modified CUBIC Reagent 2 [sucrose (44% w/w), urea (22% w/w), triethanolamine (9% w/w), triton X-100 (0.1% v/w) in distilled water] at 37°C for 24 hours (longer for thicker tissue). Tissues were imaged in a glass-bottomed ibidi dish within 1-7 days using a Leica TCS SP8 inverted confocal microscope.

2.8 Genotyping

Ear tips from experimental mice were received for genotyping. To extract DNA, 75 µl of lysis buffer 1 (0.2 mM EDTA, 25 mM NAOH, pH 12) was added to each ear sample and samples were incubated for 1 hour at 98°C on a heat block. Samples were left to cool for 30 minutes before 75 µl of neutralising buffer (40 mM Tris-HCL, pH 5.5) was added to each sample. Samples were vortexed and 1 µl DNA used per PCR reaction using GoTaq DNA polymerase and primers used at a final concentration of 200 or 400 nM (see tables below).

2.8.1 PCR mastermix composition

	K5-CreERT mastermix (µl)
B5X	5
dNTPs (10 mM)	1.25
MgCl (25 mM)	2.5
28853_K5RevM (10 µM)	1
28854_K5Fwd (10 µM)	1
28855_K5RevWT (10 µM)	1

H_2O	12
TAQ	0.25
	24

	K8-CreERT mastermix (µl)
B5X	5
dNTPs (10 mM)	1.25
MgCl (25 mM)	2.5
oIMR1084_GenCreF (10 µM)	0.5
oIMR1085_GenCreR (10 µM)	0.5
oIMR7338_IntConF (10 µM)	0.5
oIMR7339_IntConR (10 µM)	0.5
H_2O	13
TAQ	0.25
	24

	R26_mTmG mastermix (µl)
B5X	5
dNTPs (10 mM each)	1.25
MgCl (25 mM)	2.5
12177_mTmGRev (10 µM)	1
30297_mTmGFwdM (10 µM)	1
30298_mTmGFwdWT (10 µM)	1
H_2O	12
TAQ	0.25
	24

2.8.2 Primer sequences

Species	Mouse line	Gene / allele	Sequence	Primer type	Band size
Mouse	K8-CreERT2 (Generic Cre PCR)	oIMR1084_GenCreF	GCG GTC TGG CAG TAA AAA CTA TC	Cre	~100bp
		oIMR1085_GenCreR	GTG AAA CAG CAT TGC TGT CAC TT		
		oIMR7338_IntConF	CTA GGC CAC AGA ATT GAA AGA TCT	internal +ve control for Cre rxn	324bp
		oIMR7339_IntConR	GTA GGT GGA AAT TCT AGC ATC ATC C		
Mouse	K5-CreERT2	28853_K5RevM	ACC GGC CTT ATT CCA AGC	Mutant reverse	Mutant band = 190 bp
		28854_K5Fwd	GCA AGA CCC TGG TCC TCA C	common Fwd	
		28855_K5RevWT	GGA GGA AGT CAG AAC CAG GAC	wild-type reverse	Wild type band = 322 bp
Mouse	Rosa26-mTmG	12177_mTmGRev	CTT TAA GCC TGC CCA GAA GA	common Rev	Mutant band = 128 bp
		30297_mTmGFwdM	TAG AGC TTG CGG AAC CCT TC	Mut Fwd	
		30298_mTmGFwdWT	AGG GAG CTG CAG TGG AGT AG	WT Fwd	Wild type band = 212 bp

2.8.3 PCR cycling conditions

K5-CreERT2, Rosa26-mTmG:

95°C	3 minutes	
95°C	30 seconds	Loop x 35
51.7°C	1 minute	
72°C	1 minute	
72°C	10 minutes	

K8-CreERT2:

95°C	3 minutes	
95°C	30 seconds	Loop x 35

55°C	30 seconds	
72°C	30 seconds	
72°C	10 minutes	

PCR products were run on 2% agarose gels as well as a 100bp ladder.

2.9 Flow cytometry

2.9.1 Solutions

Flow buffer (50 ml) — filtered:

500 µl EDTA 0.5 M

5 ml of 10% BSA (1% final)

500 µl FBS (1% final)

250 µl DNAse 10x stock (10U/ml final)

43.75 ml DMEM-F12/ Hanks' Balanced Salt Solution (HBSS, no phenol red)

The media was aspirated from the organoids and 200 µl pre-chilled Corning Cell Recovery solution or 500 µl DMEM/F-12/PSG was added to the wells. The wells were scraped with a P1000 pipette tip to break up the Matrigel and the suspension pipetted up and down. All pipette tips used to handle the organoid suspension were pre-coated in 2.5% BSA/PBS to minimise material loss in pipette tips. The suspension was added to a 15 ml falcon and incubated on ice for 20 to 40 minutes until Matrigel matrix was broken down. The wells were washed with DMEM/F-12/PSG (approx. 500 µl per well) to maximise material recovery and resulting suspension added to a separate 15 ml falcon tube. After incubation on ice, both suspensions were centrifuged at 1500 rpm for 5 minutes. The supernatant in each falcon tube was discarded and the pellet from the falcon containing the wash was resuspended in 1 ml DMEM/F-12/PSG and added to the initial falcon tube and the suspension pipetted up and down several times to dissociate the larger organoid structures. 11 ml DMEM/F-12/PSG was added to the falcon tube and the suspension was centrifuged at 1500 rpm for 5 minutes. The supernatant was aspirated and 1 ml TrypLE added to the organoid pellet to dissociate into single cells. The suspension was pipetted up and down approx. 10 times and incubated for 5 minutes at 37°C (after 3 minutes, the falcon was mixed gently by flicking the bottom of tube). After the remaining 2 minutes, 9 ml of DMEM/F-12/PSG was added to the suspension and it was centrifuged at 1500 rpm for 5 minutes. The

organoids were resuspended in 1 ml of 5 mg/ml dispase and 200 U/ml DNase in PBS (100 µl Dispase, 100 µl DNase and 800 µl PBS was used per sample). The suspension was pipetted up and down 5-10 times and incubated at 37°C for 5 minutes before being quenched with 7 ml of HF (Hanks' Balanced Salt Solution (HBSS) + 1% FCS). The suspension was centrifuged at 1500 rpm for 5 minutes and supernatant discarded. 1 ml of HF was used to resuspend cells which were filtered through a 40 µm strainer. The original falcon tube was washed with 4 ml HF and filtered through the strainer. The suspension was centrifuged at 1500 rpm for 5 minutes and the supernatant discarded. The suspension was then resuspended in 1 ml HF and 50 µl of this suspension was added to 950 µl PBS for cell counting. For blocking, cells were resuspended at a concentration of 10^6 cells/25 µl in blocking flow buffer (standard flow buffer containing 1 µl TruStain FcX™ per 25 µl) and incubated on ice for 5-10 minutes. The antibody solution (see table above for antibodies) was prepared by adding all antibodies at a concentration of 1:250 to flow buffer, excluding CD49f which was added at a concentration of 1:50. A volume of antibody solution equal to the volume of blocking flow buffer was added to each sample and samples were incubated on ice in the dark for 15–30 minutes. The samples were washed twice with 1 ml HF and centrifuged at 2000 rpm for 5 minutes. The supernatant was discarded and samples were resuspended in 300 µl flow buffer containing DRAQ7 (1:100 of stock, 10 µl per 1 ml buffer) before being transferred to a FACS tube through a filter top. Flow cytometry was performed using a BD Fortessa flow cytometers. Cell debris and doublets were excluded by gating on FCS/SSC profiles. Subsequently dead (DRAQ7+) and CD45+ /CD31+ /Ter119+ (Lin+) non-epithelial cells were excluded. CD49f and EpCAM cell surface markers were used to identify mammary basal and luminal epithelial cells (MECs), with Tomato and GFP fluorescence selecting fluorescent cells. GFP+ MECs were then back-gated on CD49f/EpCAM profiles to assess their location within these plots.

2.9.2 Compensation set up

GFP calibration beads:

300 µl of 1X Flow Cytometer Calibration Beads Dilution Buffer was added to a standard flow cytometer sample tube. The stock tube of Calibration Beads was inverted 5 — 10 times to resuspend the beads. 6.5 µl of the bead suspension was transferred to the tube containing the dilution buffer. The diluted bead suspension was mixed well by pipetting.

BD CompBead Plus:

Beads were prepared by vortexing before adding equal numbers of drops of reagents A and B to a tube and mixed well. Per antibody/channel, 1 µl of antibody (one per colour) was added to 50 µl beads in individual Eppendorfs. Beads were incubated for at least 20 minutes on ice in the dark. 1 ml of flow buffer was added and beads were centrifuged at 2000 rpm for 5 minutes. The supernatant was discarded and 300 µl PBS added before transferring to FACS tubes.

2.10 RNA extraction from control and IL-1ß-treated mammary epithelial organoids

Eppendorf tubes were placed on ice to chill prior to the addition of RNA. The organoid media was aspirated and 1 ml of TRIzol reagent pipetted onto one well containing a Matrigel dome. The TRIzol was pipetted up and down approximately 10 times to dissolve the Matrigel. The TRIzol-Matrigel media was then pipetted onto the next well and the process repeated for 3 wells of control (PBS-treated) organoids and 3 wells of 20 ng/ml IL-1ß-treated organoids. This mixtures were then transferred to the chilled Eppendorf tubes and incubated on ice for 5 minutes. Following incubation, 0.2 ml of chloroform (per 1 ml TRIzol reagent used) was added to the Eppendorfs and the solution vortexed thoroughly before being incubated at room temperature for 5 minutes. The samples were centrifuged for 15 minutes at 11,500 rpm at 4°C. The top aqueous layer containing the RNA was removed into a clean Eppendorf and 0.5 ml of isopropanol added (per 1 ml of TRIzol reagent used). The Eppendorfs were vortexed thoroughly and left at room temperature for 10 minutes before centrifuging for 10 minutes at 11,500 rpm at 4°C. The supernatant was then aspirated to leave an RNA pellet, which was washed with 1 ml cold 75% ethanol [made using molecular grade water] per 1 ml of TRIzol used, vortexed thoroughly and centrifuged at 8,500 rpm for 5 minutes at 4°C. This wash was repeated. The supernatant was aspirated and the RNA pellet left to air dry for 5-10 minutes before being resuspended in 20-50 µl of molecular grade water. RNA was then cleaned using the Qiagen RNeasy minikit (ref 74101). Both control and IL-1ß-treated RNA samples were adjusted to a volume of 100 µl with RNase-free water. 350 µl Buffer RLT was added and the samples were mixed well before adding 250 µl ethanol (100%). After pipetting up and down, the samples were transferred to RNeasy Mini spin columns placed in 2 ml collection tubes and centrifuged for 1 minute at 10,000 rpm. The flow-through was discarded and 500 µl Buffer RPE added to the RNeasy spin columns.

The tubes were rocked several times and centrifuged for 1 minute at 10,000 rpm to wash the spin column membrane. The flow-through was discarded and the Buffer RPE wash repeated with a 2 minute centrifuge at 10,000 rpm. The flow-through was discarded and the RNeasy spin columns placed into new 2 ml collection tubes before centrifuging at 10,000 rpm) for 1 minute. The RNeasy spin columns were placed in new labelled 1.5 ml eppendorfs. 30–50 µl Rnase-free water was added directly to the spin column membrane. The samples were left at room temperature for several minutes before centrifuging for 1 minute at 13,000 rpm to elute the RNA.

2.11 cDNA synthesis

cDNA was synthesised from RNA extracted from control and IL-1ß-treated organoids using the Superscript™ IV VILO™ Master Mix (Invitrogen, cat no. 11756050). 2 µg of RNA per condition was used with 4 µl of the Superscript™ IV VILO™ Master Mix and the reaction volume made up to 20 µl with nuclease-free water. 500 ng RNA per treatment condition was used for no reverse transcriptase control reactions. The reaction mixes were prepared on ice, mixed well and subjected to the below thermocycler program:

1. 10 min @ 25^{o}C

2. 10 min @ 50^{o}C

3. 5 min @ 85^{o}C

cDNA was subsequently stored at -20 ^{o}C

2.12 Endpoint PCR for IL-6 and Cox-2

2.12.1 Primer sequences

Species	Oligo Name	Sequence	Band size
Mouse	IL-6_F	CTCATTCTGCTCTGGAGCCC	89
Mouse	IL-6R	CAACTGGATGGAAGTCTCTTGC	
Mouse	COX2_F	CCAGCACTTCACCCATCAGTT	53
Mouse	COX2_R	ACCCAGGTCCTCGCTTATGA	
Mouse	RPL13A-F	CACTCTGGAGGAGAAACGGAAGG	182
Mouse	RPL13A-R	GCAGGCATGAGGCAAACAGTC	

Mouse	GAPDH-F	TTCACCACCATGGAGAAGGC	52
Mouse	GAPDH-R	CCCTTTTGGCTCCACCCT	
Mouse	HPRT-F	CCTAAGATGAGCGCAAGTTGAA	86
Mouse	HPRT-R	CCACAGGACTAGAACACCTGCTAA	

Endpoint PCR was performed first to test the performance of the primers using cDNA synthesised from control and treated organoid RNA (described above). H_2O and the no RT Superscript™ solutions used as controls. Three mastermixes were made according to the below table for IL-6, Cox-2 and GAPDH (control housekeeping protein). 1 µl DNA was added per reaction and a final primer concentration of 400 nM used:

	Mastermix for IL-6, Cox-2 and GAPDH (µl)
B5X	5
dNTPs (10 mM)	1.25
MgCl (25 mM)	2.5
F primer (10 µM)	1
R primer (10 µM)	1
H2O	13
TAQ	0.25

PCR cycling conditions:

95°C	3 minutes	
95°C	30 seconds	Loop x 35
51.7°C	1 minute	
72°C	1 minute	
72°C	10 minutes	

PCR products were run on 2% agarose gels alongside a 100bp ladder.

2.13 RT-qPCR

RT-qPCR was performed using the PowerUp SYBR Green Master Mix (ref A25741) for the genes of interest (IL-6 and Cox-2) and three housekeeping genes (GAPDH, Rpl13a and HPRT).

The following reaction mixture was used for each gene using cDNA from vehicle control and IL-1ß-treated conditions, as well as no RT control solutions and H_2O as negative controls. 1 µl cDNA was added per reaction:

5uL PowerUp SYBR Green Master Mix

0.5 µl F primer

0.5 µl R primer

3 µl H_2O

The following RT-qPCR reaction was performed:

50°C	2 minutes	
95°C	2 minutes	
95°C	15 seconds	Loop x 40
55°C	15 seconds	
72°C	1 minute	
95°C	15 seconds	
60°C	1 minute	
95°C	15 seconds	

2.14 Bioinformatics analysis of bulk RNA sequencing data

Centonze et al. (2020) performed bulk RNA sequencing on RNA extracted from wildtype and experimental (i.e. post luminal lineage ablation) luminal, basal and 'hybrid' mouse mammary epithelial cells isolated by FACS. Htseq count files generated by Centonze et al. (2020) were accessed from the GEO accession database (Series GSE127975) and differential gene expression analysed using the DESeq2 package v1.30.1 (Love et al. 2014) in R v4.0.3 (R Core Team 2021), while correcting for multiple testing with the "fdr" method. Genes were considered to be differentially expressed if their adjusted p-value was smaller than 0.05 and the change in log2 fold exceeded 2. Volcano plots were made with the help of EnhancedVolcano v1.8.0 (Blighe et al. 2018). Raw data generated by bulk RNA sequencing of dermal fibroblasts isolated from vehicle and cisplatin-treated mice performed by Seldin and Macara (2020) was downloaded from the GEO accession database (Series GSE139272). The quality of the data was examined with FastQC v0.11.9 (Andrews, 2010). This analysis

showed that the reads were trimmed already: the sequences were of variable length and across the length of the gene the bases had a high average quality. No adapter sequences were detected, thus no further trimming was done. The reads were mapped to the mouse genome assembly GRCm38 (downloaded from Ensembl along with the .gtf file Mus_musculus.GRCm38.102.gtf) with STAR v2.7.9a (Dobin et al. 2013). Read counts were obtained using HTSeq-count v0.13.5 (Anders et al. 2015) and GNU parallel (Tange, 2011). Differential gene expression analysis was performed as for the Centonze data above. The read counts were generated and provided along with scripts for differential gene expression analysis and KEGG pathway analysis (Yu et al. 2012) data by Dr. Francisca Segers.

2.15 Image analysis

Microscopy images were analysed in ImageJ. For quantification of yH2AX staining to confirm DNA damage induction with cisplatin and mitomycin C treatment, a manual threshold was applied to the 405 (DAPI) channel to segment nuclei followed by the 'analyze particles' function to obtain a nuclear count. The find maxima tool was used to count yH2AX foci in the 647 channel and was manually set to identify genuine foci. The result was expressed as a percentage of nuclei containing yH2AX foci.

For proliferation and apoptosis analysis, the corrected total cell fluorescence (CTCF) was calculated (The Open Lab Book, 2014). Briefly, the area integrated intensity of the area of interest was measured, along with the intensity of background regions. The background intensity was subtracted from the intensity measurement of the area of interest.

3. Results

3.1 Validation of Keratin-5-mTmG and Keratin-8-mTmG lineage tracing mouse models

To characterise the baseline level of plasticity of basal and luminal mammary epithelial cells, as well as any changes in cell fate specification, morphology and behaviour in response to genotoxic damage, I used two transgenic lineage tracing mouse models that allow basal and luminal mammary epithelial cells to be specifically labelled in a temporally controlled manner. These models consist of a tamoxifen-inducible Cre-recombinase driven either by the basal-specific Keratin-5 (K5) promoter or the luminal-specific Keratin-8 (K8) promoter. In addition, mice harbour the double fluorescent reporter (mTmG) targeted to the universal Rosa26 promoter, ensuring that all cells are initially labelled with membrane tdTomato (mT) fluorescence. Upon tamoxifen administration, Cre-recombinase is activated in basal (K5 model) or luminal (K8 model) epithelial cells specifically. In these cells, Cre-recombinase excises the mTom-STOP portion of the mTmG construct by recombining the flanking loxP sites, which switches labelling from membrane tomato fluorescence to membrane Green Fluorescent Protein (GFP) expression in basal or luminal cells specifically. This GFP label is heritable and therefore permits the tracking of basal or luminal epithelial cells and their progeny over time (Figure 9).

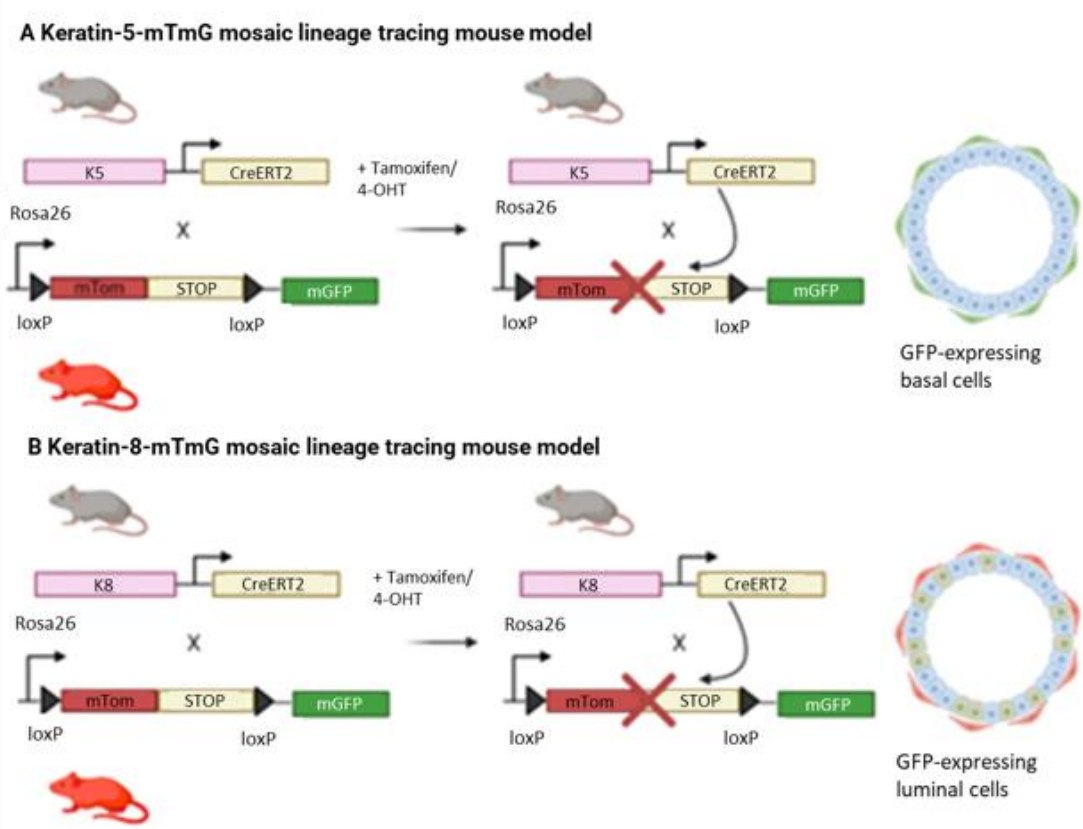

Figure 9: Schematic of Keratin-5 (K5)-mTmG (A) and Keratin-8 (K8)-mTmG (B) mosaic lineage tracing mouse models. Tamoxifen/4-OHT treatment (e.g. by injecting mice or by adding directly to isolated cells in culture) activates GFP expression in basal cells or luminal cells specifically, allowing cell fate to be traced over time. Created in BioRender.

To validate the specificity of labelling in both models, K5-mTmG and K8-mTmG mice were administered tamoxifen by intraperitoneal (IP) injection to induce Cre-recombinase activity in basal (K5+) and luminal (K8+) mammary epithelial cells respectively. All *in vivo* procedures were performed by Dr. Bethan Lloyd-Lewis who holds a Home Office Personal licence for rodent experimentation. Tissues were subsequently harvested after a short chase period for 3D wholemount immunostaining and flow cytometry analysis. As expected, in the absence of tamoxifen, no or very limited GFP was observed by flow cytometry in both K8-mTmG (Figure 10A) and K5-mTmG (Figure 10C) models. A single dose of tamoxifen followed by a 3 day chase revealed the presence of GFP+ cells in luminal ($EpCAM^{hi}/CD49f^{lo}$) and basal ($EpCAM^{lo}/CD49f^{hi}$) populations in K8-mTmG (Figure 10B) and K5-mTmG (Figure 10D) mice respectively. All GFP+ cells in response to tamoxifen in K8-mTmG mammary tissues were restricted to the luminal compartment (Figure 10B). In the K5-mTmG line, however, a very small proportion of GFP+ cells were identified in the luminal compartment by flow cytometry in response to tamoxifen (Figure 10D), suggesting a small degree of promiscuous labelling in this model. Nevertheless, immunostaining of mammary glands

isolated from tamoxifen-induced K5-mTmG and K8-mTmG mice revealed the specific expression of membrane GFP in basal and luminal cells respectively (Figure 10E). Overall, these analyses demonstrated that *in vivo*, both the K5-mTmG and K8-mTmG mouse lines represent robust systems for lineage tracing of basal and luminal mammary epithelial cells respectively.

A K8-mTmG – uninduced (no tamoxifen)

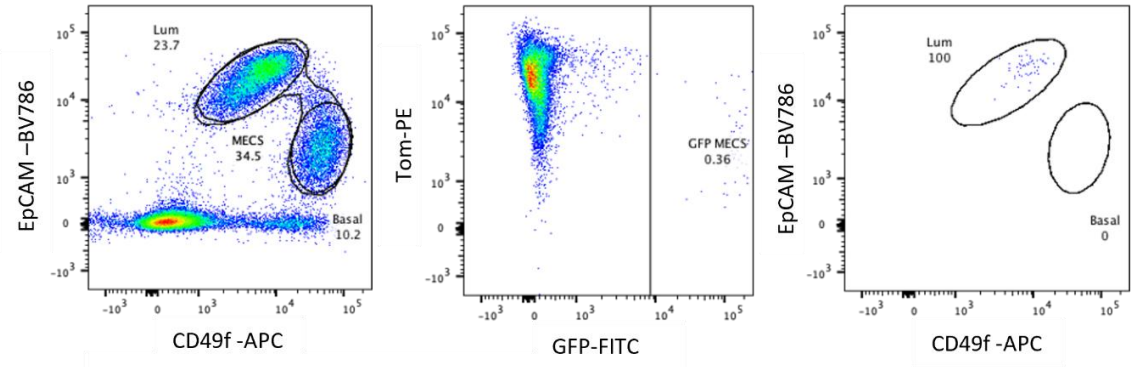

B K8-mTmG – induced (72 hours chase)

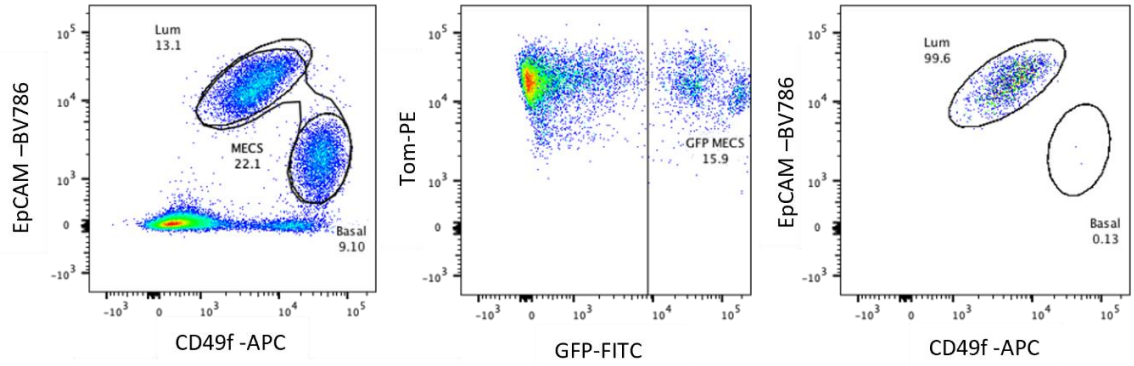

C K5-mTmG – uninduced

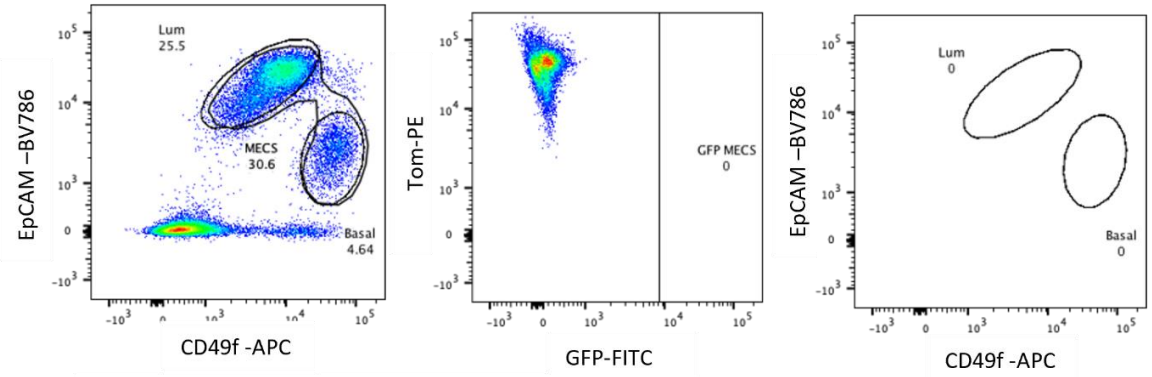

D K5-mTmG – induced (72 hour chase)

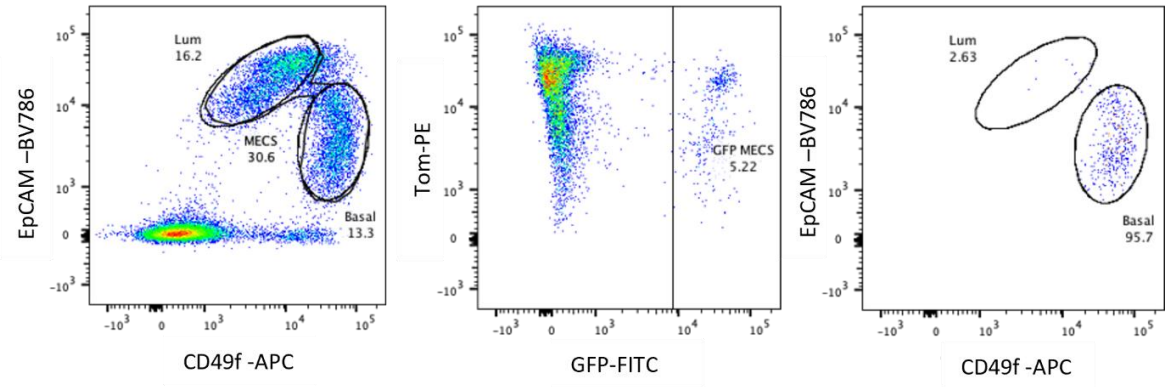

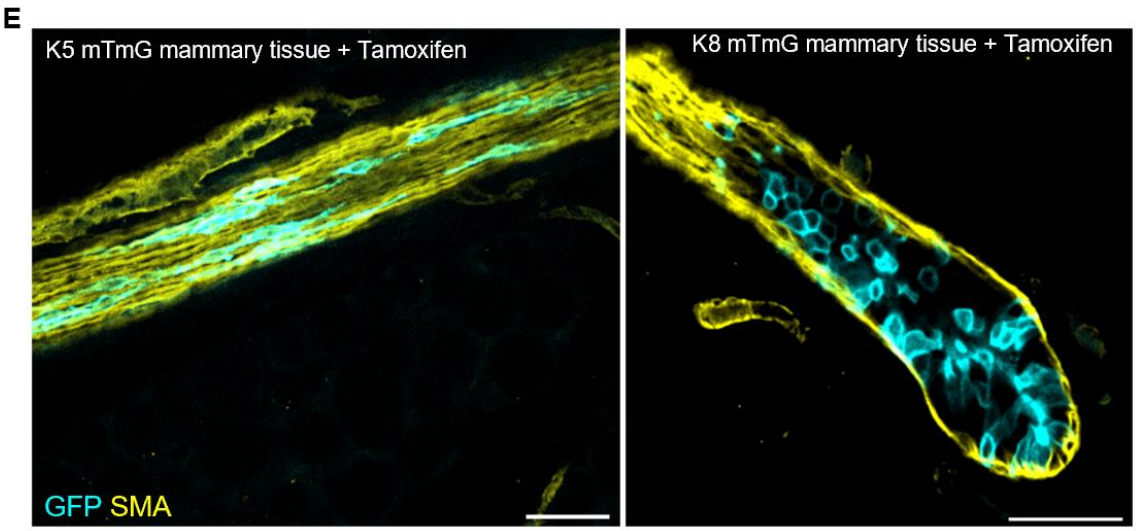

Figure 10: In vivo validation of K5-mTmG and K8-mTmG lineage tracing mouse models. A-D: Flow cytometry plots demonstrating GFP expression in mammary tissue from uninduced and tamoxifen-treated K8-mTmG and K5-mTmG mice. A: In the absence of tamoxifen, 0.36% of mammary epithelial cells express GFP in the K8-mTmG mouse line but all are luminal in origin. B: With tamoxifen treatment, the vast majority of GFP expression in the K8-mTmG mouse line remains in the luminal compartment, with only 0.13% of GFP-expressing cells identifiable as basal. C: In the absence of tamoxifen, no GFP expression is seen in the K5-mTmG mouse line. D: With tamoxifen treatment, the vast majority of GFP expression is in the basal compartment, with only 2.63% of luminal cells expressing GFP. E: Wholemount fluorescence imaging of K5-mTmG (left) and K8-mTmG (right) mammary tissue following tamoxifen induction via two tamoxifen dose injections two days apart. Tissue immunostained for the lineage marker SMA, scale bars 50 µm. Endogenous GFP expression is restricted to the basal compartment in K5-mTmG mice and the luminal compartment in K8-mTmG mice. In vivo procedures and flow cytometry undertaken by Dr. Bethan Lloyd-Lewis.

3.2 Characterising the utility of mammary organoids for lineage tracing *in vitro*

3D organoid culture systems that faithfully recapitulate the physiological cellular hierarchy and architecture of their representative epithelial tissues provide a highly tractable experimental platform that overcomes the challenges associated with *in vivo* studies. These systems also allow for epithelial specific interactions to be investigated in a stroma-free environment, facilitating the comparison of *in vivo* vs *in vitro* epithelial cellular responses to genotoxic insult. This would enable us to investigate whether any observed effects of genotoxic insult on cell fate specification, behaviour or morphology represent a cell intrinsic mechanism, or are mediated by *in vivo* microenvironmental factors (e.g. stromal cell-produced signals) that are absent *in vitro*. To this end, I established mammary epithelial cells isolated from the above transgenic mice in a 3D organoid culture system previously developed by my lab (Jardé et al. 2016). Here, mammary gland tissues are digested to isolate epithelial organoids, which are then embedded in a 3D matrix (Matrigel) and cultured in the presence of growth factors shown to be important for maintaining both luminal and basal epithelial cells (Jardé et al. 2016). These defined culture conditions enable

the sustained proliferation, stem cell maintenance and functional differentiation of mammary epithelial cells *ex vivo* for extended periods of time.

To be confident that *in vitro* responses to genotoxic damage are specific and are not simply due to abnormalities generated by the act of putting mammary epithelial cells in culture, it is essential that the structure of the mammary epithelial bilayer present in cultured 3D mammary epithelial organoids accurately recapitulates its *in vivo* counterpart. To address this, wholemount immunofluorescence staining of organoids with a range of basal (K5, P63, Smooth Muscle Actin [SMA]) and luminal (E-Cadherin [Ecad], K8) epithelial markers was performed (Figure 11). This demonstrated that our conditions facilitate the development of normal bi-layered mammary organoids that recapitulate the morphogenesis and mammary duct differentiation observed *in vivo*. The mammary epithelial organoids contain an outer basal epithelial layer positive for basal markers K5, P63 and SMA surrounding an inner luminal epithelial layer positive for luminal markers K8 and E-Cadherin. Some of the mammary epithelial organoids have formed lumens and have branched, as is seen during mammary gland development. These similarities provide confidence that any differences in cellular responses to genotoxic damage between *in vivo* and *in vitro* conditions are unlikely to be a result of structural and differentiation abnormalities in culture.

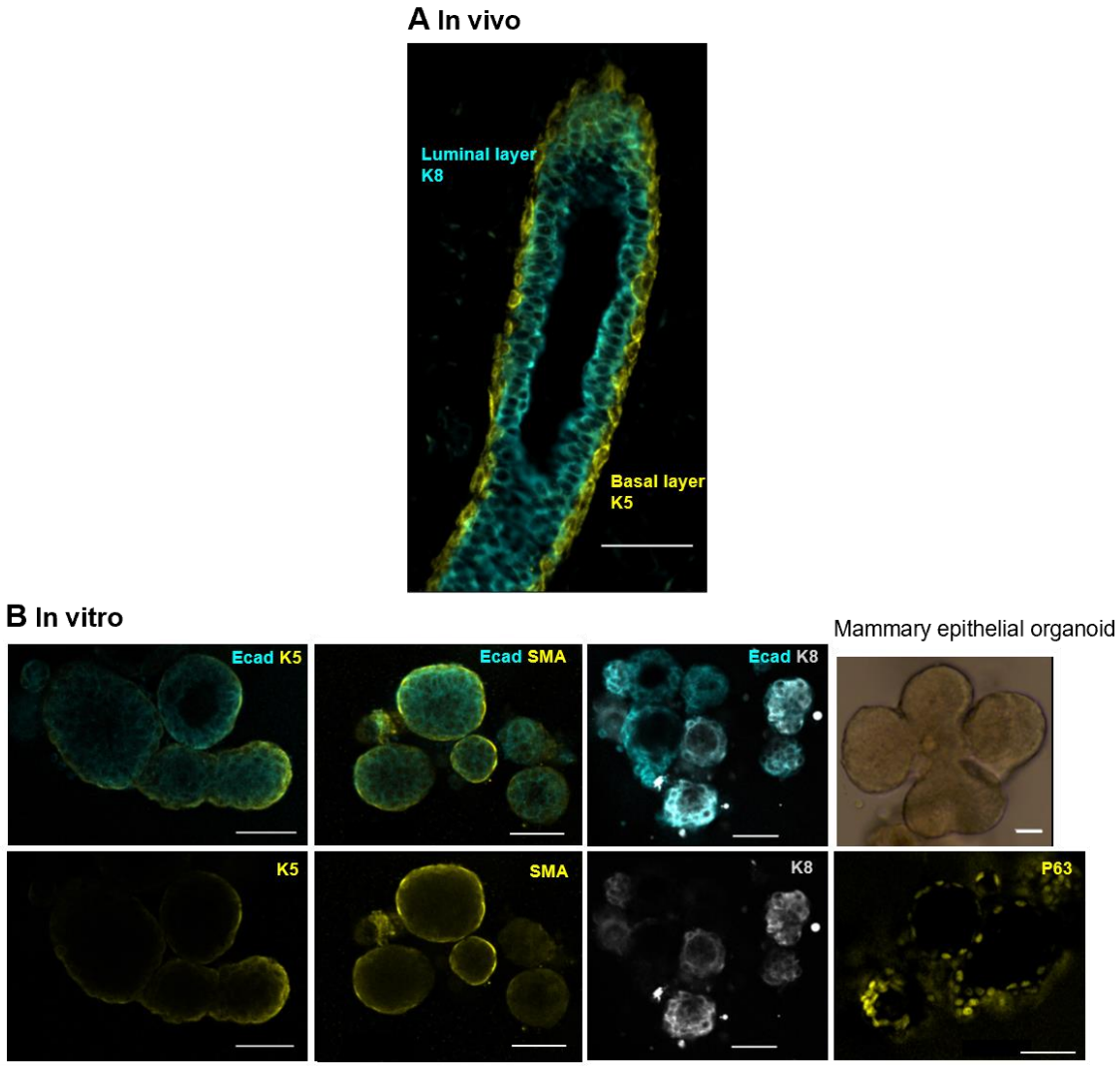

Figure 11: Characterisation of the structure of mammary epithelial organoids. A: Fluorescence microscopy image of a section of mouse mammary tissue stained for the luminal marker K8 (cyan) and the basal marker K5 (yellow). B: Wholemount fluorescence microscopy images of mammary epithelial organoids immunostained for a range of basal (K5, P63, SMA [yellow]) and luminal (K8 [gray], Ecad [cyan]) markers (representative z slices of organoids). Images demonstrate that the in vivo epithelial bilayer structure is replicated accurately in ex vivo organoid culture. Top row, far right panel: Brightfield transmitted light microscopy image of a mammary epithelial organoid derived from mammary tissue and cultured in vitro. Scale bars 50 µm.

After confirming that mammary organoids closely recapitulate the *in vivo* organisation and cellular hierarchy of the mammary epithelium, I next investigated whether this *in vitro* system would allow for accurate cell fate tracking of luminal and basal epithelial cells. Mammary epithelial cells from K5 and K8-mTmG mammary glands were isolated and established in organoid culture. As expected, in the absence of 4-OHT (the active metabolite of tamoxifen used for label induction in culture), no GFP labelling was detected in K5-mTmG organoids by flow cytometry and wholemount fluorescence imaging (Figure 12). While a small degree of labelling was evident in uninduced K8-mTmG organoids (indicative of leaky

Cre activity) via flow cytometry and wholemount fluorescence imaging (Figure 13), this was specific to the luminal lineage.

As lineage plasticity may be a relatively rare occurrence in response to damage (Centonze et al. 2020), a high degree of labelling is required to maximise the ability to observe these events in response to genotoxic damage. Thus, K5-mTmG and K8-mTmG organoids were exposed to increasing doses of 4-OHT in the culture media, namely 0 nM (PBS control), 25 nM, 50 nM or 100 nM for 24 hours (Figures 12B and 13B respectively). While increasing 4-OHT concentrations appeared to overall increase the level of GFP labelling observed by fluorescence imaging, the inherent heterogeneity of organoids meant that labelling efficiencies varied considerably between individual organoids in all treatment conditions. As such, a concentration of 500 nM – 1 µM 4-OHT was selected for all future experiments to increase the number of organoids possessing levels of GFP labelling sufficient for lineage tracing and identification of plasticity in response to genotoxic insult. These concentrations were used previously in analogous studies with no apparent detrimental effect on organoid viabilities or morphologies (Centonze et al. 2020). Importantly, wholemount immunofluorescence imaging of 4-OHT induced mammary organoids with luminal and basal specific markers (namely K8 and K5) revealed that GFP labelling was specific to basal and luminal mammary cells in the K5-mTmG and K8-mTmG models respectively (Figures 12B and 13B).

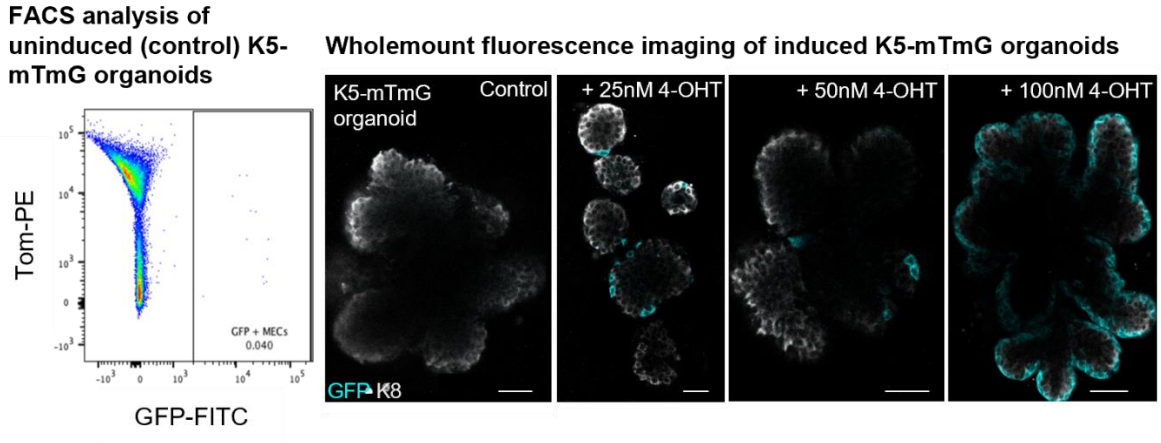

Figure 12: Validation of K5-mTmG organoids for in vitro lineage tracing. A: Flow cytometry analysis of uninduced (control) K5-mTmG organoids indicates negligible GFP expression in mammary epithelial cells. B: Wholemount fluorescence imaging of uninduced K5-mTmG organoids and K5-mTmG organoids cultured in 4-OHT-containing media for 24 hours. Organoids were fixed for staining immediately following 4-OHT removal. Organoids were co-stained for the luminal lineage marker K8. Images are representative Z slices of organoids, scale bars 50 µm. As expected, GFP expression is absent in control conditions and appears to increase with increasing concentrations of 4-OHT. Importantly, GFP expression is specific to the outer basal cell layer.

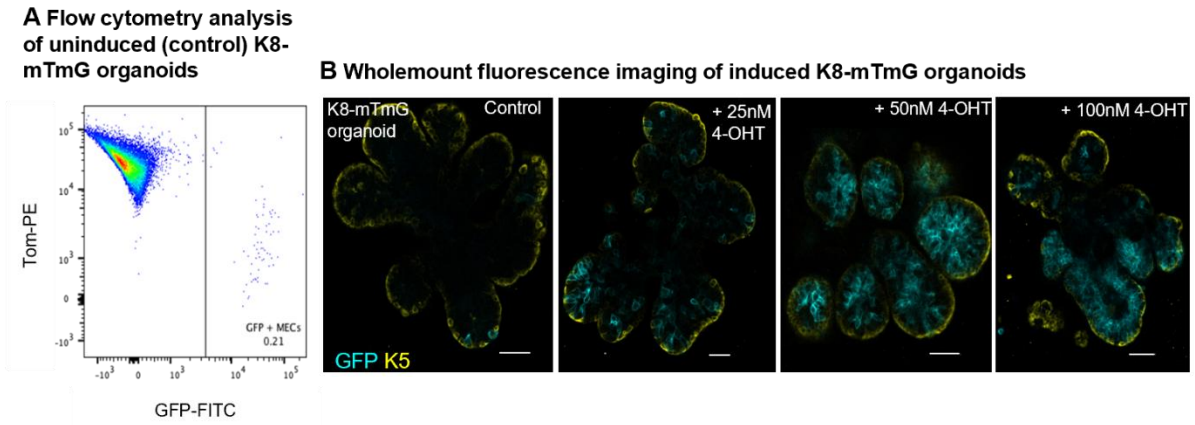

Figure 13: Validation of K8-mTmG organoids for in vitro lineage tracing. A: Flow cytometry analysis of uninduced (control) K8-mTmG organoids indicates a small amount of GFP expression, suggesting the K8-mTmG model is also slightly leaky when used in organoid culture. B: Wholemount fluorescence imaging of uninduced K8-mTmG organoids and K8-mTmG organoids cultured in 4-OHT-containing media for 24 hours. Organoids were fixed for staining immediately following 4-OHT removal. Organoids were co-stained for the basal lineage marker K5. Images are representative Z slices of organoids, scale bars 50 µm. A small number of GFP+ luminal cells are apparent in control conditions but GFP expression is much higher in 4-OHT-induced organoids and appears to increase with increasing concentrations of 4-OHT. Importantly, GFP expression is specific to inner luminal cells.

As establishing mammary epithelial cells in culture might induce plasticity, I next assessed the baseline levels of plasticity in organoid cultures. Flow cytometry analysis of 4-OHT-induced K5-mTmG and K8-mTmG organoids, using antibodies against cell surface markers that distinguish basal and luminal cell populations, detected higher levels of GFP expression in the opposing cell compartment for both models compared to that observed *in vivo* (Figure 14A and B). In the K5-mTmG model *in vitro*, approximately 20% of luminal cells were GFP+ (Figure 14A) compared with 2.63% of luminal cells *in vivo* (Figure 10D). In the K8-mTmG model *in vitro*, approximately 5% of basal cells were GFP+ (Figure 14B), compared with 0.13% of basal cells when analysed *in vivo* (Figure 10B). While this may be indicative of plasticity induced when establishing organoids from dissociated cells, these results contrast with the immunofluorescence imaging data which shows that GFP expression is lineage restricted in both models (Figures 12B and 13B). This suggests that the cell surface markers used, namely EpCAM and CD49f which are routinely used to distinguish between mammary luminal and basal cells isolated from tissues, may not be as suitable for flow cytometry analysis of cells cultured as organoids *in vitro*.

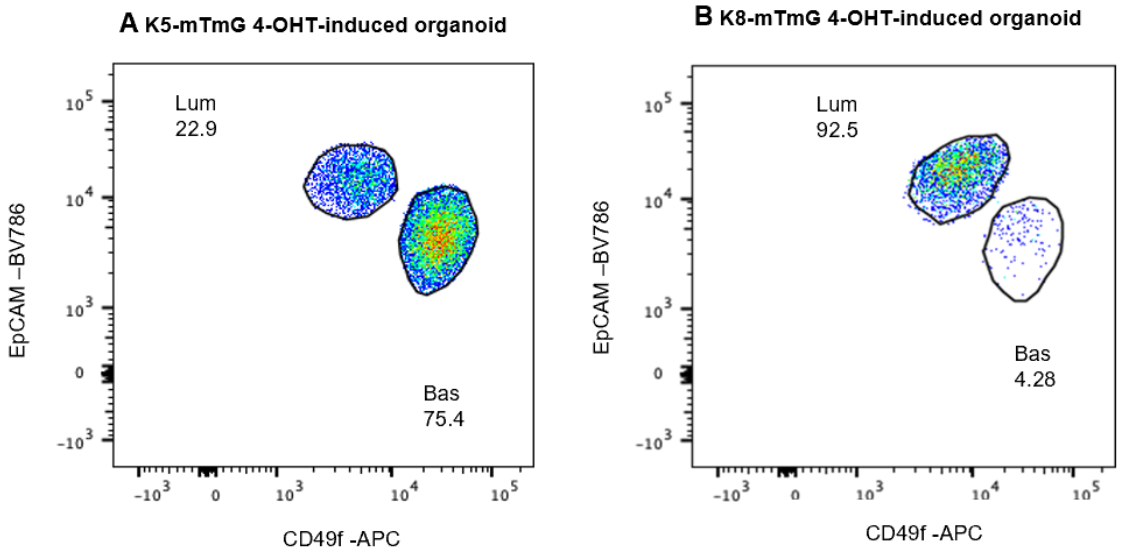

Figure 14: Flow cytometry analysis of GFP expression in K5-mTmG and K8-mTmG organoids treated with 4-OHT-containing media for 24 hours. Flow cytometry was performed on organoids one week after 4-OHT removal. A: Flow cytometry analysis of 4-OHT-induced K5-mTmG organoids. B: Flow cytometry analysis of 4-OHT-induced K8-mTmG organoids. When organoid culture is established, both models demonstrate a higher level of promiscuous labelling (GFP expression in the opposing cell compartment) upon 4-OHT induction when compared with tamoxifen-induced GFP expression in vivo.

Thus far, these results demonstrate that digesting mammary tissue from transgenic mice to establish 3D organoid cultures faithfully recapitulates the structure and organisation of mammary epithelial cells observed *in vivo*. My data also suggests that the K5-mTmG and K8-mTmG organoid models enable accurate lineage tracing of basal and luminal mammary cells respectively *in vitro* and can be used to investigate the effects of genotoxic insult on mammary epithelial cell fate specification, behaviour and morphology.

3.3 Confirmation of DNA damage induction with cisplatin treatment

Before investigating the effects of genotoxic damage on mammary epithelial cell fate and behaviour, it was necessary to establish a robust method of inducing DNA damage in organoid cultures. Previous work showed that injecting the chemotherapeutic agent cisplatin into the mammary fat pad *in vivo* leads to DNA damage, hyperproliferation and basal cell plasticity (Seldin and Macara, 2020). Therefore, cisplatin was used in this investigation to induce DNA damage and identify whether the same effects were apparent *in vitro* in mammary epithelial organoids.

To establish the concentration of cisplatin required to induce DNA damage with minimal overall toxicity (which would preclude downstream analysis), mammary epithelial organoids

were cultured for 24 hours in media containing increasing doses of cisplatin; 0 µM (PBS control), 5 µM, 10 µM, 25 µM and 50 µM. Brightfield microscopy of cisplatin-treated organoids (Figure 15) clearly demonstrated that concentrations of 25 µM cisplatin and above were too toxic for physiologically relevant analysis of the effects of genotoxic damage, as shown by the darkened colour of dying organoids. Based on these results, 5 µM cisplatin treatment for 24 hours was used for all subsequent experiments.

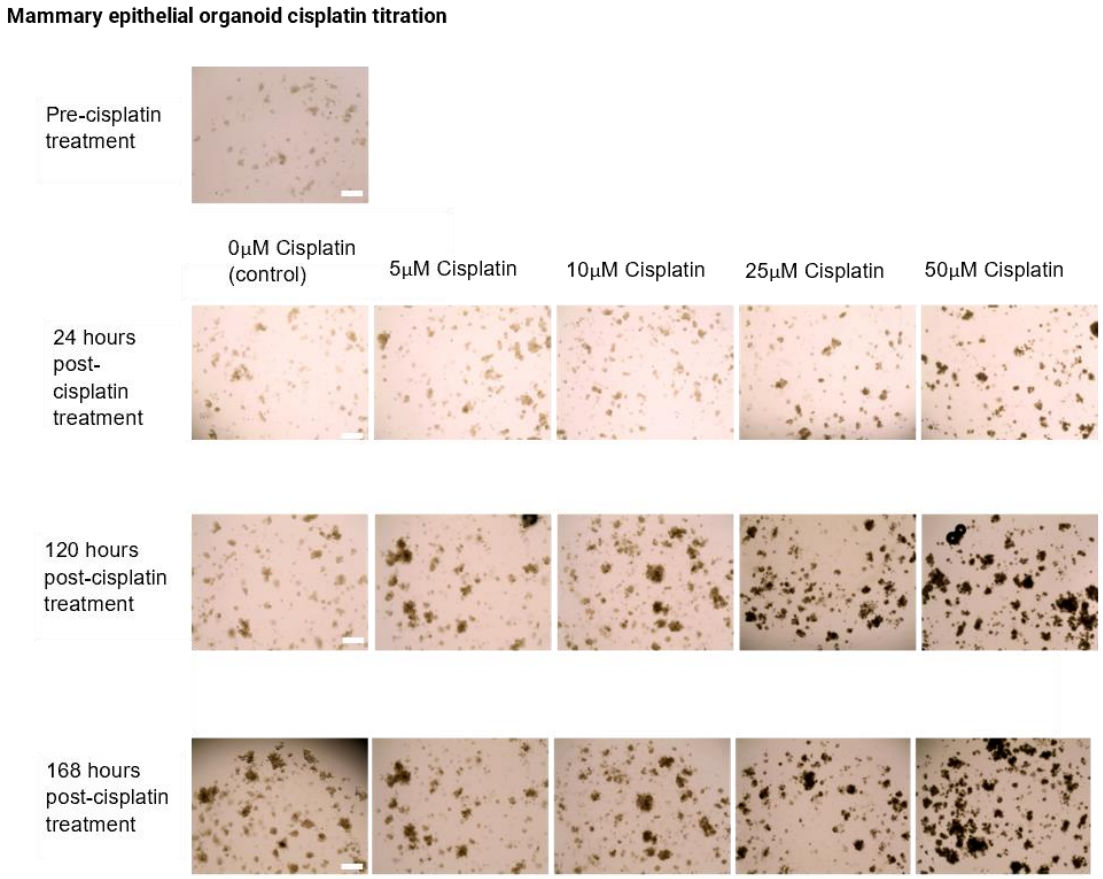

Figure 15: Mammary epithelial organoid cisplatin titration. Brightfield microscopy images of mammary epithelial organoids before and after cisplatin treatment. Scale bars 500 µm. Organoids appear sick with higher concentrations of cisplatin and longer chase times, as indicated by the dark colour and fluffy edges of the organoids, which is particularly evident in 25 µM and 50 µM-treated wells and after longer chase times (120 and 168 hours post-treatment).

To confirm that 5 µM cisplatin treatment induced DNA damage, mammary organoids were immunostained in wholemount using an antibody against yH2AX, a marker of double strand DNA breaks (DSBs). In response to DNA damage, histone H2A variant H2AX is rapidly phosphorylated at Serine residue 139, which acts as a signal to recruit DNA damage repair proteins. This phosphorylation event correlates well with DSB induction and can be detected by anti-yH2AX immunostaining, which produces nuclear foci as well as pan-nuclear staining (Sharma, Singh and Almasan, 2012). Wholemount fluorescent immunostaining of organoids,

quantification (see methods) and subsequent statistical analysis revealed significantly increased numbers of yH2AX foci in organoids exposed to 5 µM cisplatin for 24 hours compared to control conditions (Figure 16). Thus, these conditions are sufficient to induce genotoxic damage while maintaining the viability of organoids for lineage tracing analysis.

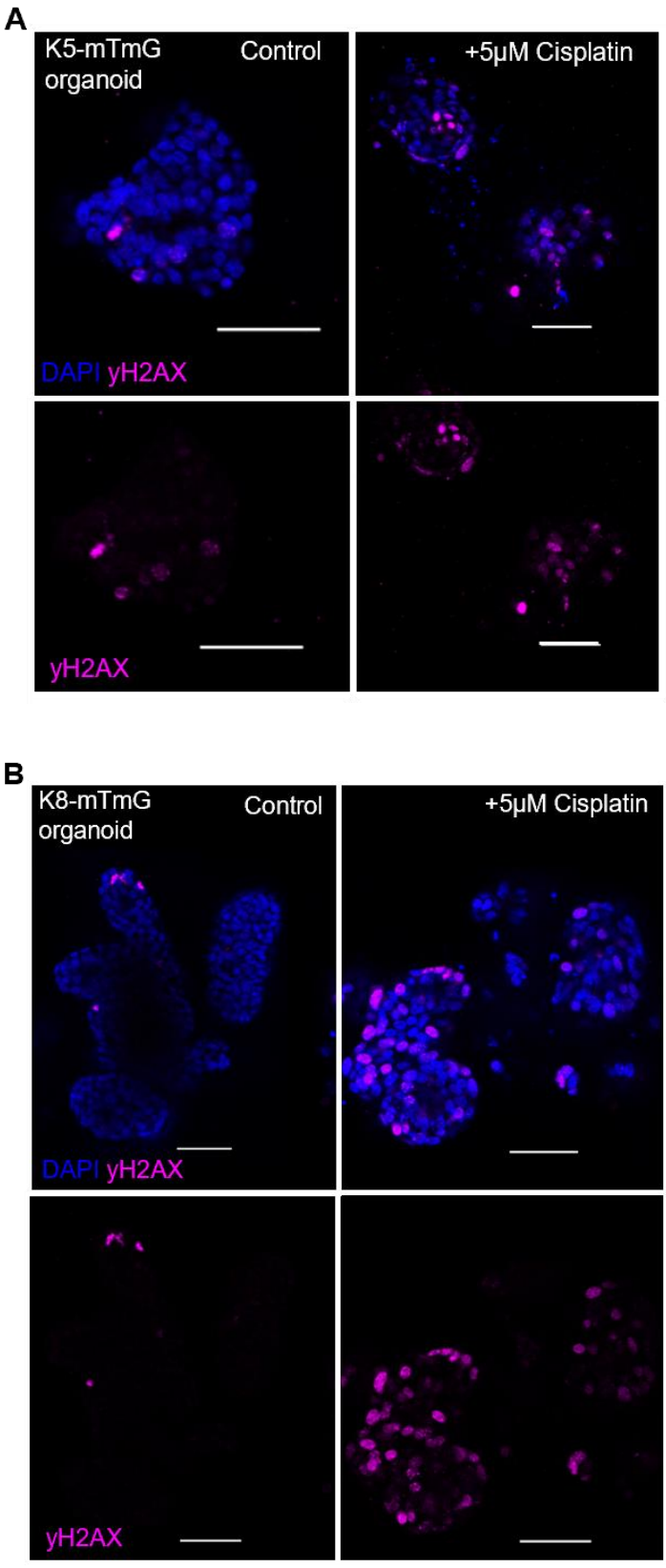
A
K5-mTmG organoid
Control
+5μM Cisplatin
DAPI yH2AX
yH2AX
B
K8-mTmG organoid
Control
+5μM Cisplatin
DAPI yH2AX
yH2AX

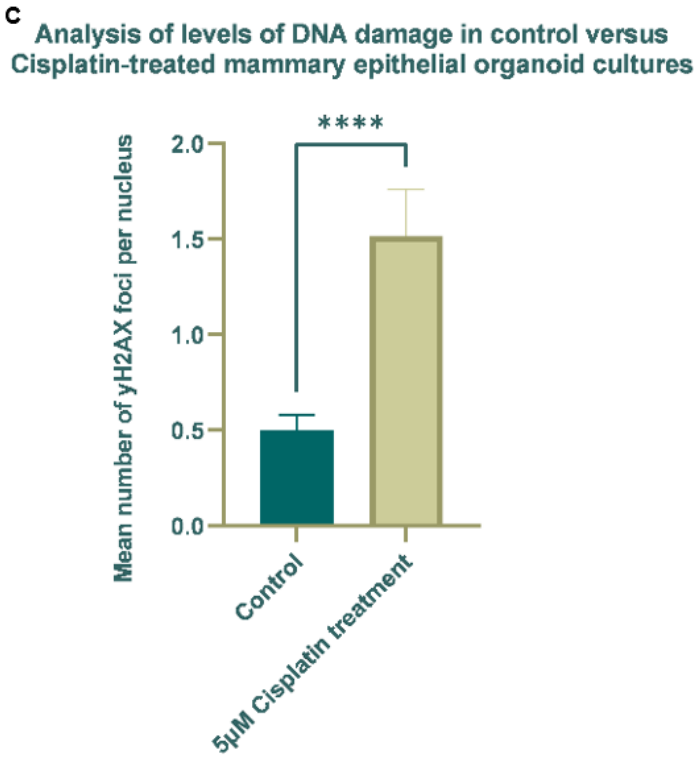

Figure 16: Cisplatin induces DNA damage in K5-mTmG and K8-mTmG organoids. Wholemount fluorescence imaging of K5-mTmG (A) and K8-mTmG (B) organoids treated with PBS (control) or 5μM cisplatin for 24 hours followed by a 4-6 day chase period. Organoids were fixed for staining immediately after the 4-6 day chase period. Organoids were immunostained using an anti-yH2AX antibody. Images are representative z slices of organoids, scale bars 50 μm. 5 μM cisplatin treatment increases yH2AX foci numbers in organoids compared to control conditions (see methods for image analysis approach). C: Bar graph showing significantly increased mean yH2AX foci per nucleus in 5 μM cisplatin-treated organoids versus control. Graph shows mean ± SEM ($p < 0.05$, Mann-Whitney test, $n = 5$).

3.4 DNA damage increases proliferation, but not apoptosis, in vitro

As Seldin and Macara (2020) reported hyperproliferation in mammary tissue *in vivo* in response to cisplatin treatment, the impact of cisplatin exposure on organoid proliferation levels *in vitro* was investigated. Alongside, the degree of cell death induced by cisplatin was also scrutinized. To achieve this, wholemount fluorescent immunostaining was performed in control and cisplatin-treated organoids using anti-Ki67 and anti-cleaved caspase-3 (CC3) antibodies respectively (Figure 17). Ki-67 is a known marker of proliferation and is expressed in all cell cycle stages excluding G0, with expression being highest during G2 and mitosis (Graefe et al. 2019). Caspases are a family of proteases that mediate apoptosis. Caspases first undergo autolytic cleavage to become active when stimulated and subsequently cleave their substrates. Many of these cleaved fragments can be detected using specific antibodies, including CC3, which is considered a reliable marker of apoptotic cells (Crowley and Waterhouse, 2016).

Surprisingly, fluorescent immunostaining for CC3 and subsequent quantification of the corrected total cell fluorescence (CTCF – a measure of fluorescence intensity that takes into account background fluorescence and cell area) indicated that levels of apoptosis were decreased in cisplatin-treated cultures compared to control conditions, although this is not statistically significant (Figure 17A). Immunostaining for Ki67 on the other hand, suggested that proliferation was increased in response to cisplatin treatment (Figure 17B), corroborating results obtained *in vivo* (Seldin and Macara, 2020).

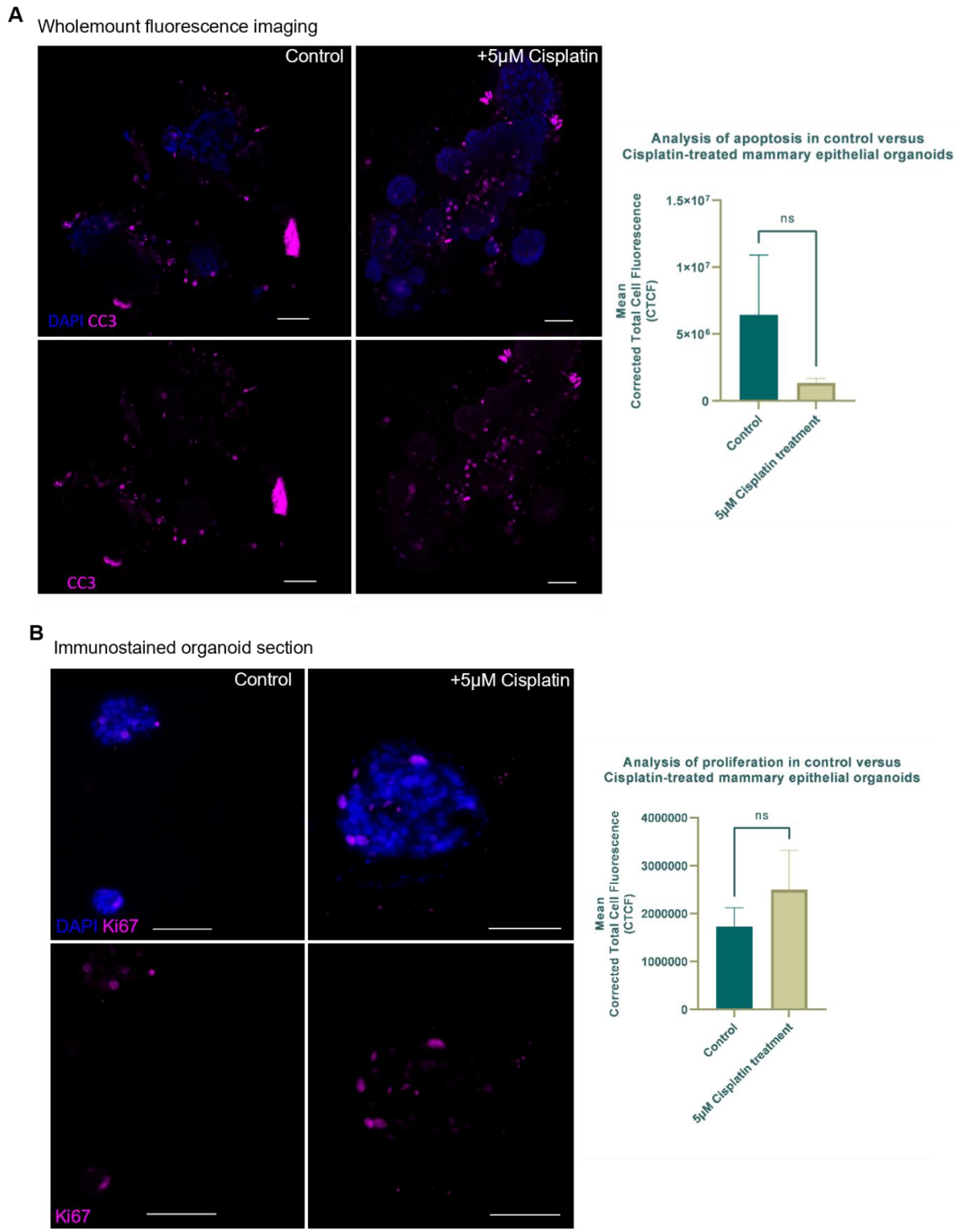

Figure 17: Cisplatin increases proliferation but not apoptosis in mammary epithelial organoids. A: Wholemount fluorescence imaging of organoids treated with PBS (control) or 5 μM cisplatin for 24 hours followed by a 4-6 day chase period. Organoids were fixed for staining immediately after the 4-6 day chase period. Organoids were immunostained using an anti-CC3 antibody. Images are representative Z slices of organoids, scale bars 50 μm. Bar graph of Corrected Total Cell Fluorescence (CTCF) (± SEM) of CC3 staining suggests apoptosis decreases with 5 μM cisplatin treatment ($p > 0.05$, Mann-Whitney test, $n = 3$). B: 2D sections of organoids treated with PBS (control) or 5 μM cisplatin for 24 hours followed by a 4-6 day chase period. Organoids were fixed following the 4-6 day chase period and subsequently embedded for sectioning. Organoids were immunostained using an anti-Ki67 antibody. Scale bars 50 μm. Bar graph of Corrected Total Cell Fluorescence (CTCF) (± SEM) of Ki67 staining suggests proliferation increases with 5 μM cisplatin treatment ($p > 0.05$, Mann-Whitney test, $n = 3$).

3.5 DNA damage does not induce plasticity *in vitro*

After confirming that cisplatin treatment induced DNA damage in mammary epithelial organoid cultures, I next investigated the impact of genotoxicity on cell behaviour and fate specification. To trace the fate of specific mammary cells after genotoxic damage, organoids were exposed to 4-OHT to induce endogenous GFP expression prior to cisplatin treatment. After 24 hours, cisplatin-containing media was removed and organoids cultured in standard media for a further 4-6 days (chase period) before being fixed and immunostained for lineage markers for confocal fluorescence imaging. If cisplatin induced cellular plasticity, this would be revealed by the presence of bi-lineage (luminal and basal) GFP+ clones i.e. GFP expression would also be observed in the opposing lineage for each organoid line. Using the K5-mTmG line as an example, this would indicate that an initially labelled basal cell had either a) undergone a direct fate switch to become luminal, or b) had produced a luminal daughter cell(s). Both scenarios are examples of cell plasticity (Figure 18).

Organoid immunostaining with a lineage marker (K5 or K8) was used to validate the lineage of GFP+ cells under the different conditions. Wholemount fluorescence microscopy for endogenous GFP and lineage marker immunostaining did not reveal any plasticity in either the K5- or K8-mTmG organoid models in response to cisplatin treatment. GFP was expressed by basal epithelial cells in the K5 line and luminal epithelial cells in the K8 line, and staining with the opposing lineage marker showed distinct separation between GFP-expressing cells and the opposing compartment (Figure 19).

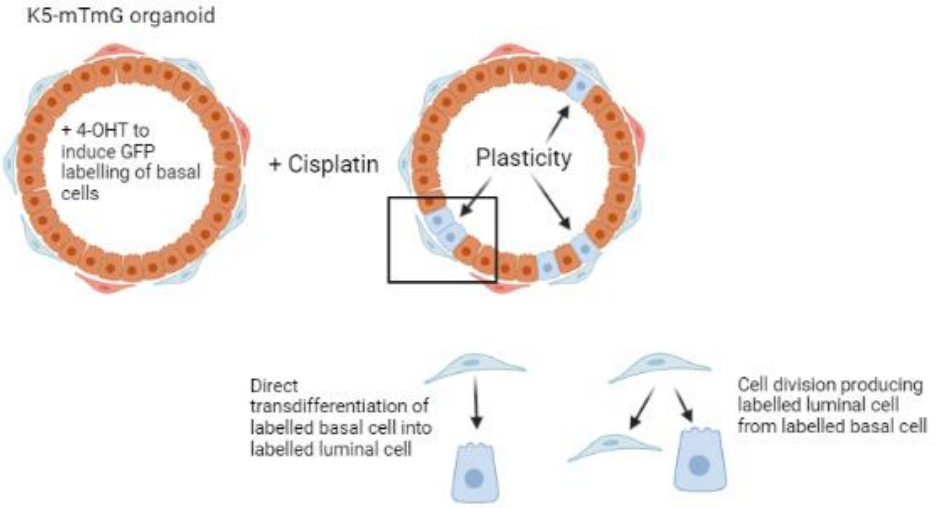

Figure 18: Schematic of hypothetical plasticity in response to cisplatin treatment. 4-OHT induction of endogenous GFP expression enables the identification of plasticity in response to cisplatin. In K5-mTmG organoids, plasticity is indicated by GFP expression in luminal cells. This could be a result of a direct basal-to-luminal fate switch of a labelled basal cell, or production of a labelled luminal daughter cell from a labelled basal cell that has regained bipotency. Created in BioRender.com.

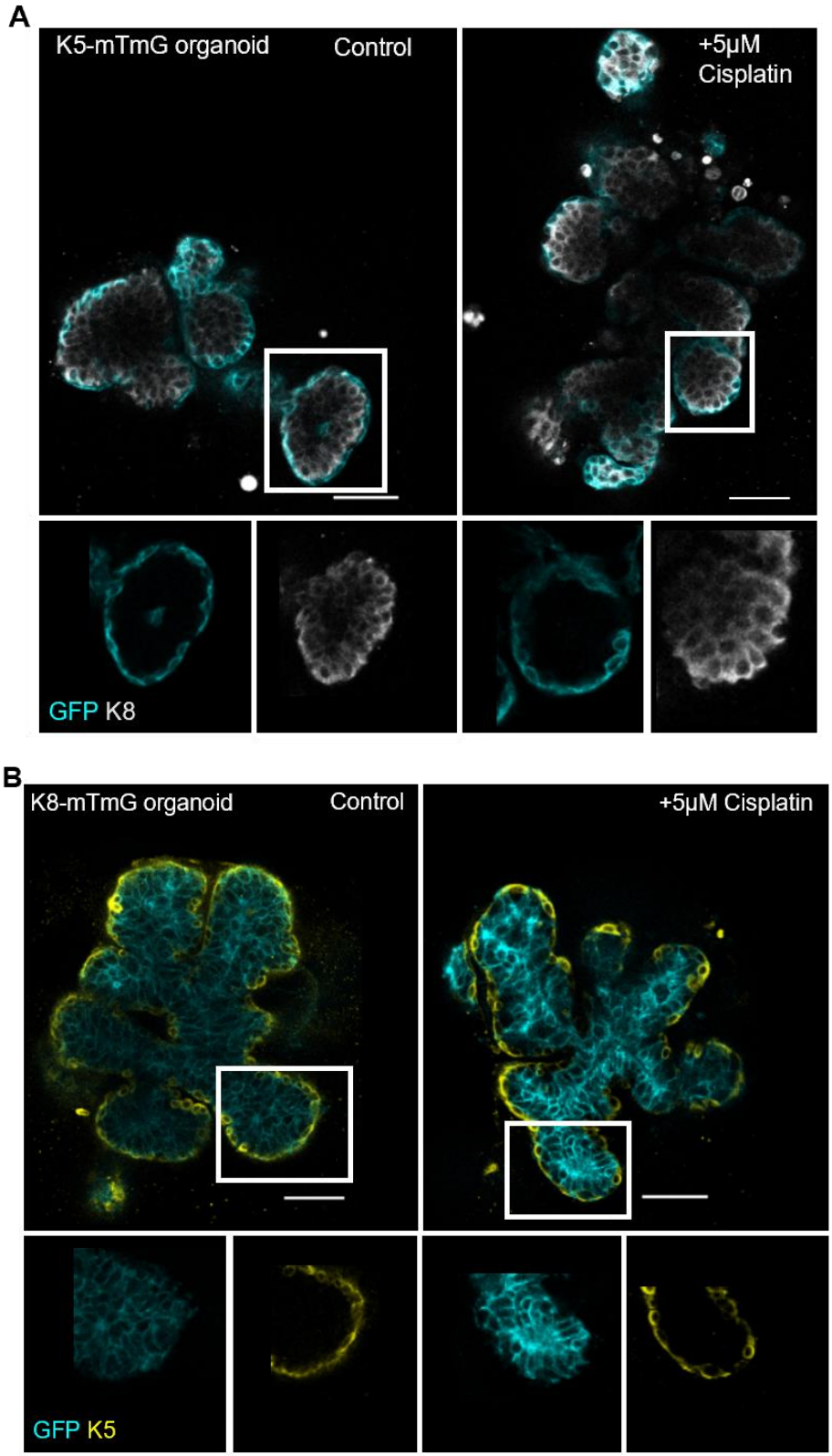

Figure 19: Cisplatin treatment does not induce plasticity in K5-mTmG or K8-mTmG organoids in vitro. Wholemount fluorescence imaging of K5-mTmG (A) and K8-mTmG (B) organoids treated with PBS (control) or 5 μM cisplatin for 24 hours followed by a 4-6 day chase. Organoids were fixed for staining immediately after the 4-6 days chase period. Organoids were immunostained for lineage markers K8 (A) and K5 (B). Images are representative Z slices of organoids, scale bars 50 μm. Endogenous GFP expression remains in the basal compartment in K5-mTmG organoids (A) and in the luminal compartment in K8-mTmG organoids (B), suggesting cisplatin treatment does not induce plasticity in vitro.

A caveat to mosaic genetic labelling of cells for lineage tracing is that rare plastic events occurring in few fluorescently labelled cells may be missed by confocal microscopy. To address this, I analysed GFP expression in vehicle and cisplatin-treated conditions using flow cytometry (Figure 20). While not as definitive as immunostaining for lineage specific markers, this approach allowed me to investigate the expression of GFP across both epithelial cell lineages in response to cisplatin treatment in substantially more organoids than can be feasibly assessed by microscopy. This analysis revealed that there were no substantial changes in GFP expression in the opposing cell lineage above baseline levels in response to cisplatin that would be indicative of cellular plasticity in either the K5- or K8-mTmG models (Figure 20). This is in line with the immunostaining data (Figure 19) and suggests that, *in vitro*, cisplatin does not induce plasticity.

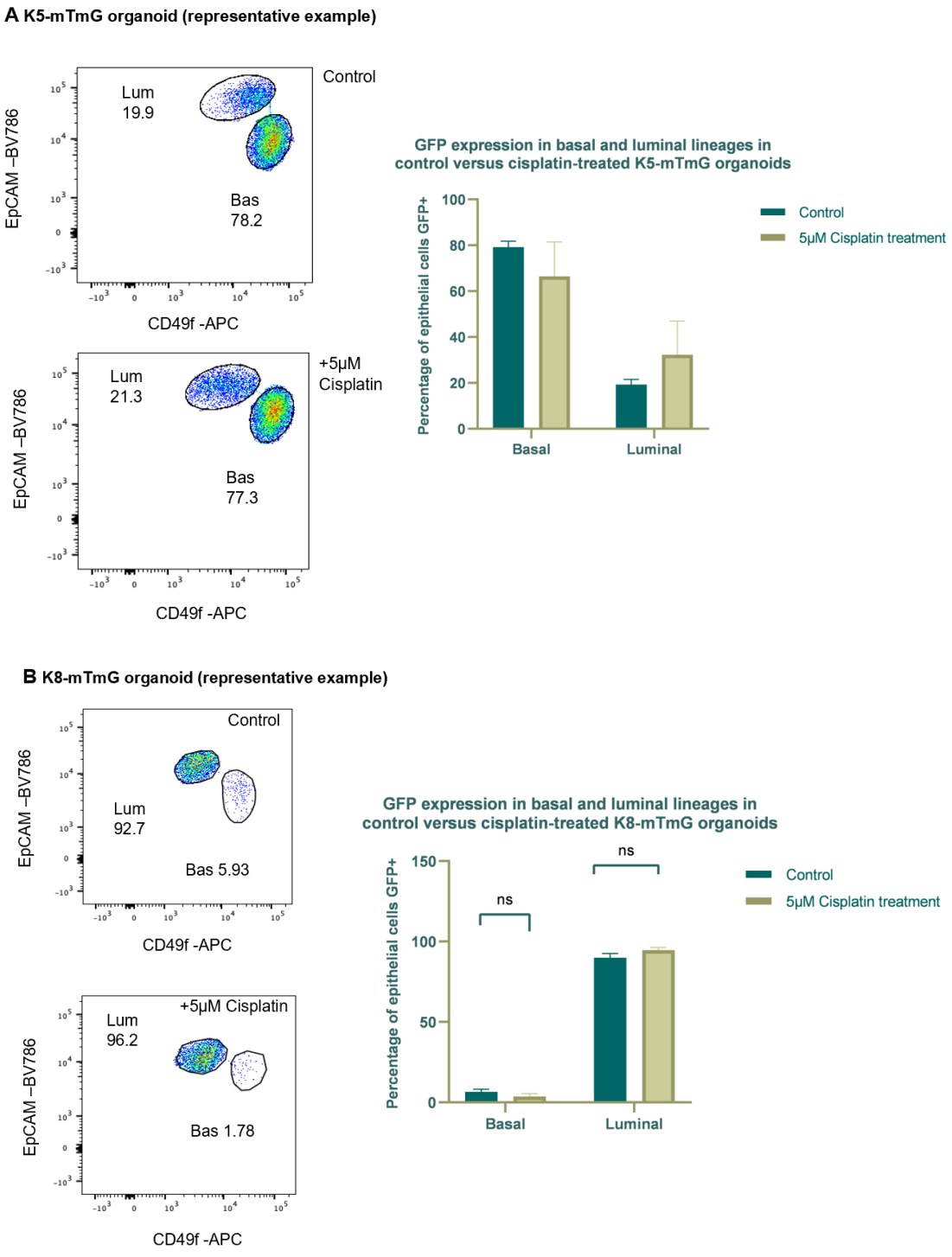

Figure 20: Flow cytometry analysis of GFP expression in K5-mTmG (A) and K8-mTmG (B) organoids treated with PBS (control) or 5 μM cisplatin for 24 hours followed by a 4-6 day chase period. Flow cytometry was performed immediately after the 4-6 day chase period. A: Flow cytometry analysis of GFP expression across basal and luminal cell populations in control and 5 μM cisplatin-treated K5-mTmG organoids. Representative flow plots and quantification shows minimal changes in GFP expression across both cell populations. Bar graph shows mean (± SEM) percentage of basal and luminal cells expressing GFP in control and 5 μM cisplatin-treated conditions (n=2). A decrease in GFP+ basal cells and accompanying increase in GFP+ luminal cells is seen with 5 μM cisplatin treatment. B: Flow cytometry analysis of GFP expression across basal and luminal cell populations in control and 5 μM cisplatin-treated K8-mTmG organoids. Representative flow plots and quantification shows minimal changes in GFP expression across both cell populations. Bar graph showing mean (± SEM) percentage of basal and luminal cells expressing GFP in control and 5 μM cisplatin-treated conditions (n=3). No significant changes in the percentage of GFP+ basal and luminal cells was seen with cisplatin treatment ($p > 0.05$, Mann-Whitney test).

To confirm whether the lack of plasticity observed with cisplatin treatment *in vitro* is an effect attributable to genotoxic damage in general and not specific to cisplatin, organoids were also treated with Mitomycin C (MMC), a different genotoxic agent that also induces DNA crosslinks (Highley et al. 2006). Immunostaining of organoids exposed to 5 µM MMC showed significantly increased levels of yH2AX staining, indicative of DNA damage (Figure 21). However, no evidence of plasticity in response to MMC was observed by confocal microscopy of endogenous GFP expression alongside wholemount immunofluorescence staining for lineage markers (Figure 22). Collectively, these data indicate that genotoxic damage does not induce mammary cellular plasticity *in vitro*.

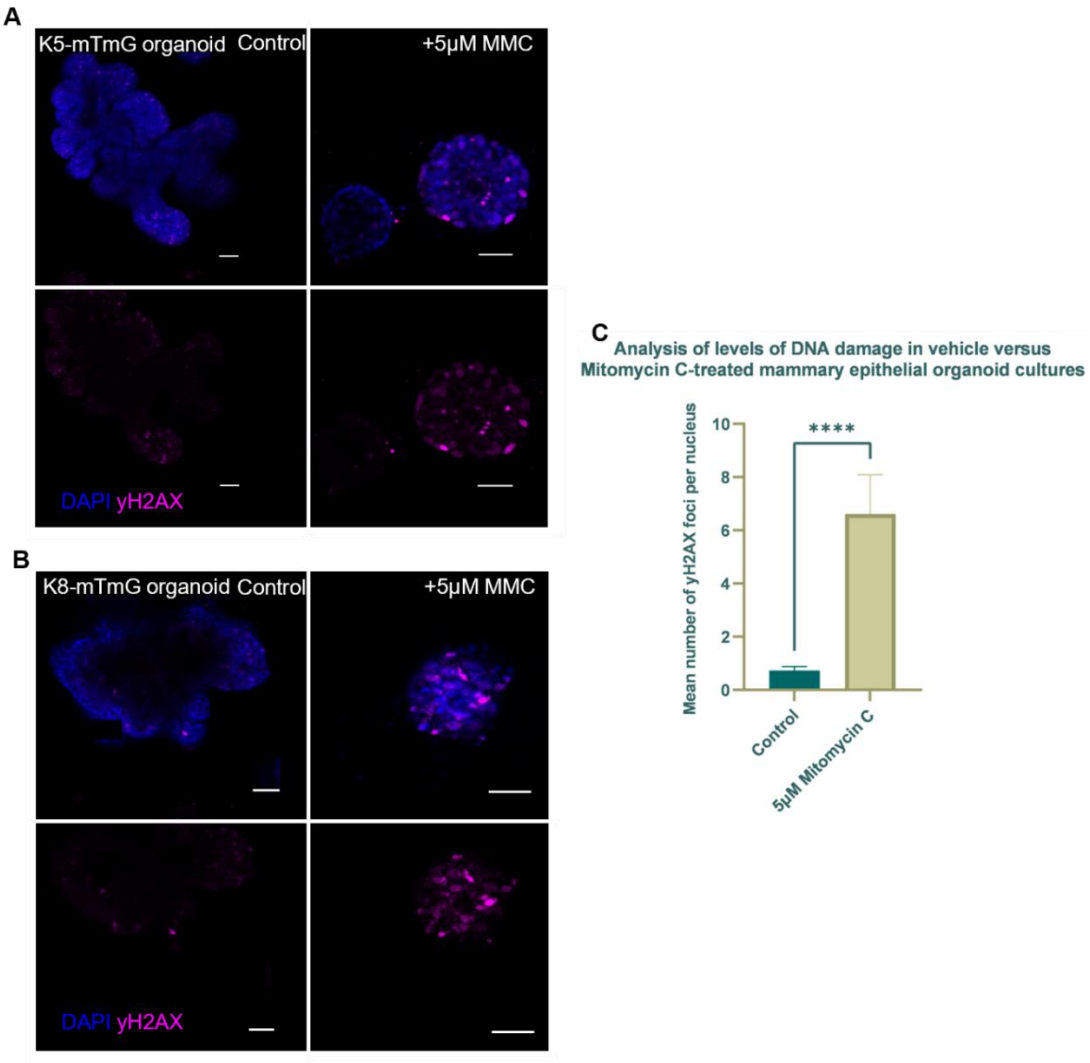

Figure 21: Mitomycin C induces DNA damage in K5-mTmG and K8-mTmG organoids. Wholemount fluorescence imaging of K5-mTmG (A) and K8-mTmG (B) organoids treated with PBS (control) or 5 µM mitomycin C (MMC) for 24 hours followed by a 4-6 day chase. Organoids were fixed for staining immediately after the 4-6 day chase period. Organoids were immunostained using an anti-yH2AX antibody. Images are representative Z slices of organoids, scale bars 50 µm. 5 µM MMC treatment increases yH2AX foci numbers compared to control conditions. C: Bar graph showing significantly increased mean yH2AX foci per nucleus in 5 µM MMC-treated organoids versus control. Graph shows mean ± SEM ($p < 0.05$, Mann-Whitney test, $n = 4$).

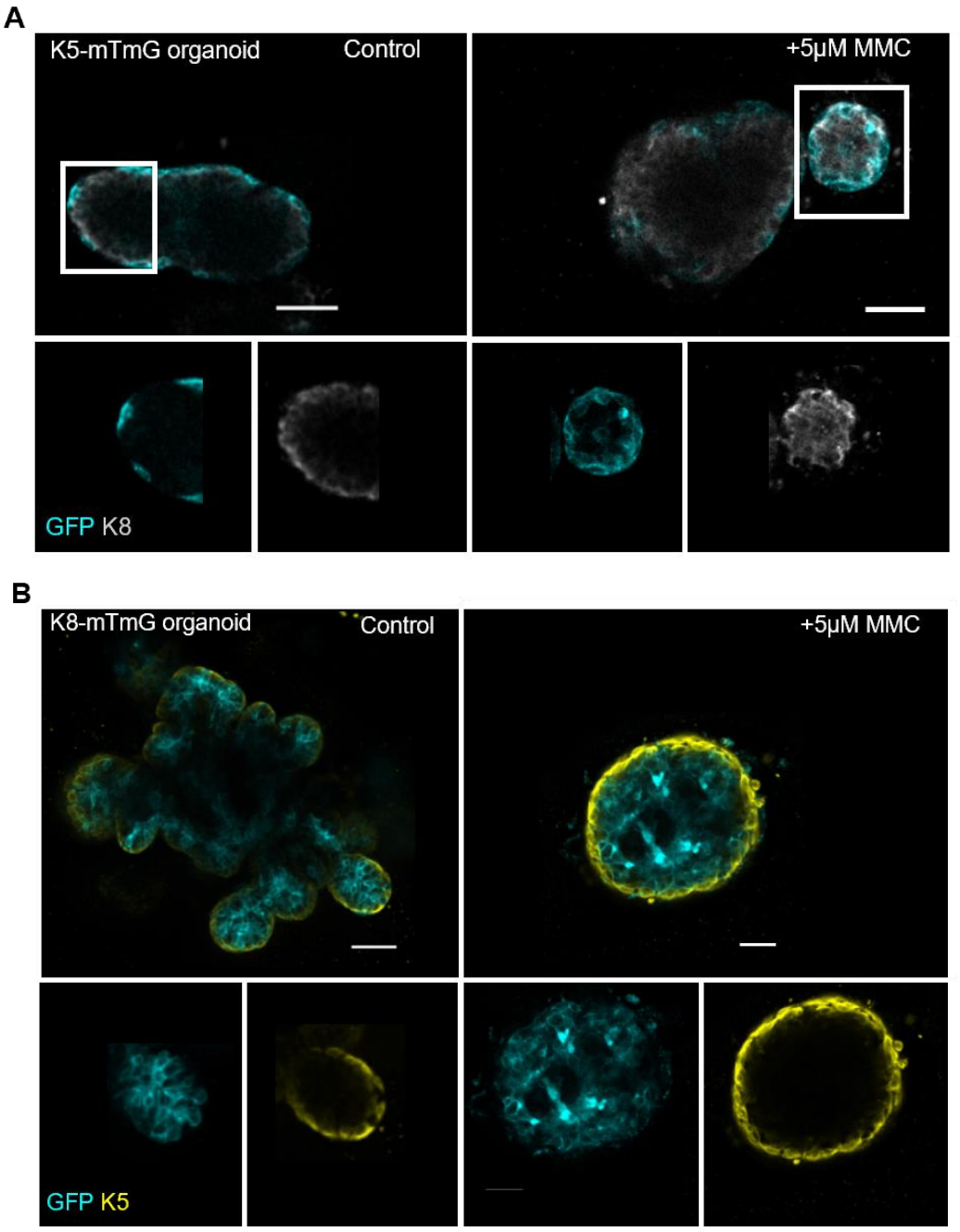

Figure 22: Mitomycin C does not induce plasticity in K5-mTmG or K8-mTmG organoids in vitro. Wholemount fluorescence imaging of K5-mTmG (A) and K8-mTmG (B) organoids treated with PBS (control) or 5 μM mitomycin C for 24 hours followed by a 4-6 day chase. Organoids were fixed for staining immediately after the 4-6 day chase period. Organoids were immunostained for lineage markers K8 (A) and K5 (B). Images are representative Z slices of organoids, scale bars 50 μm. Endogenous GFP expression remains in the basal compartment in K5-mTmG organoids and in the luminal compartment in K8-mTmG organoids, suggesting that MMC treatment does not induce plasticity in vitro.

3.6 DNA damage induces plasticity *in vivo*

The data obtained in mammary organoids suggest that genotoxic damage does not lead to cellular plasticity *in vitro.* To assess whether cisplatin-induced DNA damage could induce plasticity in the mammary gland *in vivo* as suggested by previous reports (Seldin and Macara, 2020), K5-mTmG and K8-mTmG female mice were administered two

intraperitoneal tamoxifen injections two days apart to induce GFP expression in basal and luminal cells for lineage tracing respectively. Two days after the final tamoxifen injection, PBS (vehicle control) and cisplatin (4mM) were injected directly into contralateral 4th mammary glands via a small skin incision (Figure 23). All animal procedures were performed by Dr Bethan Lloyd-Lewis. Three weeks later, the 4th mammary glands were harvested and subjected to CUBIC optical tissue clearing and wholemount immunostaining to investigate cell fate specification in response to cisplatin treatment by confocal fluorescence microscopy. In PBS-injected mammary tissues, endogenous GFP expression appeared to be restricted to the basal and luminal compartment in K5-mTmG and K8-mTmG mice respectively (Figure 24A and B, left panels), in line with data obtained in physiological (non-injected) conditions (Figure 10E). By contrast, bi-lineage GFP+ clones (i.e. luminal and basal GFP+ cells) were observed near the injection site in cisplatin-injected mammary glands from K5-mTmG mice, indicative of cellular plasticity (Figure 24A, right panel). No evidence of plasticity was observed in the K8-mTmG mammary gland following cisplatin injection, with GFP+ cells only observed in the luminal compartment (Figure 24B, right panel). Collectively, this suggests that a microenvironmental factor present *in vivo* but absent *in vitro,* such as signals produced by resident stromal cells, may mediate plasticity in mammary basal cells in response to genotoxic damage.

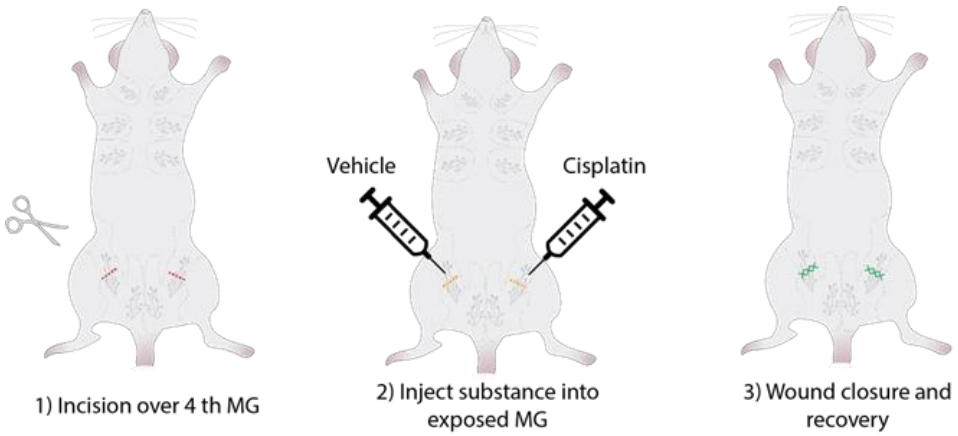

Figure 23: Schematic of surgical administration of cisplatin in vivo. Mice were administered two tamoxifen injections two days apart prior to vehicle/cisplatin injection. Two days after the final tamoxifen injection, PBS and cisplatin were injected into contralateral 4th mammary glands (MG) by making a small incision to expose the gland for injection. Mice were then left for 3 weeks chase before harvesting glands for analysis. All surgical procedures were performed by Dr. Bethan Lloyd-Lewis. Diagram provided by Dr. Bethan Lloyd-Lewis.

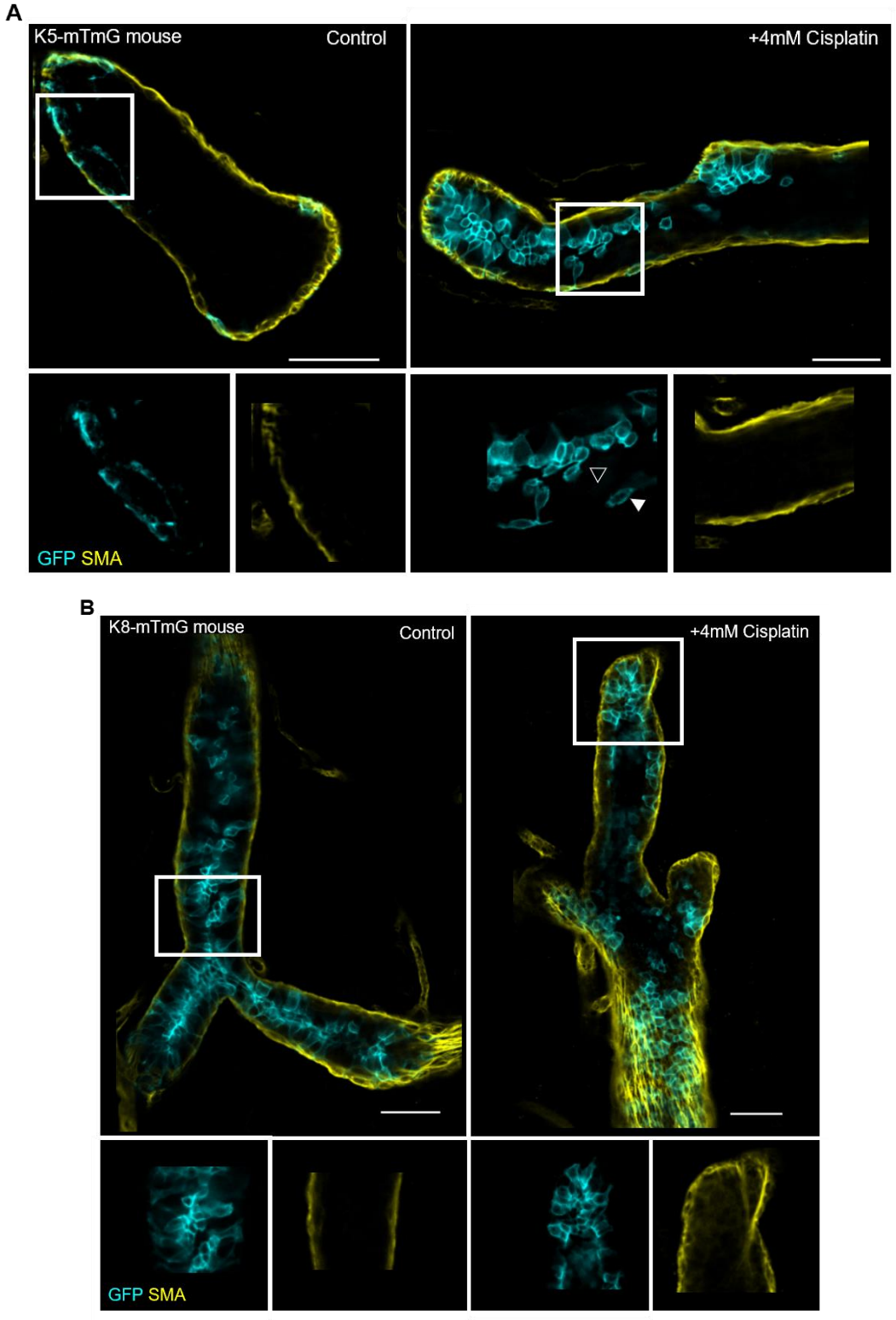

Figure 24: Cisplatin induces basal cell plasticity in vivo. Wholemount immunofluorescence imaging of CUBIC-cleared mammary tissue isolated from K5-mTmG (A) and K8-mTmG (B) mice administered intraperitoneal tamoxifen injections and subsequently intraductal PBS (control) or 4mM cisplatin injections. Mammary tissue was fixed for staining 3 weeks after PBS/cisplatin administration. Mammary tissue was immunostained with an anti-SMA antibody, scale bars 50 µm. A: K5-mTmG mammary tissue, left panel: Endogenous GFP expression remains in the basal compartment in control tissue, where it colocalises with SMA expression. Right panel: GFP+ luminal cells were identified alongside GFP+ basal cells near the injection site, suggesting that injecting cisplatin into tissues induces plasticity in basal cells in vivo. Filled arrow indicates a GFP+ basal cell and hollow arrow indicates a GFP+ luminal cell. B: K8-mTmG mammary tissue, left and right panels: Endogenous GFP expression remains in luminal compartment in both control and cisplatin-injected tissue, indicating that injecting cisplatin into tissues does not induce plasticity in luminal cells in vivo.

3.7 Investigating microenvironmental mediation of plasticity: Interleukin-1ß does not induce plasticity *in vitro*

The above *in vivo* and *in vitro* data suggests that cellular plasticity may be mediated by microenvironmental factors that are absent in our *in vitro* organoid culture system. As previously mentioned, published RNA sequencing data pointed towards Interleukin-1ß (IL-1ß) as a mediator of plasticity in the skin (Seldin and Macara, 2020) Therefore, I sought to investigate whether exposing mammary epithelial organoids to IL-1ß was sufficient to induce plasticity *in vitro*.

Mammary epithelial organoid cultures were initially treated with a titration of 0 ng/ml (PBS control), 5 ng/ml, 10 ng/ml and 20 ng/ml of IL-1ß for one (all concentrations) or two (5 ng/ml) weeks. Subsequently, cultures were fixed and immunostained for a lineage marker for wholemount fluorescence imaging to assess cell fate outcomes under these conditions. However, in both short and long timecourse experiments, endogenous GFP remained restricted to the basal compartment in K5-mTmG organoids and the luminal compartment in K8-mTmG organoids (Figure 25A and B). Thus, the IL-1ß concentrations and timeframes tested failed to induce detectable cellular plasticity in both models. To be sure that the limitations of using microscopy for lineage tracing weren't hindering our ability to identify very low levels of plasticity, flow cytometry was also performed to identify any alteration in the distribution of GFP between the basal and luminal epithelial compartments. Using this approach, no significant changes in the distribution of GFP across cell lineages was observed with IL-1ß treatment, corroborating the imaging results (Figure 26A and B). Despite this, GFP expression appeared higher in IL-1ß-treated conditions compared to control in K8-mTmG organoids by wholemount fluorescence imaging, which also revealed an increase in Ki67+ nuclei in treated conditions when immunostaining control and IL-1ß-treated K5-mTmG and K8-mTmG organoids for the proliferation marker Ki67 (Figure 27), indicating increased proliferation may be responsible for increased GFP expression. This finding corroborates Seldin and Macara's (2020) observation of hyperproliferation mediated by IL-1ß in response to cisplatin-induced DNA damage. However, GFP expression did not appear increased in control K5-mTmG organoids when compared to IL-1ß-treated conditions. To also confirm that organoids were responsive to IL-1ß, RT-qPCR for downstream IL-1ß targets IL-6 and Cox-2 was performed which showed elevated expression in response to treatment (Figure

28). Thus, the lack of plasticity observed was not due to a lack of an effect of IL-1ß treatment, further supporting the conclusion that IL-1ß does not induce plasticity *in vitro*.

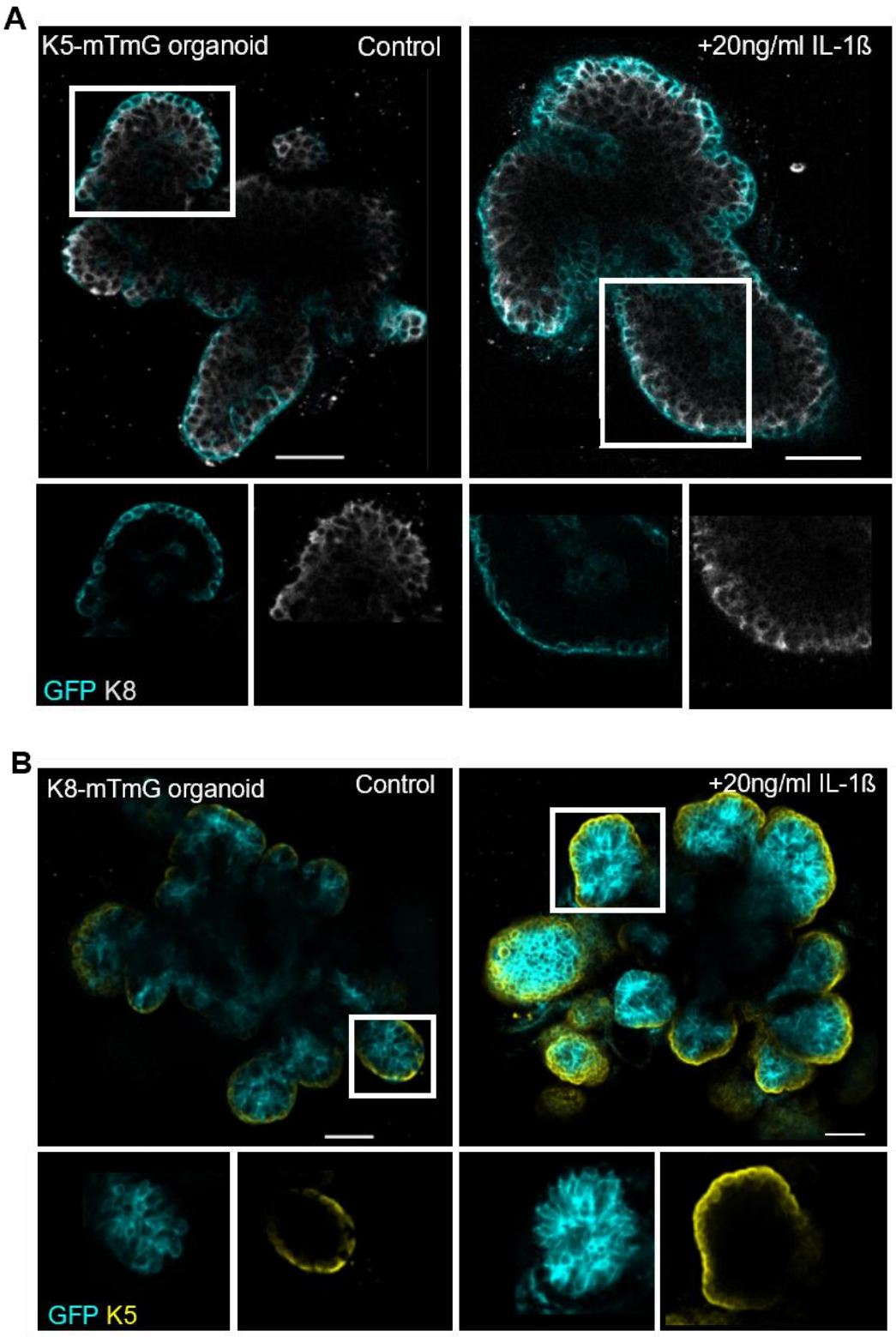

Figure 25: IL-1ß treatment does not induce plasticity in K5-mTmG or K8-mTmG organoids in vitro. Wholemount immunostaining of K5-mTmG (A) and K8-mTmG (B) organoids treated with PBS (control) or 20 ng/ml IL-1ß for 7 days. Organoids were fixed for staining immediately after PBS/IL-1ß treatment ceased. Organoids were immunostained with lineage markers K8 (A) and K5 (B). Images are representative Z slices of organoids, scale bars 50 µm. Endogenous GFP expression remains in the basal compartment in K5-mTmG organoids (A) and the luminal compartment in K8-mTmG organoids (B), suggesting IL-1ß does not induce plasticity in vitro.

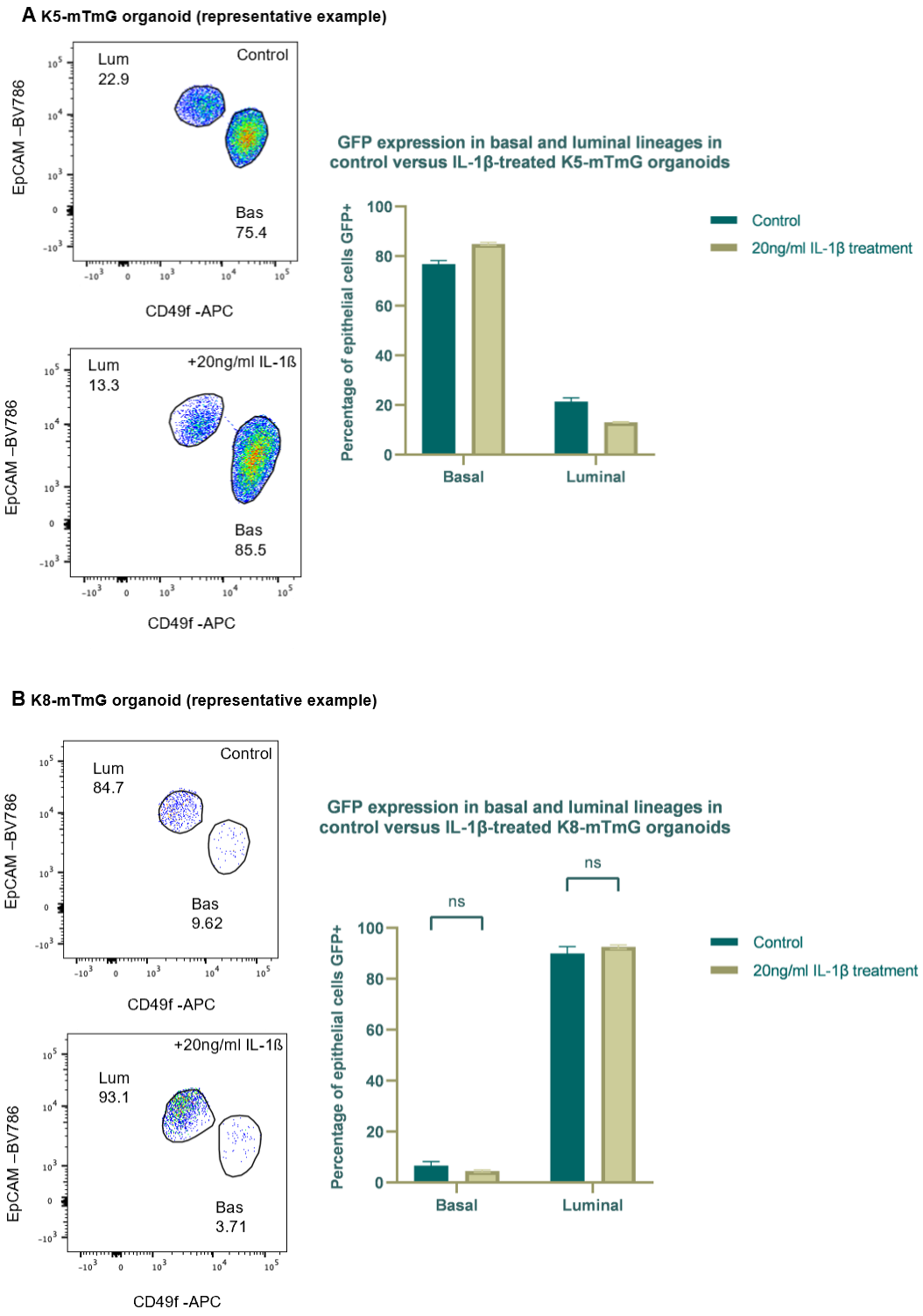

Figure 26: Flow cytometry analysis of GFP expression in K5-mTmG and K8-mTmG organoids treated with PBS (control) or 20 ng/ml IL-1ß for 7 days. Flow cytometry was performed immediately after PBS/IL-1ß treatment was ceased. A: Flow cytometry analysis of GFP expression across basal and luminal cell populations in control and 20 ng/ml IL-1ß-treated K5-mTmG organoids. Representative flow plots and quantification show minimal changes in GFP expression across both cell populations. Bar graph showing mean (± SEM) percentage of basal and luminal cells expressing GFP in control and 20 ng/ml IL-1ß—treated conditions (n=2). B: Flow cytometry analysis of GFP expression across basal and luminal cell populations in control and 20ng/ml IL-1ß-treated K8-mTmG organoids. Representative flow plot and quantification show minimal changes in GFP expression across both cell populations. Bar graph showing mean (± SEM) percentage of basal and luminal cells expressing GFP in control and 20 ng/ml IL-1ß treatment conditions (n=3). No significant change in the percentage of GFP+ basal and luminal cells was seen with IL-1ß treatment ($p > 0.05$, Mann-Whitney test).

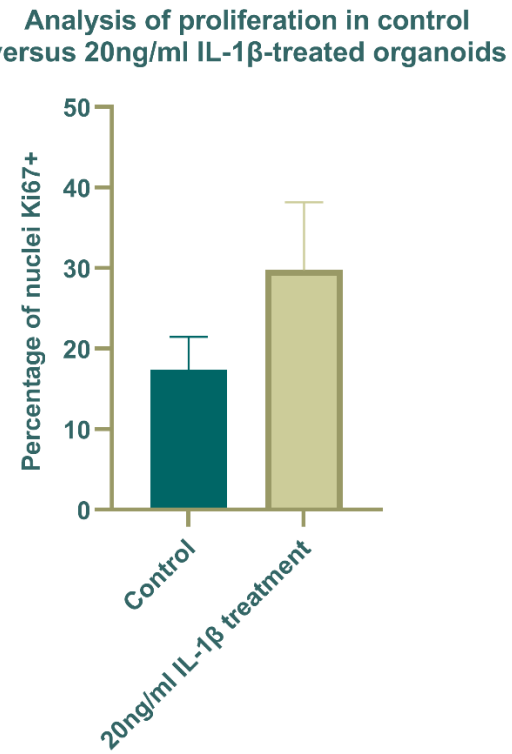

Figure 27: Analysis of proliferation in response to IL-1ß treatment. Bar graph showing mean (± SEM) percentage of Ki67+ nuclei in organoids treated with PBS (control) or 20 ng/ml IL-1ß for 7 days. Organoids were fixed for staining immediately after PBS/IL-1ß treatment ceased (n=2). Higher % of Ki67+ nuclei in IL-1ß-treated conditions suggests IL-1ß increases proliferation.

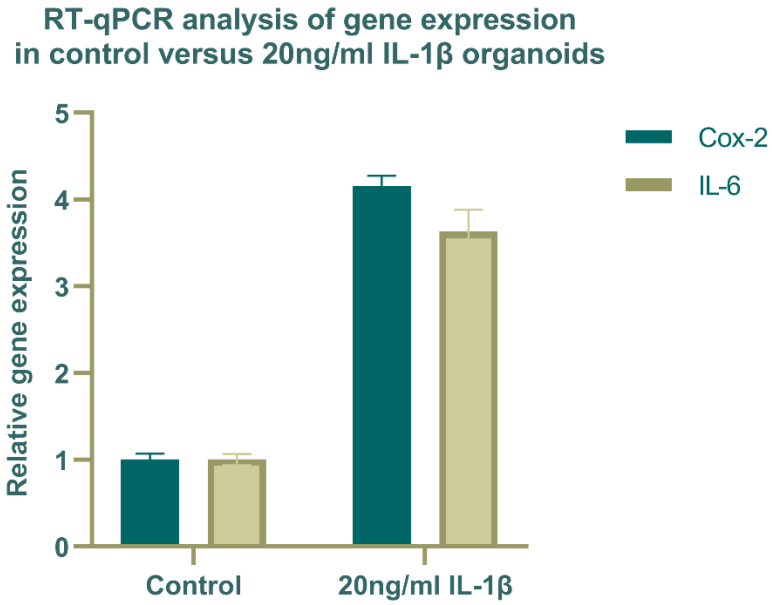

Figure 28: RT-qPCR analysis of gene expression of downstream IL-1ß gene targets in mammary epithelial organoids. Bar graph showing mean of triplicate sample (± SEM) relative gene expression of two IL-1ß target genes, IL-6 and Cox-2, in organoids treated with 20 ng/ml IL-1ß for 7 days over organoids treated with PBS (control) for 7 days (n=1). RT-qPCR was performed immediately after PBS/IL-1ß treatment ceased. Increased IL-6 and Cox-2 expression in IL-1ß-treated conditions versus control conditions confirm the responsiveness of organoids to IL-1ß.

3.8 Investigating microenvironmental mediation of plasticity: Evidence of plasticity in response to Adalimumab treatment *in vitro*

Previous work by Centonze et al. (2020) identified TNF as a restrictor of plasticity in the mammary gland, showing that exposure to the Tumour Necrosis Factor (TNF) inhibitor Adalimumab was capable of inducing plasticity in basal mammary cells. To investigate whether this effect could be replicated in our *in vitro* models, both K5-mTmG and K8-mTmG organoids were exposed to 2 μg/ml Adalimumab for 48 hours, followed by a 3 day chase period prior to cell fate analysis by fluorescence microscopy and flow cytometry (data not shown). No evidence of plasticity was observed in either K5 or K8-mTmG organoids using this treatment protocol. However, by increasing Adalimumab treatment to 5 μg/ml for 5 days, bilineage GFP+ clones were observed by fluorescence microscopy in K5-mTmG organoids, with GFP+ luminal cells residing alongside GFP+ basal cells (Figure 29A). In contrast, no evidence of plasticity was seen via fluorescence microscopy in K8-mTmG organoids (Figure 29B). Despite these observations, flow cytometry analysis showed no changes in GFP distribution across cell lineages in response to 5 days of 5 μg/ml Adalimumab treatment in both K5-mTmG and K8-mTmG organoids (Figure 30). Thus, to be able to draw firm conclusions on whether TNF inhibition can induce mammary cell plasticity *in vitro*, further fluorescence imaging experiments are required to enable careful quantification of the percentage of bi-lineage GFP clones observed with Adalimumab treatment.

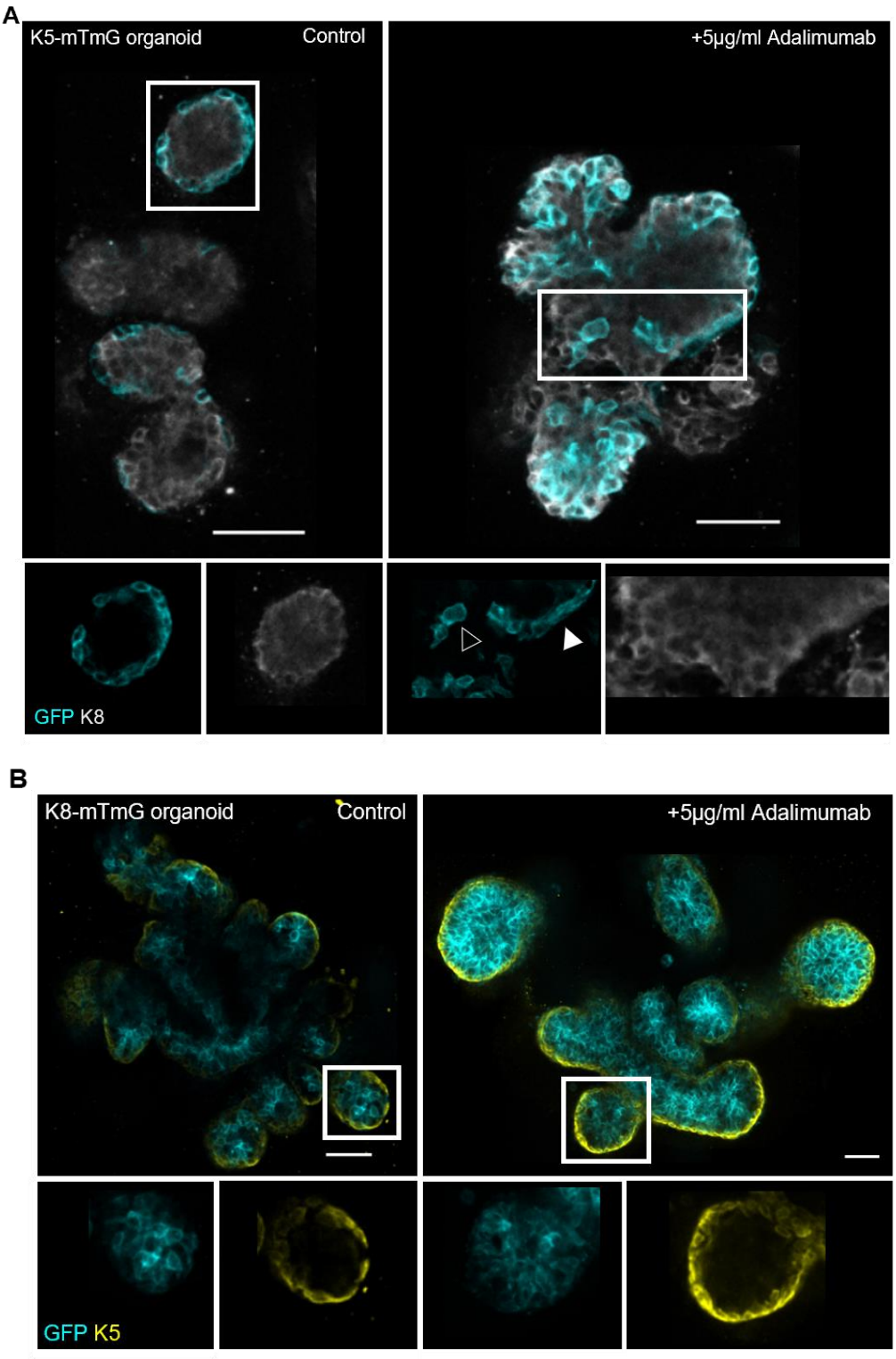

Figure 29: Analysis of plasticity of K5-mTmG (A) and K8-mTmG (B) organoids treated with PBS (control) or 5 µg/ml Adalimumab for 5 days. Organoids were fixed for staining immediately after PBS/Adalimumab treatment ceased. Images are representative z slices of organoids, scale bars 50 µm . A: Wholemount fluorescence imaging of control and 5 µg/ml Adalimumab-treated K5-mTmG organoid immunostained for the lineage marker K8. Endogenous GFP expression remains in the basal compartment in control conditions (left panel) but bilineage clones are apparent in Adalimumab-treated conditions (right panel), with GFP+ luminal cells (hollow arrow) residing near GFP+ basal cells (filled arrow), suggesting Adalimumab may induce plasticity in basal cells in vitro. B: Wholemount fluorescence imaging of control and 5 µg/ml Adalimumab-treated K8-mTmG organoid immunostained for the lineage marker K5. Endogenous GFP expression remains in the luminal compartment in control and treated conditions, suggesting Adalimumab does not induce plasticity in luminal cells in vitro.

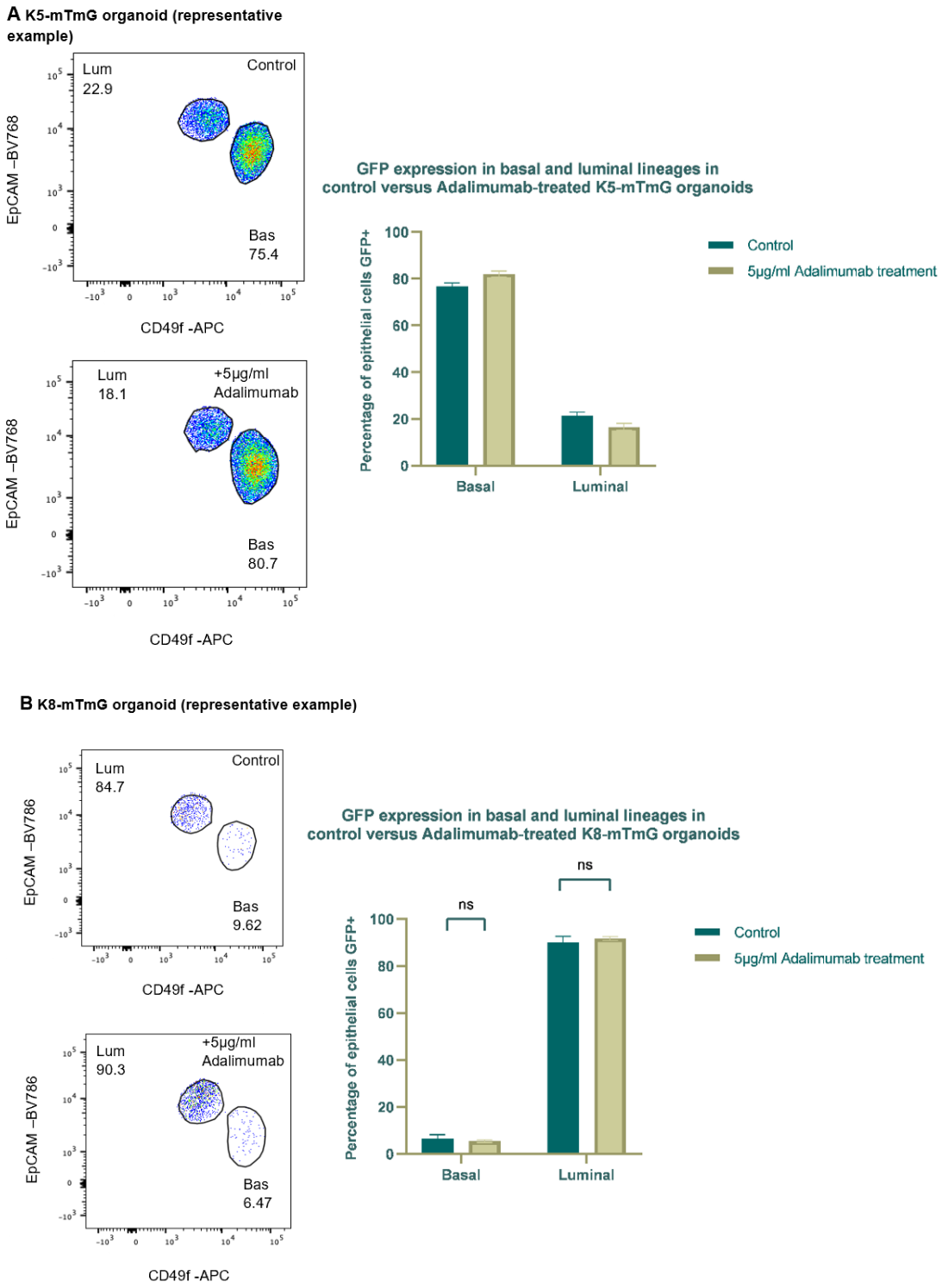

Figure 30: Flow cytometry analysis of GFP expression in K5-mTmG (A) and K8-mTmG (B) organoids treated with PBS (control) or 5 µg/ml Adalimumab for 5 days. Flow cytometry was performed 2 days following PBS/Adalimumab removal, during which time organoids were cultured in normal media. A: Flow cytometry analysis of GFP expression across basal and luminal cell populations in control and 5 µg/ml Adalimumab-treated K5-mTmG organoids. Representative flow plot and quantification show minimal changes in GFP expression across both cell populations. Bar graph showing mean (± SEM) percentage of basal and luminal cells expressing GFP in control and 5 µg/ml Adalimumab treatment conditions (n=2). B: Flow cytometry analysis of GFP expression across basal and luminal cell populations in control and 5 µg/ml Adalimumab-treated K8-mTmG organoids. Representative flow plot and quantification show minimal changes in GFP expression across both cell populations. Bar graph showing mean (± SEM) percentage of basal and luminal cells expressing GFP in control and 5 µg/ml Adalimumab treatment conditions (n=3). No significant change in the percentage of GFP+ basal and luminal cells was seen with Adalimumab treatment ($p > 0.05$, Mann-Whitney test).

3.9 Identifying novel putative microenvironmental-induced factors and pathways underpinning mammary epithelial cell plasticity

As treating mammary organoids with promising candidate agents (IL-1ß or the TNF inhibitor Adalimumab) had no (IL-1ß) or subtle (Adalimumab) impact on mammary cellular plasticity *in vitro*, I next sought to identify other potential microenvironmental mediators of plasticity by interrogating published RNA sequencing data sets of cells undergoing fate changes in response to damage (Centonze et al. 2020, Seldin and Macara 2020).

Using a transgenic mouse model that allowed the specific ablation of luminal cells, Centonze et. al (2020) performed bulk RNA sequencing on luminal and basal cells before and after luminal cell ablation, in addition to a 'hybrid' mammary cell population that emerged in response to ablation. With this data, I first performed principal component analysis (PCA) to understand the variance between control and experimental cell populations (summarised in Table 1). PCA demonstrated high variance between the reference and comparison population in all of the comparisons performed for differential gene expression (DEG) analysis (summarised in Table 2). On a basic level, this suggests that ablation of luminal cells leads to changes in gene expression, which may underpin the plasticity observed in basal cells in response to luminal cell ablation (Figure 31).

Table 1: Description of cell type and treatment conditions of samples subjected to RNA sequencing by Centonze et. al (2020) (2 replicates per condition) and analysed for differential gene expression.

Sample	***Cell type***	***Experimental condition***
BC_S44 and BC-WT_S80	*Basal*	*Pre-ablation (WT)*
LC_S45 and LC-WT_S81	*Luminal*	*Pre-ablation (WT)*
TBC_S46 and TBC_S82	*Basal*	*Post-ablation*
TLC_S48 and TLC_S84	*Luminal*	*Post-ablation*
THC_S83 and THC_S47	*Hybrid*	*Post-ablation*

To try to identify potential mediators of plasticity, I focused my analysis on the luminal post-ablation and hybrid cell populations. As the sequenced luminal post-ablation cells were known to arise from basal cells that had re-acquired bipotency, any differentially expressed genes when comparing luminal post-ablation cells to their luminal pre-ablation (wildtype) counterparts may represent candidate plasticity mediators. Similarly, the hybrid cell population arose only following luminal cell ablation, thus comparing their similarity to wildtype luminal and basal cells, as well as post-ablation luminal cells, would indicate

whether this hybrid population represents an intermediate cell state existing solely under plastic conditions. The comparisons performed are summarised in Table 2.

Table 2: Summary of comparisons of cell populations from Centonze et al. (2020) dataset used for differential gene expression analysis. Hybrid cells only arise under ablation conditions.

Reference population	***Cell population compared to reference population***
Luminal pre-ablation	*Luminal post-ablation*
Luminal pre-ablation	*Hybrid*
Basal pre-ablation	*Hybrid*
Luminal post-ablation	*Hybrid*

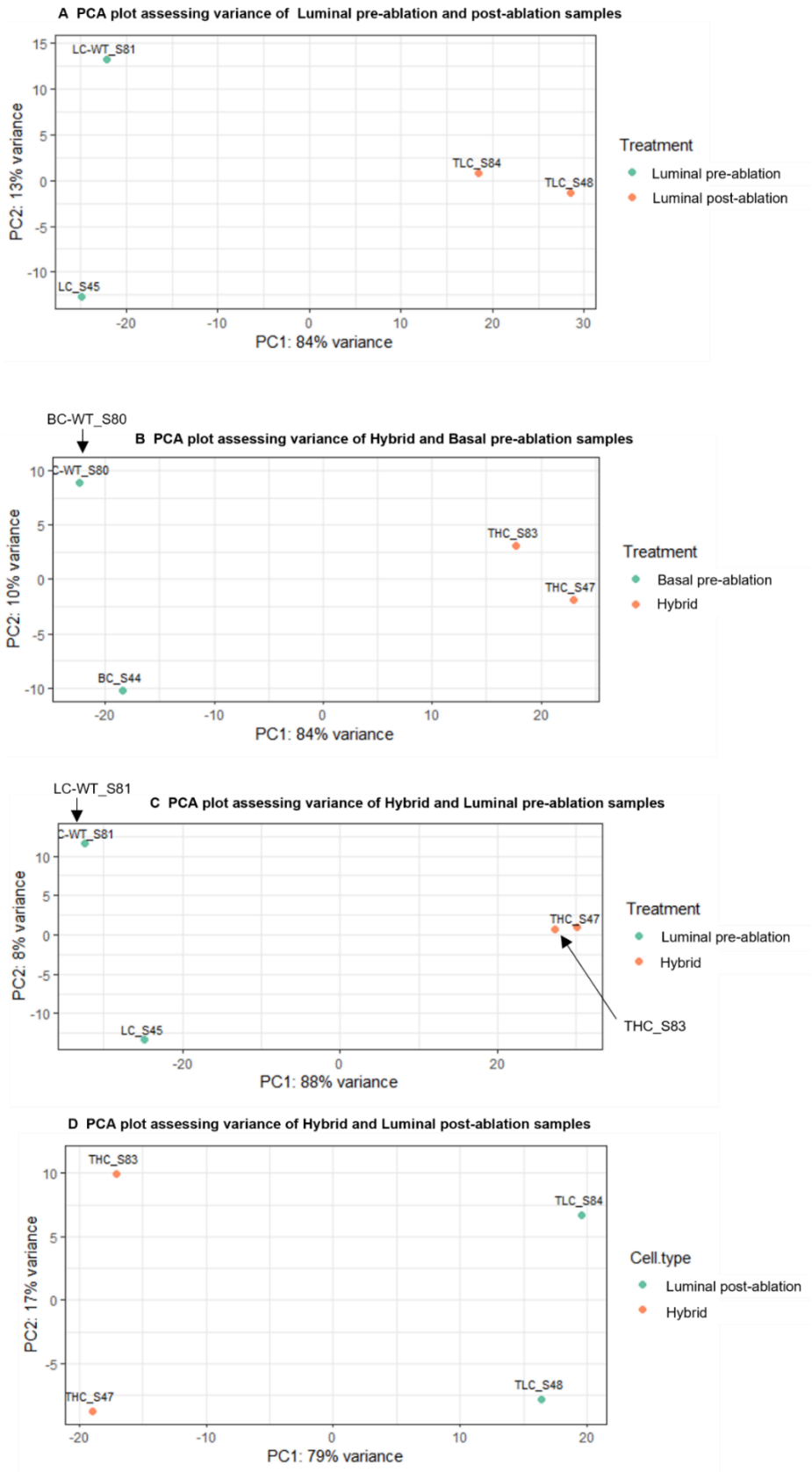

Figure 31: Principal Component Analysis of sample comparisons. Principal Component Analysis (PCA) plots measuring the variance between luminal pre-ablation (WT) and luminal post-ablation samples (A), hybrid (arising after ablation) and basal pre-ablation (WT) samples (B), hybrid (post-ablation) and luminal pre-ablation (WT) samples (C) and hybrid and luminal post-ablation samples (D). All experimental treatments were performed on duplicate samples. High variance between the populations compared suggests that luminal cell ablation leads to differential gene expression. PCA plots were generated using scripts written by Dr. Francisca Segers in R.

To assess how the identity of the experimental cell populations arising after luminal cell ablation, namely the hybrid cells and post-ablation luminal cells, differ from wildtype basal and luminal cells, I compared the expression of known basal and luminal lineage markers in these distinct populations (Figure 32). Post-ablation luminal cells that have arisen from bipotent basal cells appear to be more 'basal' in character than pre-ablation (wildtype) luminal cells, as they express higher levels of common basal markers such as P63, SMA (Acta2) and Keratin 5 (Krt5) and lower levels of the luminal markers Keratin 8 (Krt8) and Keratin 18 (Krt18) (Figure 32A). The identity of the hybrid cells that emerge post-luminal cell ablation appears less defined. In comparison to basal pre-ablation (wildtype) cells they are more 'luminal' in nature, with higher expression levels of all luminal markers and lower levels of basal marker expression (Figure 32B). In comparison to luminal pre-ablation cells however, hybrid cells appear more 'basal', with higher basal marker expression levels and lower luminal marker expression levels (Figure 32C). Thus, hybrid cells may represent an intermediate cell state between basal and luminal cells. When comparing hybrid cells to luminal post-ablation cells, the situation appears more complex. Although hybrid cells express higher levels of basal markers than luminal post-ablation cells, the expression of luminal markers is fairly comparable across both cell populations, perhaps due to lower expression of luminal markers by the more 'basal-like' post-ablation luminal cells (Figure 32D).

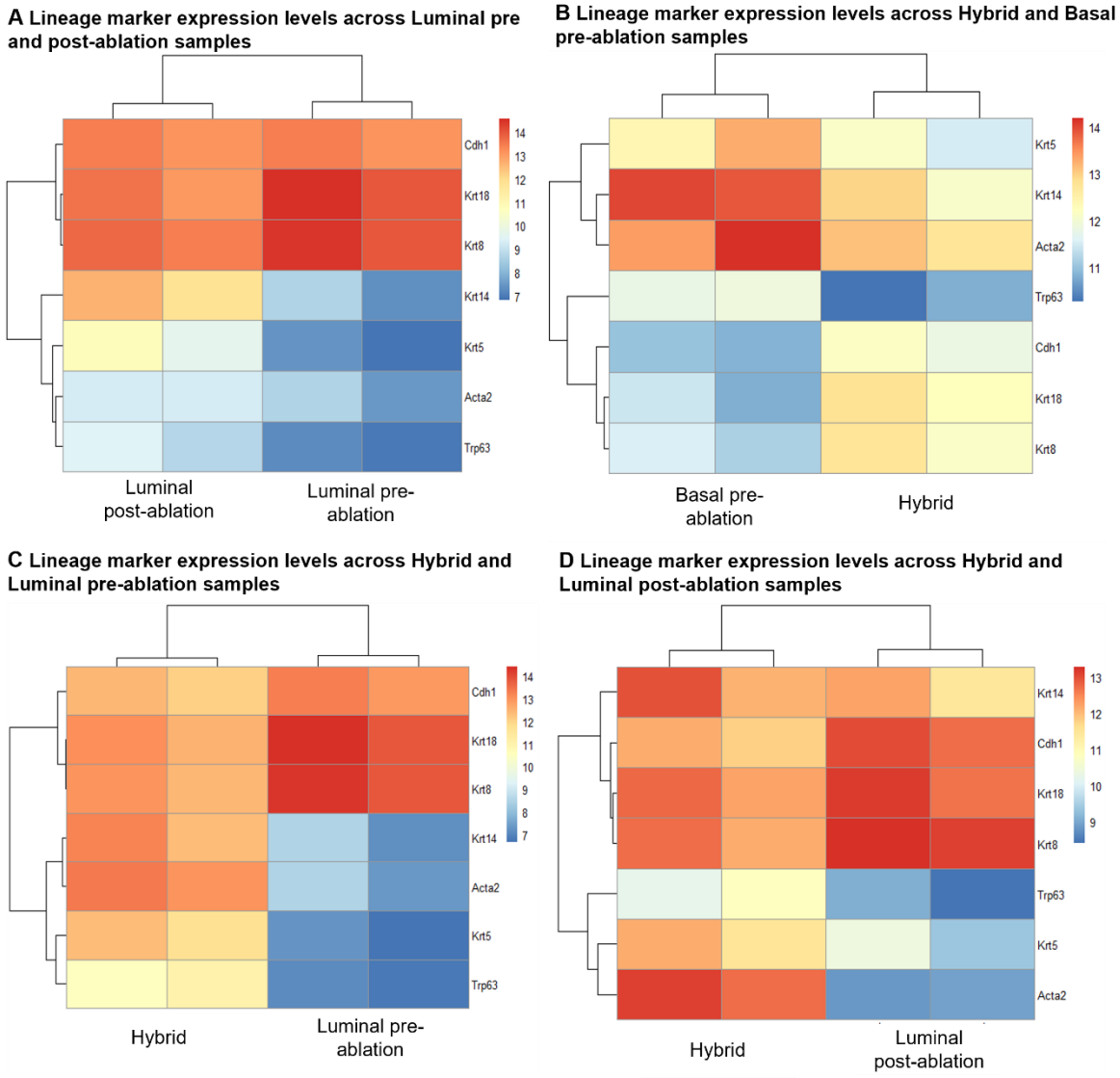

Figure 32: Heat maps showing gene expression (normalized read counts on a log2 scale) of a range of known basal and luminal mammary epithelial markers across sample comparisons. A: Lineage marker gene expression across luminal pre-ablation (WT) and post-ablation cells showing higher levels of basal marker and lower levels of luminal marker expression in luminal post-ablation cells compared with WT luminal cells. B: Lineage marker gene expression across hybrid (arising post-ablation) and basal pre-ablation (WT) cells showing higher levels of luminal marker and lower levels of basal marker expression in hybrid cells compared with WT basal cells. C: Lineage marker expression across hybrid and luminal pre-ablation cells showing higher levels of basal marker and lower levels of luminal marker expression in hybrid cells compared with WT luminal cells. D: Lineage marker expression across hybrid cells and luminal post-ablation cells showing higher levels of basal marker expression in hybrid cells compared with luminal post-ablation cells, but similar levels of luminal marker expression across both cell populations. Heat maps generated using scripts written by Dr. Francisca Segers in R.

Volcano plots displaying the differentially expressed genes in the above comparisons revealed the overall spread of the data (Figure 33). The level of differential gene expression appears highest between luminal pre- and post-ablation samples (Figure 33A), with many significantly upregulated and downregulated genes in post-ablation samples when compared to pre-ablation (wildtype) samples. When comparing (post-ablation) hybrid to

basal and luminal pre-ablation (wildtype) samples, more upregulated genes were identified, with fewer downregulated genes observed compared to the luminal pre- and post-ablation comparison (Figures 33B and 33C). This effect is even more noticeable in the hybrid to luminal post-ablation comparison, where very few significantly downregulated genes are identified. The number of significantly differentially expressed genes was overall lower in this comparison, with fewer upregulated genes also detected (Figure 33D). This likely reflects the degree of similarity between samples, with luminal pre- and post-ablation samples being the most different and therefore having the highest level of differential gene expression and luminal post-ablation and hybrid (post-ablation) samples being the most similar and therefore having lower levels of differential gene expression.

The identified differentially expressed genes between these cell populations (Table 2) were then subjected to KEGG pathway analysis (Yu et al. 2012). This revealed several commonly upregulated pathways and associated genes. No significantly downregulated pathways were identified. Interestingly, there appeared to be more commonly upregulated genes in comparisons between control and experimental cell populations (i.e. luminal pre and post-ablation and hybrid and basal/luminal pre-ablation) than when comparing experimental populations (hybrid and luminal post-ablation). This again implies that inducing luminal cell ablation triggers significant changes in gene expression as compared to wildtype (pre-ablation) controls.

Of the identified commonly upregulated pathways (and associated genes), my analysis showed that the cell cycle is commonly upregulated in response to luminal cell ablation, with regulators such as Cdk1 and Cdc20 increasing in expression by at least 2-fold in experimental compared with control populations (Table 3). Extracellular Matrix (ECM)-receptor interactions was also a commonly upregulated pathway across the populations compared, with upregulation of several genes encoding collagen components (examples provided in Table 3) by at least 2.7-fold in experimental compared with control populations. Intriguingly this was also seen for some collagen component-encoding genes in the hybrid vs luminal post-ablation comparison. Furthermore, cytokine/chemokine signalling pathways were also detected as upregulated by KEGG pathway analysis, with many factors upregulated in experimental when compared with control populations by at least 2-fold (examples in Table 3). Although not detected by KEGG pathway analysis, many alterations in

histone marker expression (e.g. H4C12 and H2ac10) were apparent across the control and experimental comparisons, potentially implicating changes in the chromatin landscape as important for plasticity induction.

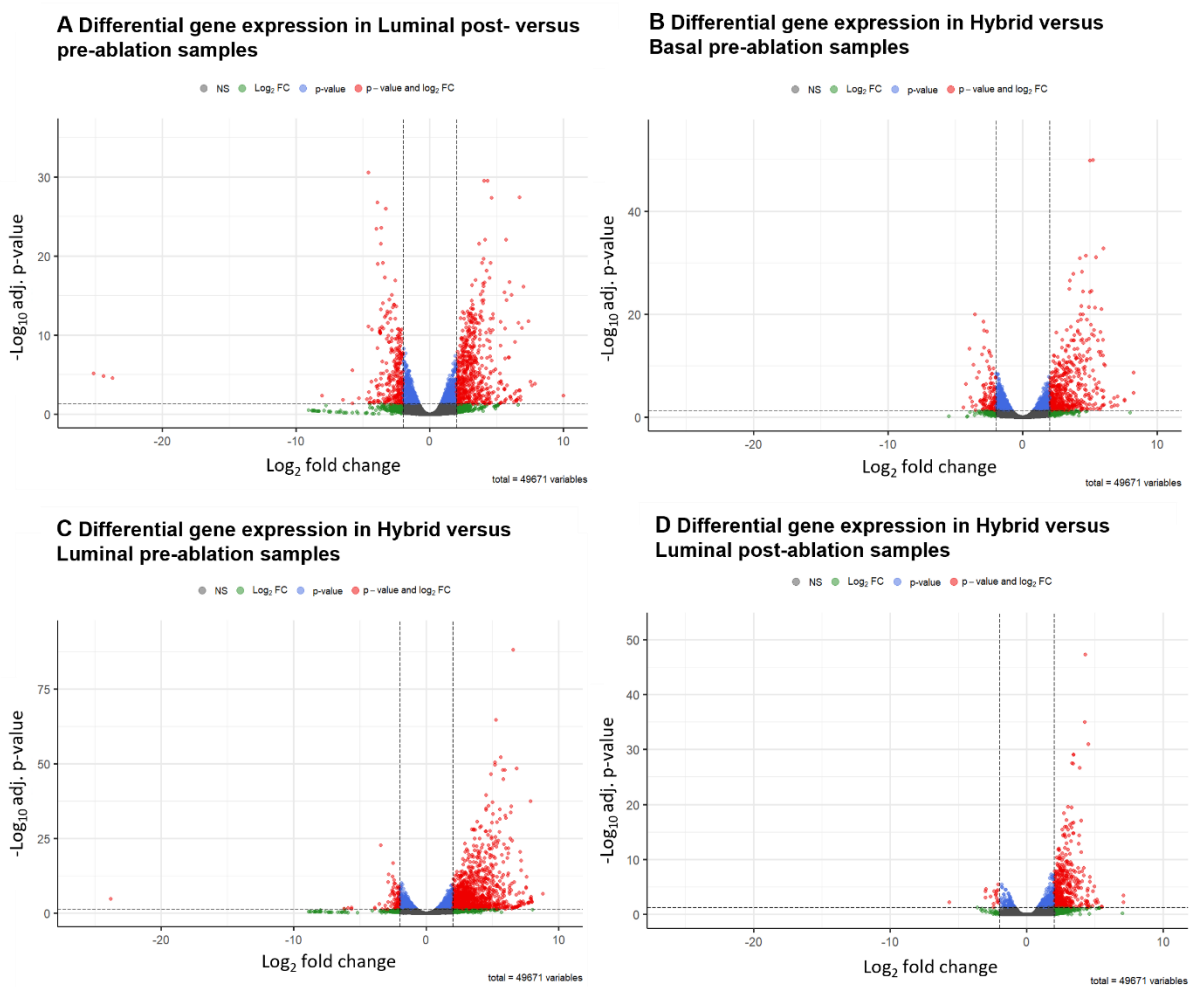

Figure 33: Volcano plots displaying differential gene expression across sample comparisons. Red dots indicate differentially expressed genes with a significant adjusted p- value and log2fold change. Blue dots represent genes with a significant p value only. Green dots represent genes with a significant log2fold change only. Grey dots represent unsignificant differentially expressed genes (see methods). A: Differentially expressed genes in luminal post-ablation samples compared with luminal pre-ablation (wildtype) samples. B: Differentially expressed genes in hybrid (post-ablation) samples compared with basal pre-ablation (wildtype) samples. C: Differentially expressed genes in hybrid samples compared with luminal pre-ablation samples. D: Differentially expressed genes in hybrid compared with luminal post-ablation samples. Volcano plots generated using scripts written by Dr. Francisca Segers in R.

Table 3: Summary of common upregulated genes between the samples compared within the Centonze et al. (2020) dataset (see Table 2 for comparisons). Table shows gene names and their associated KEGG pathway, as well as log2fold increases in gene expression in each comparison. All adjusted p values of log2fold change increases in gene expression were < 0.05. Script for differential gene expression analysis provided by Dr. Francisca Segers performed in R. Where the specified gene was not significantly differentially expressed in a population comparison, X is used.

KEGG pathway	***Gene name***	***Log2fold change***			
		Luminal pre & post-ablation	***Hybrid & Basal pre-ablation***	***Hybrid & Luminal pre-ablation***	***Hybrid & Luminal post-ablation***
Cell cycle	*Cdk1*	*3.58*	*4.81*	*3.57*	*X*
Cell cycle	*Cdc20*	*2.40*	*2.76*	*2.48*	*X*
ECM-receptor interactions	*Col5a2*	*2.74*	*X*	*5.18*	*2.41*
ECM-receptor interactions	*Col1a1*	*3.82*	*4.11*	*6.38*	*X*
Chemokine/ Cytokine signalling	*Ccl6*	*X*	*3.95*	*4.45*	*2.27*
Chemokine/ Cytokine signalling	*IL-19*	*7.51*	*3.85*	*7.32*	*X*
	H4C12	*2.20*	*2.02*	*2.26*	*X*
	H2ac10	*2.87*	*4.42*	*2.48*	*X*

To assess whether the genes and pathways identified above might also be relevant for genotoxic damage-induced cell fate plasticity, I used a similar work flow to analyse the bulk RNA sequencing datasets available from the work of Seldin and Macara (2020). Here, the authors sequenced dermal fibroblasts isolated from vehicle-injected (PBS control) and cisplatin-injected mice to try to identify the microenvironmentally-produced factors that induced epidermal cell plasticity. PCA analysis again demonstrated high variance between vehicle and cisplatin-treated samples, suggesting cisplatin treatment is causing differential gene expression which may be mediating the epidermal cell plasticity observed in response to genotoxic damage (Figure 34).

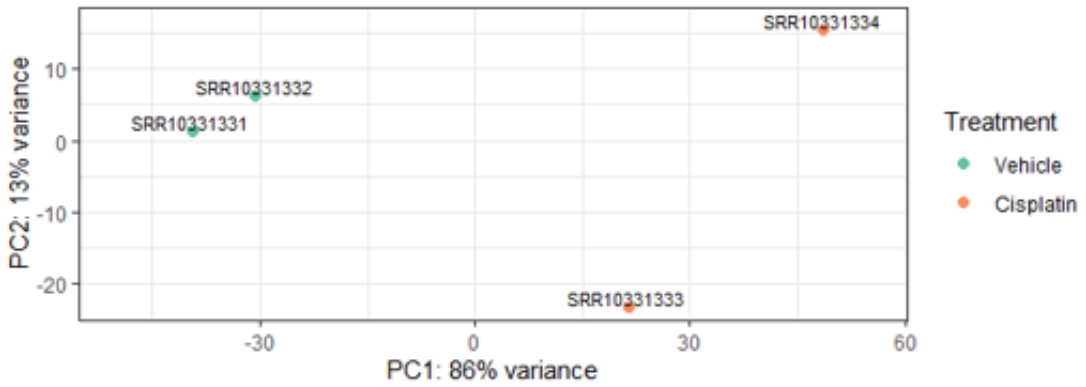

Figure 34: Principal Component Analysis (PCA) plots measuring the variance between vehicle-treated (control) and cisplatin-treated samples. High variance between samples compared suggests cisplatin treatment is leading to differential gene expression. PCA plots generated using scripts written by Dr. Francisca Segers in R.

Initially I sought to identify commonly differentially expressed genes between the Centonze et al. (2020) and Seldin and Macara (2020) data sets. However, correlation testing in R indicated that there was minimal correlation between the log2fold changes in gene expression between the two data sets (examples shown in Figure 35). This suggests that there is little overlap in differential gene expression and that there would be limited benefit in identifying commonly differentially expressed genes between the two studies. Visualisation of differential gene expression by volcano plot further highlights differences between the Seldin and Centonze datasets. The Seldin dataset displays a much broader range of levels of upregulated gene expression, with even fewer significantly downregulated genes (Figure 36). Thus, whilst I considered similarly upregulated pathways between the Centonze et al. (2020) and Seldin and Macara (2020) datasets, I interrogated the results of the differential gene expression analysis separately.

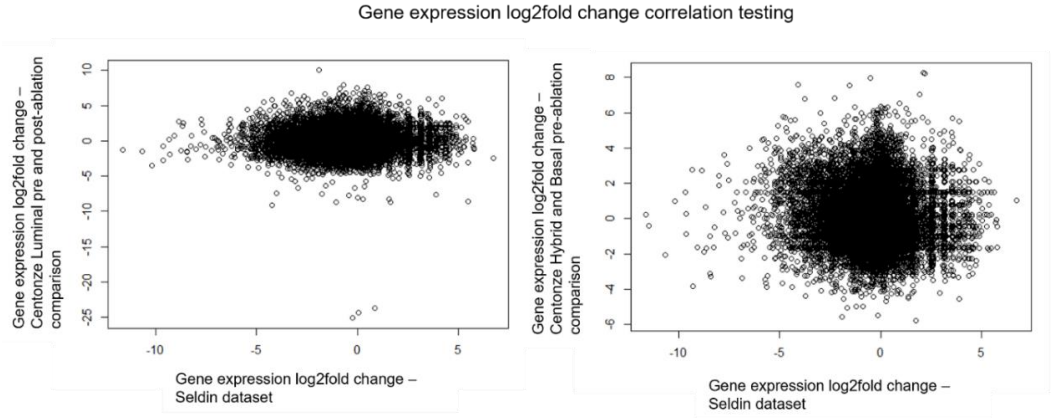

Figure 35: Example of correlation testing for log2fold changes in gene expression between Seldin and Macara (2020) and Centonze et al. (2020) data sets. Left panel assesses correlation between log2fold changes in gene expression between the Seldin comparison and the luminal pre- and post-ablation Centonze comparison. Right panel assesses correlation between the Seldin comparison and the hybrid and basal pre-ablation Centonze comparison. Both graphs show no correlation between log2fold changes in gene expression. Correlation graphs generated using script provided by Dr. Francisca Segers in R.

Interestingly, despite the limited correlation in specific differentially expressed genes between the two studies, similarly to the Centonze et al. (2020) dataset, KEGG pathway analysis (Yu et al. 2012) of the identified differentially expressed genes in the Seldin dataset also identified chemokine/cytokine signalling and ECM-receptor interaction pathways as being upregulated in response to genotoxic cell ablation (see examples in Table 4). TNF and NF-KB pathways were specifically upregulated, which are known to play a role in inflammatory cell recruitment, ECM remodelling, cell adhesion and cell survival (Liu et al. 2017, Aggarwal, 2003). This further supports a potential role for ECM regulators and chemokine/cytokine signalling in response to damage in plasticity induction, as indicated in my analysis of the Centonze et al's dataset. Upregulation of the TNF pathway is particularly of note considering Centonze et al's (2020) observation that TNF restricts basal mammary epithelial cell potential. Collectively, this suggests that chemokine/cytokine signalling pathways are differentially regulated in response to both lineage ablation (Centonze et al. 2020) and genotoxic damage (Seldin and Macara, 2020).

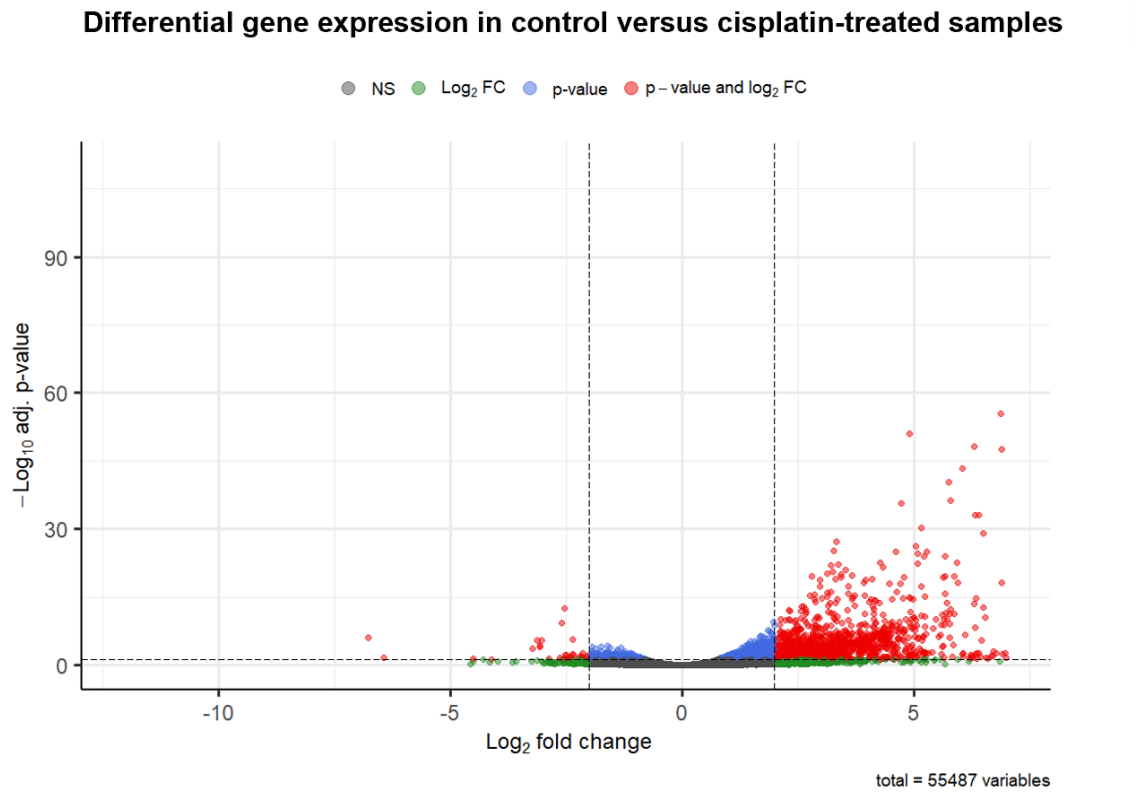

Figure 36: Volcano plot displaying differential gene expression in cisplatin-treated samples compared to control (vehicle-treated) samples. Red dots indicate differentially expressed genes with a significant adjusted p-value and log2fold change. Blue dots represent genes with a significant p value only. Green dots represent genes with a significant log2fold change only. Grey dots represent unsignificant differentially expressed genes (see methods). Volcano plots generated using scripts written by Dr. Francisca Segers in R.

Table 4: Summary of commonly upregulated genes in cisplatin-treated populations versus control populations in the Seldin and Macara (2020) dataset. Table shows gene names and their associated KEGG pathway as well as log2fold increases in gene expression. All adjusted p values of log2fold change increases in gene expression were < 0.05. Script for differential gene expression analysis provided by Dr. Francisca Segers performed in R.

KEGG pathway	***Gene name***	***Log2fold change***
Chemokine/Cytokine signalling	*Ccl3*	*4.33*
ECM-receptor interactions	*Col6a1*	*2.31*
TNF pathway	*Mmp11*	*2.55*
NF-KB pathway	*Bcl2a1a*	*5.64*

In summary, analysis of bulk RNA sequencing datasets from Centonze et al. (2020) revealed that plasticity in basal cells triggered by luminal cell ablation leads to the generation of luminal cells that are more 'basal' in nature, alongside the emergence of a hybrid cell population that may represent an intermediate basal-luminal state. When considered alongside bulk RNA sequencing data from Seldin and Macara (2020), ECM-receptor interaction and chemokine/cytokine signalling pathways are commonly upregulated in response to damage. This provides a focus for future investigations towards identifying the microenvironmental factor(s) that mediate cisplatin-induced mammary basal cell plasticity *in vivo*.

4. Discussion

The mammary gland is a highly dynamic, regenerative system. Recent advances in technologies such as genetic lineage tracing and whole tissue 3D imaging have revealed that while distinct unipotent progenitors maintain the basal and luminal epithelial bilayer under homeostatic conditions, these progenitors are highly plastic and can produce cells of the opposing lineage under certain conditions. Cell dissociation for culture and transplantation, oncogene activation and genotoxic damage in the form of cisplatin treatment have all been demonstrated to induce plasticity in mammary epithelial cells. These findings have potentially important implications for the treatment and prevention of disease such as breast cancer. This project aimed to further investigate the impact of genotoxic damage on mammary epithelial cell fate, with a focus on comparing cellular responses *in vivo* and *in vitro* to better understand the mechanisms behind genotoxic-induced mammary epithelial cell plasticity.

4.1 Establishment of an *in vitro* experimental model for mammary cell fate mapping in response to genotoxic damage

To be able to compare mammary cell fate outcomes in response to genotoxic damage *in vivo* vs *in vitro*, I isolated mammary epithelial cells from our transgenic lineage tracing models and established them in 3D organoid culture. Firstly, it was important to ensure that the organisation of the mammary epithelial organoids accurately recapitulated the *in vivo* mammary gland. This allows confidence that any differences in cell fate specification or behaviour in response to genotoxic damage is not a result of differences in epithelial structure and organisation between *in vivo* and culture conditions. Fluorescence microscopy of mammary epithelial organoids immunostained for a range of basal and luminal epithelial markers demonstrated that the mammary epithelial bilayer in cultured organoids is structurally very similar to the *in vivo* mammary gland, with basal and luminal markers being predominantly expressed in the correct compartments. Mammary epithelial organoids, like their *in vivo* counterpart, were capable of branching and forming lumens. However, there are some important differences between mammary organoids and the *in vivo* epithelium that must be considered when interpreting responses to cisplatin treatment. Mammary organoids are grown in Matrigel and supplemented with growth factor-containing media. This introduces variability within and between cultures depending on, for example, the specific batch/lot of these factors. An individual organoids' position in the Matrigel influences its exposure level to growth factors and may also expose them to different levels of tension. This variability is potentially reflected by some organoids not forming complete bilayers, with budding branches often more similar to the stratified TEBs present *in vivo* during puberty than an elongated bi-layered duct. Moreover, organoids gradually lost smooth muscle actin (SMA) expression, a marker for differentiated basal cells, over time and luminal cells in stratified organoids' buds occasionally expressed basal markers, such as P63. Like other tissue organoid systems, mammary organoids exhibit a high level of heterogeneity in terms of morphology and size, which poses challenges when drawing conclusions regarding the organoid's response to treatment. Nevertheless, fluorescence wholemount imaging routinely and clearly showed luminal cells enveloped by a layer of basal cells within the organoid system, closely mimicking the compartmentalisation observed *in vivo.* This provides confidence that any differences observed in cell fate and

behaviour in response to genotoxic insult between *in vivo* and *in vitro* systems are likely biologically relevant and not due to culture-induced perturbations to epithelial organisation and architecture.

As well as validating the *in vitro* organoid system as a model, it was also important to confirm the robustness of the two transgenic mouse lines used for lineage tracing *in vivo*, namely K5-mTmG and K8-mTmG mice which are used for tracing basal and luminal cells respectively. This was necessary to be able to accurately lineage trace individual mammary epithelial cells after exposure to genotoxic agents. These models were previously validated for *in vivo* lineage tracing by Dr. Bethan Lloyd-Lewis. In the absence of tamoxifen induction, negligible GFP+ cells were observed by flow cytometry in both models. Moreover, administering tamoxifen to K5-mTmG and K8-mTmG mice induced GFP expression in basal and luminal mammary cells respectively with a high degree of specificity, as observed by wholemount fluorescence microscopy and flow cytometry.

The performance of these lineage tracing models in *in vitro* organoid culture models, however, had not been investigated. As dissociating cells for culture can induce plasticity, it was necessary to ensure that GFP expression was a) only being induced in response to 4-OHT (the active metabolite of tamoxifen used in culture) treatment and b) expressed in the cell lineage specified by the promoter. Encouragingly, levels of GFP expression were similarly negligible or very low without 4-OHT treatment in both K5-mTmG and K8-mTmG organoids. While a small degree of leakiness was apparent in K8-mTmG organoids, rare GFP+ cells were restricted to the luminal compartment. For the purposes of this study, the small amount of GFP expression observed in the absence of 4-OHT treatment is of little concern as responses to genotoxic damage in specific developmental windows were not being investigated.

After 4-OHT treatment, wholemount fluorescence imaging of K5- and K8-mTmG organoids immunostained for basal and luminal specific markers revealed that GFP fluorescence was mostly restricted to the respective basal and luminal compartments in these models. However, more GFP expression in the opposing compartment was observed in organoid cultures compared to *in vivo*, suggesting that placing mammary epithelial cells in culture induced a baseline level of plasticity. Surprisingly, flow cytometry analysis using cell surface markers commonly used to separate luminal and basal mammary cells (EpCAM and CD49f)

isolated from tissues showed an increased number of mis-specified GFP+ cells compared to that visualised by microscopy, particularly in K5-mTmG organoids. The precise reason(s) for these differences remains unclear. Flow cytometry is more sensitive than wholemount fluorescence microscopy (due to the depth of imaging required to visualise whole organoids within Matrigel drops) and allows for more organoids to be analysed. Thus, the level of baseline plasticity observed by imaging may be an underestimation. Alternatively, baseline levels of plasticity may appear higher by flow cytometry due to culture-induced perturbations in the specificity of the cell surface markers used to define these populations. It is conceivable that the expression and distribution of the cell adhesion proteins EpCAM and CD49f (Integrin α6) may change in the presence of Matrigel, which does not fully recapitulate the basement membrane observed *in vivo*.

Higher background levels of plasticity in the organoid cultures could falsely give the impression of plasticity induction in response to treatment, impeding the identification of subtle changes in true drug-induced levels of plasticity. However, this issue does not impede the identification of significant changes in cell fate specification in response to genotoxic damage, especially when considering vehicle control treatments were always performed alongside genotoxic treatments, thus allowing baseline levels of plasticity to be considered. Furthermore, using both fluorescence microscopy image analysis and flow cytometry to assess GFP lineage expression allows for any treatment-induced plasticity to be detected more robustly than using a single technique alone.

Although the K5-mTmG and K8-mTmG lineage tracing mouse models facilitate accurate cell fate mapping in response to genotoxic damage in this study, some features of these models must be considered when interpreting results. Firstly, they facilitate population-based/mosaic lineage tracing with comparatively low levels of fluorescent labelling when using tamoxifen/4-OHT doses that do not negatively affect normal mammary biology. Tamoxifen is anti-oestrogenic and thus cannot be used to induce cell labelling at saturation. Therefore, it is possible that any effects relating to cell fate specification in response to genotoxic damage may be missed if they occur in unlabelled cells. To maximise labelling levels to increase the chance of observing plasticity in response to treatment, I increased the concentration of 4-OHT used in cultures to 500 nM – 1 μM. These concentrations have been used previously in organoids with no reported detrimental effects (Centonze et al.

2020). However, this did not lead to 100% of basal and luminal cells being labelled with GFP in both K5-mTmG and K8-mTmG organoids respectively. Thus, in future studies, it would be desirable to use models that do not rely on tamoxifen for inducing Cre activity e.g. doxycycline-based models, which have no reported effects on normal mammary gland biology. Importantly, this would enable us to label 100% of cells within the luminal and basal compartments. In turn, this would allow us to more easily detect any drug-induced effects on cell fate outcomes via the dilution of labelled cells by the unlabelled progeny of mis-specified cells from the opposing compartment (as undertaken by Wuidart et al. 2016). It may also be beneficial to move away from a K8-driven lineage tracing system for the luminal compartment, due to evidence suggesting that K8 expression may preferentially label a subset of luminal cells (Davis et al. 2016).

To investigate the effects of genotoxic damage on cell fate specification, it was necessary to carefully titrate the doses of cisplatin used to induce DNA damage. Cisplatin was very effective at damaging organoids, as revealed by their dark and 'fluffy'-edged appearance by light microscopy at higher concentrations. As organoid death in these contexts could have been related to a non-DNA damage effect (e.g. perturbed metabolism), it was important to confirm that DNA damage was indeed being induced at the selected cisplatin concentration by immunostaining treated organoids with yH2AX, a marker of DNA double strand breaks. Quantification of yH2AX foci in organoids using ImageJ revealed that there were significantly higher numbers of yH2AX foci per nucleus in cisplatin-treated organoids when compared to control (PBS) treated organoids. This confirmed that the selected cisplatin dose induced DNA damage in organoids while remaining sub-lethal, allowing the effect of genotoxic damage on mammary epithelial plasticity to be thoroughly investigated.

It is worth noting that cisplatin induces crosslinks in DNA, which often result in double strand breaks when repair is attempted, rather than double strand breaks directly. Therefore, although using an anti-yH2AX antibody to quantify the numbers of double strand breaks in organoids is sufficient to confirm that cisplatin has induced DNA damage, it may not be the most accurate assessment of how cisplatin affects organoid DNA. The mechanism by which DNA damage is induced (i.e. DNA crosslinks as opposed to double strand breaks) may be important in its ability to cause plasticity and other potentially relevant changes in cell behaviours. Thus, measuring DNA crosslinking directly using techniques such as a comet

assay, whereby the contents of lysed cells suspended in an agarose layer on a microscope slide are electrophorised, would be beneficial (Zhang et al. 2009). The inherent heterogeneity of organoid cultures also presented difficulties as their sensitivity to cisplatin treatment varied. Typically, denser cultures with larger individual organoids tended to be more resistant to cisplatin-induced damage, whereas sparser cultures with smaller organoids were more sensitive. To overcome this, efforts were made to repeat experiments in organoids of a similar density/size and multiple repeats performed to be sure of damage induction.

A previous report showed that cisplatin induced skin and mammary cell hyperproliferation *in vivo* (Seldin and Macara, 2020). To characterise the impact of genotoxic treatment on cellular proliferation under *in vitro* conditions, organoids were immunostained with an anti-Ki67 antibody. Image analysis suggested that cisplatin treatment led to increased cell proliferation in organoids, corroborating *in vivo* results (Seldin and Macara, 2020). This is seemingly counterintuitive, as the DNA damage response leads to cell cycle arrest to prevent the transmission of potentially catastrophic DNA damage to daughter cells (Ruiz-Losada et al. 2022). Indeed, the increase in proliferation in organoids was not statistically significant. However, it is possible that during the chase period following cisplatin exposure, any repairable DNA damage has been resolved, meaning proliferation can resume. Moreover, proliferation may be increased to replace cells killed by cisplatin exposure. To investigate this, organoids were immunostained for cleaved caspase 3 (CC3), a reliable indicator of apoptosis. Surprisingly, despite organoids showing morphological signs of damage by brightfield microscopy, CC3 levels appeared to decrease with cisplatin treatment. However, this decrease was not significantly significant and was likely reflective of the difficulties experienced when immunostaining paraffin-embedded organoid sections, rendering image analysis challenging. For instance, the CC3 antibody often bound non-specifically to the lumens of the organoids, which caused high levels of background staining that masked genuine antibody signal. I sought to improve the quality of staining in many ways during the project, including comparing different solvents used for de-paraffinisation (histoclear vs xylene), using different antigen retrieval buffers as well as including Triton-X100 detergent into PBS wash steps, which failed to improve the staining. Marginal improvements were made by changing the specific fluorophore of the conjugated secondary

antibody used for detection, which facilitated the extraction of some quantitative data from the acquired images. As this analysis was only performed on a small subset of organoids, further repeats are necessary to gain better insights into whether the decrease in apoptosis observed is biologically relevant and not an artefact of immunostaining/image analysis. It would also be prudent to incorporate another method of analysing apoptosis levels in organoids to confirm whether difficulties in imaging are confounding results, such as the analysis of Annexin V by flow cytometry.

After ensuring that cisplatin reliably induced DNA damage in mammary epithelial organoids, I next investigated whether this led to cellular plasticity *in vitro*. Fluorescence microscopy to visualise endogenous GFP, alongside immunostaining for a lineage marker expressed by the opposing compartment, indicated that DNA damage does not induce plasticity *in vitro*. GFP was only observed in the basal compartment in K5-mTmG organoids and in the luminal compartment in K8-mTmG organoids, being distinctly separate from the stained opposing cell lineage. It is possible that the levels of GFP expression induced by 4-OHT treatment was a limiting factor, as plasticity would only be apparent in GFP-expressing cells. To identify whether there were very low levels of plasticity that might be undetectable by fluorescence microscopy, flow cytometry was also performed. This revealed a small increase in luminal GFP expression above baseline levels in response to cisplatin treatment in K5-mTmG organoids, which is suggestive of plasticity in the basal compartment. Interestingly this was also accompanied by a small decrease in basal GFP expression, which may be a result of basal cell death due to cisplatin-induced damage. Indeed, it would be interesting to investigate whether cisplatin preferentially damages basal or luminal cells. It would be logical to assume that basal cells might be more prone to damage by cisplatin given their location on the outer surface of the epithelial bilayer and that the repair process triggered by damage may result in plasticity, leading to higher numbers of luminal cells. However, in K8-mTmG organoids, cisplatin treatment led to an increase in GFP in the luminal compartment and corresponding decrease in the basal compartment. If cisplatin was indeed inducing plasticity in basal cells and causing them to produce luminal cells, a decrease in the number of GFP+ cells in the luminal compartment would be expected in K8-mTmG organoids due to dilution of the GFP+ luminal cell pool by unlabelled luminal cells generated by plasticity in unlabelled basal cells. The higher baseline levels of mis-specified

cells observed using flow cytometry in control conditions (as discussed in the results section above) also render small changes induced by cisplatin treatment more difficult to detect using this approach. Thus, while overall it appears that no substantial plasticity is induced by genotoxic damage in organoids, further experiments are required prior to drawing any conclusions.

To confirm that the lack of plasticity in response to cisplatin treatment was not agent specific, I performed similar experiments using mitomycin C, a chemically distinct agent that also induces DNA crosslinks. yH2AX immunostaining and subsequent fluorescence microscopy and image analysis confirmed that mitomycin C induced DNA damage in the organoids. Similar to the cisplatin experiments, no evidence of plasticity was observed in both K5-mTmG and K8-mTmG organoids in response to mitomycin C exposure. This increases confidence in the conclusion that genotoxic damage does not induce plasticity *in vitro*.

Considering the results of the *in vitro* experiments, we also assessed the impact of genotoxic damage on cell fate plasticity *in vivo* in K5-mTmG and K8-mTmG mice. Previous work showed that injecting cisplatin or mitomycin C directly into the mammary gland *in vivo* induced basal cell plasticity (Seldin and Macara, 2020). The impact of genotoxic damage on luminal cell plasticity, however, remained unexplored. To replicate these findings, cisplatin was injected directly into the mammary fat pads of pubertal K5-mTmG and K8-mTmG mice. 3D wholemount fluorescence imaging of optically cleared and immunostained tissues harvested 3-4 weeks after administration revealed that cisplatin exposure induced basal cell plasticity in K5-mTmG mice, while no evidence of luminal cell plasticity was detected in K8-mTmG mammary tissues. While further replicate experiments and yH2AX immunostaining analysis are ongoing, particularly to corroborate results obtained in K8-mTmG mice, these data indicate that cisplatin-driven DNA damage can induce cellular plasticity *in vivo*, but likely only in basal cells. Taken together, the apparent lack of cellular plasticity observed in organoids *in vitro* in response to genotoxic damage suggests that the effect observed *in vivo* might be mediated by signals from the mammary microenvironment that are absent in our culture conditions. To investigate this hypothesis further, I selected two candidate factors implicated in mammary epithelial cell plasticity *in vivo* (Centonze et al. 2020, Seldin and

Macara, 2020) for *in vitro* studies, namely Interleukin-1ß (IL-1ß) and Adalimumab, a Tumour Necrosis Factor (TNF) inhibitor.

4.2 Investigating the impact of IL-1ß and TNF inhibition on mammary epithelial cell fate plasticity *in vitro*

Interleukin-1ß is a pro-inflammatory cytokine that affects nearly all cells, often in concert with TNF (also a pro-inflammatory cytokine) to upregulate host responses to disease/damage (Dinarello, 1997). Previous studies showed that plasticity in epidermal cells in response to genotoxic damage was mediated by IL-1ß secreted by resident skin fibroblasts (Seldin and Macara, 2020). Injecting IL-1ß directly into the backskin of wildtype mice was shown to stimulate epidermal plasticity, which could be blocked in the presence of an IL-1ß blocking antibody. Based on this intriguing observation and the evolutionary and structural similarities between the epidermis and mammary epithelium, K5-mTmG and K8-mTmG epithelial organoids were cultured in the presence of IL-1ß to investigate whether this factor could induce mammary epithelial cell plasticity *in vitro*. RT-qPCR analysis revealed that the IL-1ß target genes IL-6 and Cox-2 were upregulated in response to treatment, confirming that mammary epithelial cells are responsive to IL-1ß. However, microscopic analysis showed that IL-1ß treatment did not induce discernible plasticity in organoids, with endogenous GFP expression remaining in the basal and luminal compartment in K5- and K8-mTmG organoids respectively. Similarly, flow cytometry did not show any increases in GFP expression in the opposing lineage over baseline control levels for both organoid models. Interestingly, the number of GFP+ cells appeared to increase in treated samples, suggesting that IL-1ß stimulated cell proliferation. This was confirmed by wholemount fluorescence microscopy of control and IL-1ß-treated organoids immunostained for the proliferation marker Ki67, which revealed increased numbers of Ki67+ nuclei in treated organoids. This corroborates Seldin and Macara's (2020) findings that IL-1ß induces hyperproliferation in response to cisplatin-induced DNA damage. Collectively, these results indicate that IL-1ß does not stimulate plasticity in mammary epithelial organoids *in vitro*. This suggests that the ability of IL-1ß to induce cellular plasticity may be specific to epidermal cells. Indeed, Seldin and Macara did not investigate whether the plastic response to IL-1ß injection was also seen in the mammary gland. In future work, it would be interesting to investigate whether

injecting IL-1ß directly into the mammary gland *in vivo* leads to changes in cell fate specification.

Recent *in vitro* genetic lineage ablation studies suggested that the multipotency of mammary epithelial cells is restricted under physiological conditions by cell-cell TNF signalling, as treating mammary cells with the TNF inhibitor Adalimumab resulted in basal cell plasticity (Centonze et al. 2020). The impact of TNF signalling blockade on luminal cell fate outcomes, however, was not investigated. I thus attempted to replicate this effect in K5-mTmG organoids and to test whether Adalimumab exposure also induces plasticity in luminal cells using K8-mTmG organoids. Preliminary flow cytometry experiments suggested that no plasticity above baseline levels was induced in response to Adalimumab exposure. However, corresponding imaging studies using traditional intracellular lineage markers to distinguish the luminal and basal compartments provided some evidence of basal cell plasticity in response to TNF signalling inhibition. It is conceivable that this effect was more apparent for Centonze et al. due to their ability to fluorescently label basal cells to saturation in their study, which is not possible in our experimental models (as discussed above). Moreover, the impact of Adalimumab on mammary cell fate plasticity *in vitro* was subtle in this study (only a 3% increase in labelled luminal cells), which may be difficult to replicate when using different models. Thus, further replicate experiments are required to confirm our initial observations. Moreover, while I attempted to validate the responsiveness of mammary organoids to Adalimumab by performing immunostaining for NF-KB (a downstream target of the TNF pathway), these experiments were inconclusive. Thus, validation experiments are required to confirm the efficacy of Adalimumab in blocking TNF signalling in our experimental system, such as analysing the expression of TNF target genes in organoids by RT-qPCR.

It is also important to acknowledge the differences between the experimental system used by Centonze et al. (2020) and that used in this study. In their work, the authors used a genetic model that facilitated the specific ablation of vast swathes of the luminal cell compartment, whereas here genotoxic damage was being induced in both luminal and basal cells at levels insufficient to cause mass cell death. Therefore, the signals induced by these different stressors are likely distinct and may influence cell behaviour and fate specification

differently. Thus, care is required when making comparisons between our work and this study and their observations.

4.3 Identifying putative microenvironmental factors that might mediate cisplatin-induced mammary epithelial plasticity *in vivo*

My data suggested that, unlike in *in vivo* contexts, genotoxic damage fails to induce mammary epithelial plasticity *in vitro*. I therefore sought to identify novel putative microenvironmental mediators of plasticity that could be prioritised for functional analysis in future studies. To achieve this, I interrogated and cross compared two bulk RNA sequencing datasets, namely RNA sequencing data from mammary luminal, basal and "hybrid" epithelial cells pre and post-luminal cell ablation (Centonze et al. 2020) and fibroblasts isolated from vehicle and cisplatin-treated mice (Seldin and Macara, 2020). HTseqcount files were generated and analysed for differential gene expression using the DESeq2 package in R (see methods). For both datasets, initial principal component analysis indicated high variance between control and experimental populations, with individual replicate samples within control and experimental conditions tending to cluster closely together. This increases confidence that luminal cell ablation (Centonze et al. 2020) and cisplatin treatment (Seldin and Macara, 2020) leads to differential gene expression profiles, which could reveal candidate mediators of the plastic responses seen in treated conditions.

When interrogating the Centonze et al. (2020) dataset, I first analysed the expression of a range of well-defined luminal and basal cell markers to understand the process by which luminal cells emerged from basal cells that had regained bipotency in response to luminal cell ablation. My comparative analysis of lineage marker expression across distinct cell populations suggested a mechanism whereby hybrid cells arising in response to luminal cell ablation represent an intermediate, potentially transient, cell state. Indeed, hybrid cells displayed both 'basal-like' and 'luminal-like' marker expression characteristics, seemingly in-between normal basal and luminal cells. When compared to post-ablation luminal cells, however, basal marker expression in hybrid cells was higher, while luminal marker expression was similar. It is therefore possible that in response to luminal cell ablation, basal cells themselves, or their daughter cells, begin to lose basal marker expression and gain low levels of luminal marker expression in order to replace luminal cells lost to ablation.

To try to identify factors which may mediate this plastic process, differential gene expression and KEGG pathway analyses were performed to identify upregulated genes and pathways respectively (see methods). This revealed that cell cycle, ECM-receptor interaction and chemokine/cytokine signalling pathways were all upregulated in experimental versus control conditions. Considering long-term self-renewal to support the maintenance of a range of differentiation outcomes is a defining feature of bi/multipotent cells, it is reasonable to hypothesise that the induction of plasticity involves alterations to the cell cycle. Indeed, multipotent cells are known to progress through the cell cycle quickly with short gap (G) phases. Since progression through the cell cycle is regulated by factors such cyclin-dependent kinases, it is possible the induction of plasticity is mediated in part by altered cyclin-dependent kinase expression, or perhaps altered expression is a result of plasticity induction (Boward, Wu and Dalton, 2016). ECM-cell interactions are also likely crucial in the maintenance of a cell's identity due to the role of the ECM in establishing a cell's niche and dictating the signals which cells are exposed to. Changes in the nearby ECM may therefore lead to alterations in cell fate (Ka Yan Ma, 2020). Chemokine and cytokine signalling has already been implicated in plasticity mediation by the Centonze et al. (2020) and Seldin and Macara (2020) studies which identified TNF and IL-1ß as regulators of plasticity respectively. Analysis of upregulated genes in the Seldin and Macara (2020) dataset specified the TNF and NF-KB pathways, chemokine signalling networks that regulate ECM alterations, cell adhesion and cell survival among other functions. It is possible that DNA damage/luminal cell ablation activates these pathways which encompass signalling factors that work individually or in concert to trigger plasticity as a response. The increased histone modification expression, whilst not highlighted by KEGG pathway analysis, is an area of particular interest considering the role of the chromatin landscape and epigenetic regulation in stabilising cell fates during development. It is possible that DNA damage/luminal cell ablation alters chromatin states, rendering the epigenetic landscape more permissive and allowing non-physiological cell fate choices to occur (Flahavan, Gaskell and Bernstein, 2017). This might represent the mechanism underpinning the alterations in lineage marker expression seen across cell population comparisons of data from the Centonze et al. (2020) study.

Despite highlighting candidate pathways for future studies aimed at identifying important mediators of mammary cell plasticity in response to genotoxic damage, there are some limitations to the RNA sequencing analysis performed herein to consider. For example, while there are evolutionary similarities between the skin and mammary epithelium as previously mentioned, the Seldin and Macara (2020) dataset consists of RNA extracted from fibroblasts isolated from vehicle and cisplatin-treated mice, which are distinct from the cells residing in the mammary gland. Moreover, perhaps unsurprisingly, correlation testing revealed minimal correlation between differential gene expression in the Centonze et al. (2020) and Seldin and Macara (2020) datasets. Thus, the likelihood that potential candidate plasticity mediators identified in the Seldin and Macara (2020) dataset have the same effect in the mammary gland is slim. This may explain why treating mammary organoids with IL-1ß - the factor secreted by skin fibroblasts in response to cisplatin treatment that mediates epidermal plasticity (Seldin and Macara, 2020) – had no discernible effect on mammary cell fate outcomes *in vitro*. Conversely, the experimental system employed by Seldin and Macara's (2020) is much closer to that used in this study compared to the diphtheria toxin-based genetic lineage ablation approach used by Centonze et al. (2020), despite its use in mammary epithelial cells.

4.4 Future perspectives

While taking the aforementioned limitations into account, an immediate priority for future work would be to investigate factors that regulate the overlapping pathways identified between the Centonze and Seldin RNA sequencing data to assess whether they are able to induce plasticity when added to mammary epithelial organoid cultures. For example, alongside other soluble cytokines/chemokines that affect TNF and NF-KB signalling such as Interleukin-19, organoids could be treated with agents that impact ECM-receptor interactions, for example blocking antibodies against key mammary epithelial cell integrin proteins. Longer term, as cisplatin was able to induce mammary epithelial cell plasticity *in vivo*, it would be desirable to perform RNA sequencing on mammary gland tissues injected with vehicle control and cisplatin solutions to identify differences in gene expression between the two treatment conditions. This may reveal factors capable of inducing plasticity in organoid cultures. With regards to organoid cultures, it would be interesting to

investigate the effect of cisplatin when co-culturing mammary epithelial organoids with fibroblasts/immune cells given their importance for normal mammary gland development and tissue homeostasis and the fact that the RNA sequencing analysis performed implicates signals regulated by these cell types in plasticity induction, such as collagen components produced by fibroblasts and cytokines/chemokines involved in immune cell recruitment. If cisplatin induces plasticity in this context, this would suggest that the co-cultured cells are the source of factors that mediate plasticity, which in turn would aid their identification. On a more technical note, this study has highlighted the continuing limitations of using a tamoxifen-inducible population-based lineage tracing model for studies of this nature. Harnessing a more neutral or saturation-based system that does not rely on tamoxifen for labelling would be beneficial in future work.

4.5 Conclusion

During this project, I have optimised the establishment of 3D mammary organoids isolated from K5-mTmG and K8-mTmG lineage-tracing transgenic mice and validated that their architecture and behaviour accurately recapitulates the *in vivo* mammary gland. I also confirmed their suitability for *in vitro* lineage tracing. Lineage tracing experiments in 3D cultures demonstrated that cisplatin-induced genotoxic damage does not trigger plasticity in K5-mTmG or K8-mTmG organoids *in vitro*, but does lead to increased proliferation. This was corroborated by the lack of plasticity seen in response to mitomycin C-induced genotoxic damage, which confirmed the response was not specific to cisplatin. Induction of plasticity in response to cisplatin treatment *in vivo* suggested microenvironmental factors may mediate plasticity, however two factors referenced in recent literature – IL-1ß and the TNF inhibitor Adalimumab (Seldin and Macara, 2020, Centonze et al. 2020) - failed to conclusively induce plasticity *in vitro*. By analysing publicly available bulk RNA sequencing data generated in the Centonze et al. (2020) and Seldin and Macara (2020) studies, I have identified a range of pathways and genes commonly upregulated in response to damage that might represent putative mediators of plasticity which could be further investigated in future work.

References

Aggarwal, B. (2003) 'Signalling pathways of the TNF superfamily: a double-edged sword'. Nat Reviews Immunology, 3, pp. 745–756.

Anders, S. Pyl, P. T. Huber, W. (2015) 'HTSeq—a Python framework to work with high-throughput sequencing data'. Bioinformatics, 31(2), pp. 166-169.

Andrews, S. (2010) 'FastQC: A Quality Control Tool for High Throughput Sequence Data' [Online]. Available online at: http://www.bioinformatics.babraham.ac.uk/projects/fastqc/ (Accessed 10th June 2022)

Blaas, L. Pucci, F. Messal, H. Andersson, A. Ruiz, E. Gerling, M. Douagi, I. Spencer-Dene, B. Much, A. Mitter, R. Bhaw, L. Stone, R. Bornhorst, D. Sesay, A. Jonkers, J. Stamp, G. Malanchi, I. Toftgård, R. Behrens, A. (2016) 'Lgr6 labels a rare population of mammary gland progenitor cells that are able to originate luminal mammary tumours'. Nature Cell Biology, 18, pp. 1346-1356.

Blighe, K. Rana, S. Lewis, M. (2022) 'Enhanced Volcano: Publication-ready volcano plots with enhanced colouring and labeling'. R package version; 1.8.0.

Boward, B. Wu, T. Dalton, S. (2016) 'Concise Review: Control of Cell Fate Through Cell Cycle and Pluripotency Networks'. Stem Cells, 34, pp. 1427–1436.

Bray, F. Ferlay, J. Soerjomataram, I. Siegel, R. L. Torre, L. A. Jemal, A. (2018) 'Global cancer statistics 2018: GLOBOCAN estimates of incidence and mortality worldwide for 36 cancers in 185 countries'. CA: A Cancer Journal for Clinicians, 68(6), pp. 394-424.

Centonze, A. Lin, S. Tika, E. Sifrim, A. Fioramonti, M. Malfait, M. Song, Y. Wuidart, A. Van Herck, J. Dannau, A. Bouvencourt, G. Dubois, C. Dedoncker, N. Sahay, A. de Maertelaer, V. Siebel, CW. Van Keymeulen, A. Voet, T. Blanpain, C. (2020) 'Heterotypic cell-cell communication regulates glandular stem cell multipotency'. Nature, 584(7822), pp. 608-613.

Crowley, L. Waterhouse, N. (2016) 'Detecting Cleaved Caspase-3 in Apoptotic Cells by Flow Cytometry'. Cold Spring Harbour Protocols, 11.

Davis, F. Lloyd-Lewis, B. Harris, O. Kozar, S. Winton, D. Muresan, L. Watson, C. (2016) 'Single-cell lineage tracing in the mammary gland reveals stochastic clonal dispersion of stem/progenitor cell progeny'. Nature Communications, 25(7), pp. 1-13.

DeOme, K. Faulkin, L. Bern, H. Blair, P. (1959) 'Development of Mammary Tumors from Hyperplastic Alveolar Nodules Transplanted into Gland-free Mammary Fat Pads of Female C3H Mice'. Cancer Research, 19(5), pp. 515-520.

Dinarello, C.A. (1997) 'Interleukin-1'. Cytokine & Growth Factor Reviews, 8, pp. 253-265.

Dobin, A. Davis, C. A. Schlesinger, F. Drenkow, J. Zaleski, C. Jha, S. Batut, P. Chaisson, M. Gingeras, T. R. (2013) 'STAR: ultrafast universal RNA-seq aligner'. Bioinformatics, 29(1), pp. 15-21.

Flahavan, W. Gaskell, E. Bernstein, B. (2017) 'Epigenetic plasticity and the hallmarks of cancer'. Science, 357(6348), pp. 1-29.

Graefe, C. Eichhorn, L. Wurst, P. Kleiner, J. Heine, A. Panetas, I. Abdulla, Z. Hoeft, A. Frede, S. Kurts, C. Endl, E. Weisheit, C. (2019) 'Optimized Ki-67 staining in murine cells: a tool to determine cell proliferation'. Molecular Biology Reports, 46, pp. 4631-4643.

Hein, S. M. Haricharan, S. Johnston, A. N. Toneff, M. J. Reddy, J. P. Dong, J. Bu, W. Li, Y. (2016) 'Luminal epithelial cells within the mammary gland can produce basal cells upon oncogenic stress'. Oncogene, 35(11), pp. 1461-1467.

Highley, M. Harper, B. Harper, P. Dumez, H. Guetens, G. De Boeck, G. Prenen, H. Schrijvers, D. Maes, R. de Bruijn, E. (2006) 'The pharmacokinetics of mitomycin C in the mitomycin C, ifosfamide and cisplatin (MIC) regimen'. International Journal of Pharmacology, 2, pp. 293-296.

Honvo-Hueto, E. Turchet, S. (2015) 'Indirect Immunofluorescence on Frozen Sections of Mouse Mammary Gland'. Journal of Visualized Experiments, 106(53179), pp. 1-44.

Inman, J. L. Robertson, C. Mott, J. D. Bissell, M. J. (2015) 'Mammary gland development: cell fate specification, stem cells and the microenvironment'. Development, 142(6), pp. 1028-1042.

Jardé, T. Lloyd-Lewis, B. Thomas, M. Kendrick, H. Melchor, L. Bougaret, L. Watson, P. Ewan, K. Smalley, M. Dale, T. (2016) 'Wnt and Neuregulin1/ErbB signalling extends 3D culture of hormone responsive mammary organoids'. Nature Communications, 7(13207), pp. 1-14.

Ka Yan Ma, S. Shing Fung Chan, A. Rubab, A. Cheuk Wing Chan, W. Chan, D. (2020) 'Extracellular Matrix and Cellular Plasticity in Musculoskeletal Development'. Frontiers in Cell and Developmental Biology, 8(781), pp. 1-20.

Khan, S. Suryavanshi, M. Kaur, J. Nayak, D. Khurana, A. Manchanda, R. K. Tandon, C. Tandon, S. (2021) 'Stem cell therapy: A paradigm shift in breast cancer treatment'. World Journal of Stem Cells, 13(7), pp. 841–860.

Koren, S. Reavie, L. Couto, J. P. De Silva, D. Stadler, M. B. Roloff, T. Britschgi, A. Eichlisberger, T. Kohler, H. Aina, O. Cardiff, R. D. Bentires-Alj, M. (2015) 'PIK3CA(H1047R) induces multipotency and multi-lineage mammary tumours'. Nature, 525(7567), pp. 114-118.

Liang, Y. Lin, S.Y. Brunicardi, F.C. Goss, J. Li, K. (2009) 'DNA Damage Response Pathways in Tumor Suppression and Cancer Treatment'. World Journal of Surgery, 33, pp. 661–666.
Liu, T. Zhang, L. Joo, D. Sun, S. (2017) 'NF-κB signaling in inflammation'. Signal Transduction and Targeted Therapy, 2(17023), pp. 1-9.

Lloyd-Lewis, B. Davis, F. Harris, O. Hitchcock, J. Watson, C. (2018) 'Neutral lineage tracing of proliferative embryonic and adult mammary stem/progenitor cells'. Development, 145(14), pp. 1-9.

Lloyd-Lewis, B. Harris, O. Watson, C. Davis, F. (2017) 'Mammary Stem Cells: Premise, Properties, and Perspectives'. Trends in Cell Biology, 27(8), pp. 556-567.

Lord, C. Ashworth, A. (2012) 'The DNA damage response and cancer therapy'. Nature, 481, pp. 287–294.

Love, M. I. Huber, W. Anders, S. (2014) 'Moderated estimation of fold change and dispersion for RNA-seq data with DESeq2'. Genome biology, 15(12), pp. 1-21.

Meier-Abt, F. Bentires-Alj, M. (2014) 'How pregnancy at early age protects against breast cancer'. Trends in Molecular Medicine, 20(3), pp. 143-153.

Molyneux, G. Geyer, F. C. Magnay, F. A. McCarthy, A. Kendrick, H. Natrajan, R. Mackay, A. Grigoriadis, A. Tutt, A. Ashworth, A. Reis-Filho, J. S. Smalley, M. J. (2010) 'BRCA1 basal-like breast cancers originate from luminal epithelial progenitors and not from basal stem cells'. Cell Stem Cell, 7(3), pp. 403-41.

Muzumdar, M.D. Tasic, B. Miyamichi, K. Li, L. Luo, L. (2007) 'A global double-fluorescent Cre reporter mouse'. Genesis, 45, pp. 593-605.

Oun, R. Moussa, Y. Wheate, N. (2018) 'The side effects of platinum-based chemotherapy drugs: a review for chemists'. Dalton Transactions, 47(19), pp. 6645-6653.

Prater, M. Petit, V. Russell, A. Giraddi, R. Shehata, M. Menon, S. Schulte, R. Kalajzic, I. Rath, N. Olson, M. Metzger, D. Faraldo, M. Deugnier, M. Glukhova, M. Stingl, J. (2014) 'Mammary stem cells have myoepithelial cell properties'. Nature Cell Biology, 16(10), pp. 942–947.

Przepiorski, A. Sander, V. Tran, T. Hollywood, J. A. Sorrenson, B. Shih, J. H. Wolvetang, E. J. McMahon, A. P. Holm, T. M. Davidson, A. J. (2018) 'A Simple Bioreactor-Based Method to Generate Kidney Organoids from Pluripotent Stem Cells'. Stem Cell Reports, 11(2), pp. 470-484.

Rios, A. Yang Fu, N. Lindeman, G. Visvader, J. (2014) 'In situ identification of bipotent stem cells in the mammary gland'. Nature, 506, pp. 322-327.

Ruiz-Losada, M. Gonzalez, R. Peropadre, A. Gil-Galvez, A. Tena, J. Baonza, A. Estella, C. (2022) 'Coordination between cell proliferation and apoptosis after DNA damage in Drosophila'. Cell Death & Differentiation, 29, pp. 832-845.

Scheele, C. Hannezo, E. Muraro, M. Zomer, A. Langedijk, N. van Oudenaarden, A. Simons, B. Rheenen, J. (2017) 'Identity and Dynamics of mammary stem cells during branching morphogenesis'. Nature, 542, pp. 313–317.

Seldin, L. Le Guelte, A. Macara, I. (2017) ‘Epithelial plasticity in the mammary gland’. Current Opinion in Cell Biology, 49, pp. 59-63.

Seldin, L. Macara, I. (2020) ‘DNA Damage Promotes Epithelial Hyperplasia and Fate Mis-specification via Fibroblast Inflammasome Activation’. Cell Press: Developmental Cell, 55, pp. 558-573.

Sharma, A. Singh, K. Almasan, A. (2012) ‘Histone H2AX Phosphorylation: A Marker for DNA Damage’ in Bjergbæk, L. (ed.) DNA Repair Protocols. Methods in Molecular Biology (Methods and Protocols), vol 920. Totowa, NJ. Humana Press.

Siddik, Z. (2003) ‘Cisplatin: mode of cytotoxic action and molecular basis of resistance’. Oncogene, 22, pp. 7265-7279.

Slepicka, P. Somasondara, A. Dos Santos, C. (2021) ‘The molecular basis of mammary gland development and epithelial differentiation’. Seminars in Cell & Developmental Biology. 114, pp. 93-112.

Stevenson, A. Vanwalleghem, G. Stewart, T. Condon, N. Lloyd-Lewis, B. Marino, N. Putney, J. Scott, E. Ewing, A. Davis, F. (2020) ‘Multiscale imaging of basal cell dynamics in the functionally mature mammary gland’. Proceedings of the National Academy of Sciences, 117(43), pp. 26822-26832.

Sumbal, J. Budkova, Z. Traustadóttir, G. Á. Koledova, Z. (2020) ‘Mammary Organoids and 3D Cell Cultures: Old Dogs with New Tricks’. Journal of Mammary Gland Biology and Neoplasia, 25(4), pp. 273-288.

Tange, O. (2011) ‘Gnu parallel-the command-line power tool’. The USENIX Magazine, 36(1), pp. 42-47.

The Open Lab Book (2014). Measuring cell fluorescence using ImageJ. Available at: https://theolb.readthedocs.io/en/latest/imaging/measuring-cell-fluorescence-using-imagej.html#:~:text=Measuring%20cell%20fluorescence%20using%20ImageJ%20%C2%B6%201%20From,has%20no%20fluroence%2C%20this%20will%20be%20your%20background. (Accessed 02/09/2022).

Tiede, B. Kang, Y. (2011) ‘From milk to malignancy: the role of mammary stem cells in development, pregnancy and breast cancer’. Cell Research, 21(2), pp. 245-257.

Van Amerongen, R. Bowman, A. Nusse, R. (2012) ‘Developmental Stage and Time Dictate the Fate of Wnt/b-Catenin-Responsive Stem Cells in the Mammary Gland’. Cell Stem Cell, 11, pp. 387-400.

Van Keymeulen, A. Lee, M. Y. Ousset, M. Brohée, S. Rorive, S. Giraddi, R. R. Wuidart, A. Bouvencourt, G. Dubois, C. Salmon, I. Sotiriou, C. Phillips, W. A. Blanpain, C. (2015)

‘Reactivation of multipotency by oncogenic PIK3CA induces breast tumour heterogeneity’. Nature, 525(7567), pp. 119-123.

Van Keymeulen, A. Rocha, A. Ousset, M. Beck, B. Bouvencourt, G. Rock, J. Sharma, N. Dekoninck, S. Blanpain, C. (2011) ‘Distinct stem cells contribute to mammary gland development and maintenance’. Nature, 479, pp. 189-193.

Vinuesa-Pitarch, E. Ortega-Álvarez, D. Rodilla, V. (2022) ‘How Lineage Tracing Studies Can Unveil Tumor Heterogeneity in Breast Cancer’. Biomedicines, 10(3), pp. 1-15.

Wuidart, A. Ousset, M. Rulands, S. Simons, B. Van Keymeulen, A. Blanpain, C. (2016) ‘Quantitative lineage tracing strategies to resolve multipotency in tissue-specific stem cells’. Genes & Development, 30, pp. 1261-1277.

Yu, G. Wang, L. G. Han, Y. He, Q. Y. (2012) ‘clusterProfiler: an R package for comparing biological themes among gene clusters’. Omics: a journal of integrative biology, 16(5) pp. 284-287.

Zhang, K. Qi, H. Liu, Y. Chen, W. (2009) ‘Visualization of Cellular DNA Crosslinks by Atomic Force Microscopy’. Scanning, 31(2), pp. 75-82.